The Geochemistry and Ecotoxicity of Offshore New Zealand Phosphorites

BY

Grace Elizabeth Frontin-Rollet

A thesis submitted to Victoria University of Wellington in partial fulfilment of requirements for the degree of Master of Geology.

School of Geography, Environment and Earth Sciences

Victoria University of Wellington

2017

Abstract

The New Zealand offshore seabed hosts diverse resources including phosphate rich rocks. Phosphate rock deposits on the Chatham Rise have been the focus of previous investigations into their composition and mining potential; however, the diversity of the geochemistry of phosphate deposits, including their wider distribution beyond the Chatham Rise, their trace metal budget, and potential for ecotoxicity, remain poorly characterised. This study addresses some of these gaps by presenting a geochemical investigation, including trace metals, for a range of phosphate nodules from across the Chatham Rise, Bollons Seamount and offshore southeastern South Island. Elutriate and reconnaissance bioaccumulation experiments provide insights into the potential for ecotoxic trace metal release and effects on biota should sediment disturbance through mining activities occur.

The bulk chemistry of Bollons Seamount phosphorite nodules have been characterised for the first time, and show significant enrichment in first row transition metals; Co, Ni, Cu, Zn, in addition to Sr, Y, Mo, U, MnO, CaO and P_2O_5, and depletion in TiO_2, Al_2O_3, MgO, K_2O, FeO, SiO_2, Sc, Cr, Ga, Rb, Cs, Hf, and Th relative to average upper continental crust. The cores of these nodules are dominated by apatite, quartz and anorthoclase phases, which are cross cut by Mn rich dendrites. The abundant presence of these minerals results in the significant differences in chemistry observed relative to Chatham Rise phosphorite nodules. The nodules also contain a secondary authigenic apatite phase, with a Mn crust rim. Significant rare earth element enrichment (REE) is most likely due to efficient scavenging by the Mn crust, resulting in seawater REE patterns characterised by negative Ce and Eu anomalies and heavy rare earth element enrichment.

The bulk geochemistry of the Chatham Rise and offshore South Island phosphorite nodules is characterised by enrichment in CaO, P_2O_5, Sr, U, Y, Mo and depletion in TiO_2, Al_2O_3, MnO, MgO, FeO, K_2O, Sc, Cr, Cu, Ga, Rb, Cs, Ba, Hf, Ta, Pb and Th relative to average upper continental crust. The low concentrations of Cd in Chatham Rise, offshore South Island, and Bollons Seamount phosphorites make them potentially suitable sources for direct application fertilizers.

The New Zealand marine phosphorite nodule deposits formed by repeated cycles of erosive bottom currents and phosphogenesis, resulting in the winnowing and concentration of the

deposits. The iron pump model is proposed as a mechanism for the formation of apatite and associated mineral phases, giving the nodules their characteristic concentric zoning. The migration of the nodules through the oxic, suboxic, and anoxic zones of the sediment profile led to the formation of glaucony, apatite (suboxic zone), goethite (oxic zone), and pyrite with associated U enriched (anoxic zone) minerals. Rare earth elements (REE) in the Chatham Rise phosphorite nodules are associated with the glaucony rim minerals, and indicate that since the formation of the rims, very little diagenesis has occurred, preserving seawater REE patterns characterised by negative Ce and Eu anomalies and heavy REE enrichment. Site specific enrichments in trace elements Ba, V, Co, Ni, Cu, Zn, Y, Cd and Pb are attributed to either differences in incorporation of material into precursor carbonate e.g. volcanic materials, or higher fluxes of organic matter, delivering high concentrations of essential metals from biota, especially Cu and Zn.

Direct pore water measurements from surficial sediment of the Chatham Rise show high concentrations of dissolved Fe and Mn, along with Cu, indicating suboxic conditions. High Cu concentrations measured in sediment pore water suggest that Cu release requires monitoring should seafloor surficial sediments on the Chatham Rise be disturbed. However, the elutriate experiments were not able to resolve if Cu release by sediment disturbance would exceed Australian and New Zealand Environment Conservation Council (2000) environmental guideline trigger values.

The surrogate amphipod species *Chaetocorophium* c.f. *lucasi* shows promise as a biomonitor for disturbed marine sediments. Elements enriched in surficial sediments and phosphorite nodules, Hg, Pb, Fe, U and V, were not observed to bioaccumulate. Site specific differences in chemistry were observed, specifically in the different total relative bioaccumulation of Mo between amphipods exposed to sediments from two different sites. This suggests that future monitoring of chemical release during marine sediment disturbance requires the full geochemical characterisation of the substrate. Furthermore, fresh sediment and deep water should be used for future elutriate experiments, as storage of material by freeze-thawing and/or refrigeration causes mobilisation of some key trace metals such as U, V, Mo, Mn.

Acknowledgements

Firstly, I'd like to thank my supervisors Dr. Monica Handler, Dr. Richard Wysoczanski, and Dr. Chris Hickey. Without your patience and support I would not have completed this thesis. Your time and effort, especially with editing, has been greatly appreciated.

Secondly, I'd like to thank those who provided technical and analytical assistance. This includes the SGEES technical staff, especially Sabrina Lange, Jane Chewings, and Bruce Charlier. I'd also like to thank the staff at NIWA, wellington, especially Lisa Northcote, Graeme Moss, Diana Macpherson, Sadie Mills, Sarah Allen, and Neil Barr. Big thanks to Dr. Michael Gazley (CSIRO) for making μXRF and SEM maps, as well as the many interesting and inspiring conversations about compositional data analysis. To Dr. Katie Collins, your patience and assistance with teaching me how to use R is greatly appreciated. To the crew and science team of TAN1503 for their efforts in ensuring we had fresh samples for this thesis. Thank you for your patience, especially the voyage leader Dr. Malcolm Clark, and Di Tracey. I'd also like to acknowledge Chatham Rock Phosphate Ltd for giving us permission to retrieve a box core from within the mining permit area. Thank-you Professor Terry Seward for giving your time and expertise regarding chemistry matters related to this thesis.

Financial support and encouragement generously given by Education Endowment Trust AUSIMM scholarship, and the John Gamble Geology Prize is gratefully acknowledged.

The funding for this thesis was provided by NIWA through a Ministry of Business, Innovation and Employment (MBIE) grant for Enabling the Management of Offshore Mining (EMOM) project, 2012-2016.

Finally I'd like to thank my families for their love and support. To my partner Kade Earl and his amazing family. I could not have done this without you all. To my parents Brett Frontin-Rollet and Janine Wearne for your encouragement and support, especially my father for your engineering expertise and assistance building the column apparatus. I'd like to acknowledge my academic siblings; Alex Zohrab and Andrea Davies, the current inhabitants of the CO421 masters office, the inhabitants of the old masters office CO422, and fellow students from the geochemistry laboratory, especially Elliot Swallow for your assistance.

Table of Contents

List of Figures

List of Tables

Glossary of terms and abbreviations used

1 ppm	Equivalent to; 1 g/m^3 , mg/kg
99% species protection	If the concentrations of potentially ecotoxic metals are below trigger guidelines derived for this this threshold, then statistically it is expected that 99% of species will survive. This level of protection is used for pristine and undisturbed environments (Australian and New Zealand Environment Conservation Council, 2000a).
Amphipod	An invertebrate from the order Crustacea.
ANZECC	Australian and New Zealand Environment Conservation Council
Benthic	Organisms whose habitat consists of just above/ below the sediment surface. (Australian and New Zealand Environment Conservation Council, 2000a).
Bioaccumulation	The uptake of substances (e.g. metals) into an organism's body tissues which is maintained due to exposure either from direct ingestion or from water in the immediate environment. (Australian and New Zealand Environment Conservation Council, 2000a).
Bioassay	Usually a laboratory experiment where a test organism is exposed to different concentrations of a potential toxicant to assess the response of the biota. (Australian and New Zealand Environment Conservation Council, 2000a).
Bioconcentration	A general process where a net concentration of contaminants such as metals are concentrated into an organism's body tissues. (Australian and New Zealand Environment Conservation Council, 2000a).
Bioconcentration factor (BCF)	An empirical estimate of concentration of contaminant in an organism's tissue whereby the absolute concentration of a contaminant in an organism's tissues is divided by the concentration in the water of which the organism has been living. (Australian and New

	Zealand Environment Conservation Council, 2000a).
Bottom water	Water directly above the seabed.
CFA	Carbonate fluorapatite; carbonate apatite, or francolite
Chronic	Refers to the long-term exposure of an organism to a contaminant in a laboratory experiment. A chronic can include: growth, lethality, effects on reproduction or any other related effects. (Australian and New Zealand Environment Conservation Council, 2000a).
CRP	Chatham Rock Phosphate Limited.
CTD	Conductivity, temperature, depth.
Elutriate	"Process of elutriating fine particles and pore water from sediments". (Hickey et al., 2014, p. 20).
EPA	Environmental Protection Agency
GDP	Gross Domestic Product
Guideline	"Numerical concentration limit or narrative statement recommended to support and maintain a designated water use." (Australian and New Zealand Environment Conservation Council, 2000a, p.A-11).
Guideline trigger levels/value	Environment trigger values are concentrations of known ecotoxic elements below which there is a low risk of toxic effects. If the trigger values are exceeded, this is an indication that action in the form of either monitoring or further investigation is needed (Australian and New Zealand Environment Conservation Council, 2000a).
Phosphate	Phase rich in phosphorus.
Phosphorite	Marine sedimentary rock where phosphate is the main constituent.

Stressor	"Physical, chemical, or biological factors that can cause an adverse effect in an aquatic ecosystem". (Australian and New Zealand Environment Conservation Council, 2000a, p. A-18).
Toxicant	A chemical contaminant, which is in excess in the environment, that can cause harmful and adverse effects to local biota (Australian and New Zealand Environment Conservation Council, 2000a).
Toxicity	"The inherent potential or capacity of a material to cause adverse effects on a living organism". (Australian and New Zealand Environment Conservation Council, 2000a, p. A-19).

Chapter 1. Background

1.1 Introduction

Phosphate rocks are enriched in phosphorus (>18 wt%), and are found in limited deposits around the world. They are critical to society forming the basis of phosphate fertilizers that underpin high production of food. As land based mineral resources become exhausted, the seafloor will become a more attractive exploration frontier to find more resources.

Phosphate rock deposits are dominantly composed of apatite family minerals. Trace metals can substitute into the apatite crystal lattice, or be contained in other phases that co-exist with apatite phases. The levels of trace metals can vary drastically from deposit to deposit due different processes of formation. Some of these trace metals may be ecotoxic, thus their release could be of concern if the phosphate rock is used as an agricultural fertilizer, or disturbed in the seafloor environment during potential mining operations.

With the renewed global interest in marine phosphorite deposits, this study aims to characterise the chemistry of New Zealand's principal offshore phosphorite deposits and examine any potential ecotoxic effects of their extraction from the seafloor. This study will achieve these aims through:

1. Characterising the bulk geochemistry of offshore New Zealand phosphorites from Chatham Rise and Bollons Seamount.
2. Evaluating potential levels of ecotoxic trace metal release by conducting elutriate leaching and column experiments.
3. Evaluating the potential of an amphipod species to monitor the effects of ecotoxic metal levels through bioaccumulation experiments.

1.2 Thesis Structure

The investigations into bulk chemistry characterisation and ecotoxicity are undertaken in separate chapters. The following section gives an outline for the six chapters presented in this thesis.

Chapter 1. Background: This chapter provides a background to the use of phosphate rock as a resource, exploring its economic effects on both a global scale and in relation to New Zealand.

Chapter 2. Phosphorite formation: A Review: This chapter reviews the formation processes relevant to offshore New Zealand phosphorites and the implications for incorporation of unwanted trace metals into the deposit.

Chapter 3. Geological Setting and Palaeoceanography: A background to the geological and palaeoceanographic processes and events that ultimately lead to the formation of seafloor phosphorite nodules. There is emphasis on the Chatham Rise region, as this area has the highest concentrations of phosphorite deposits and hence has been studied in the most detail.

Chapter 4. Geochemistry: The bulk major and trace element chemistry of offshore New Zealand phosphorite nodules, and some associated surficial sediments, are characterised in this chapter. An overview of the analytical methods used to obtain results is included. The key results are presented and split into different sections depending on sample type. The discussion is an interpretation of the results exploring formation models, the conditions of diagenesis, and the geochemical considerations of offshore New Zealand phosphorites as an agricultural fertilizer.

Chapter 5. Ecotoxicity Experiments: This chapter explores the potential release of ecotoxic trace metals resulting from sediment disturbance related to seafloor mining methods. An overview of methods, such as standard elutriate testing, column leaching experiments, and bioaccumulation experiments is given. Key results from the different methods are presented, along with some key baseline data for the Chatham Rise seafloor environment. The discussion interprets the significance of the results in relation to potential ecotoxicity resultant from surficial sediment disturbance and assesses the use of amphipods as

environmental biomonitors. A comparison between previous standard elutriate results for surficial Chatham Rise sediments is also included.

Chapter 6. Conclusions: A summary of key findings from Chapter 4. and Chapter 5. Recommendations for future work that could not be conducted in this thesis is given.

Appendices. Supplementary information: Three appendices (labelled A-C) are included in this thesis. Appendix A includes all geochemical data collected and sample information for Chapter 4. Appendix B includes all data collected and sample information for Chapter 5. Appendix C gives an overview of the design and construction of the leaching column apparatus used in Chapter 5.

1.3 The Study Area

Phosphorite sediments have been observed in a handful of localities both onshore and on the continental shelf of New Zealand (Figure 1-1). Onshore deposits have been found at Stoneyhurst, and Oamaru, on the South Island of New Zealand (Walsh, 2009), and on the Chatham Islands (Wood et al., 1989). Offshore deposits have been observed on Chatham Rise at ~ 400 mbsl (metres below sea level) (Cullen, 1980; Cullen, 1987), and on Campbell Plateau in Snares Depression and, Pukaki Saddle (Summerhayes, 1967).

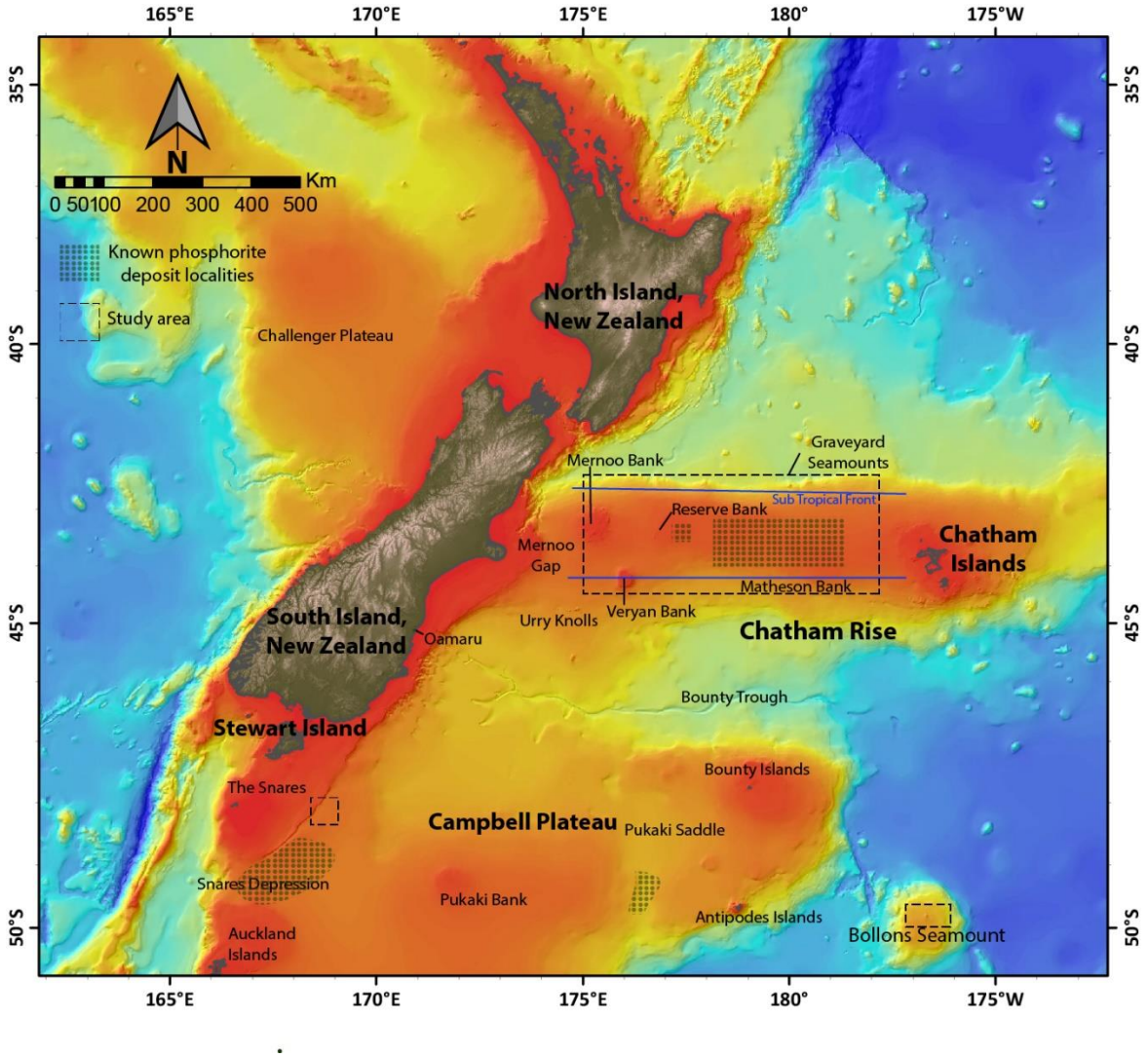

Figure 1-1: Map of the study area, areas of known phosphorite deposits (Cullen, 1987; Summerhayes, 1967), and topographical features. Approximate location of the Sub Tropical Front from Nodder et al. (2003) Base map compiled by Dr. Richard Wysoczanski, NIWA.

Samples investigated in this study are from various locations on Chatham Rise, Bollons Seamount, and Campbell Plateau, and were collected from research cruises conducted from the 1950's to the 1980's, and in 2007. Two additional box core samples and seawater samples were collected for this study during April 2015 on the TAN1503 voyage of the *R.V. Tangaroa*. The majority of samples used in this study come from Chatham Rise, as this area has highly concentrated deposits and have thus been sampled more thoroughly.

1.4 Global Rock Phosphate

Due to its important role as an agricultural fertilizer, rock phosphate plays a key role in the global economy with over 90% of phosphate mined being used for fertilizer production (Hughes, 2015). However, there are concerns about the longevity of phosphate reserves. Global reserves may only last up to 300-400 years into the future, based on the prediction that global demand for phosphate will increase by 1% p.a. between 2010 and 2050, then stabilize until 2100 at 100 Mt per year (Cooper et al., 2011). Other estimates of phosphate reserve longevity range from as little as 30 % to as much as 90 % of reserves left by the end of the century (Van Vuuren et al., 2010). A peak in phosphate production coeval with a decrease in ore quality as deposits run out could cause a supply deficit in rock phosphate (Cordell et al., 2009), which could be up to 200 Mt per year by 2075 (Cooper et al., 2011).

One of the more concerning aspects of global rock phosphate production is the global distribution of deposits. Morocco currently holds 15% of global phosphate rock production, by 2100 it is predicted to be as high as 80% which has the potential to create a very volatile geopolitical situation between major nations that rely on rock phosphate imports to support their economies (Cooper et al., 2011). Despite debate and uncertainty over details, there is consensus that phosphate rock is a finite resource that will only increase in demand, leading to depletion in the future (Cooper et al., 2011; Cordell et al., 2009; Vaccari & Strigul, 2011; Van Vuuren et al., 2010).

1.5 New Zealand Phosphates and the Economy

New Zealand soils have low quantities of minerals that contain plant available phosphorous, resulting in depletion in pasture soils (Burns, 1952). This was realised realitvely early on during the first development of farmland in New Zealand with the first phosphate fertilizer imported in 1867, and the first superphosphate in 1880 (Burns, 1952). Since 2010, more than 50% of New Zealand's phosphate rock has been imported from Morocco, with other main suppliers being Vietnam, South Africa, and Nauru (Figure 1-2).

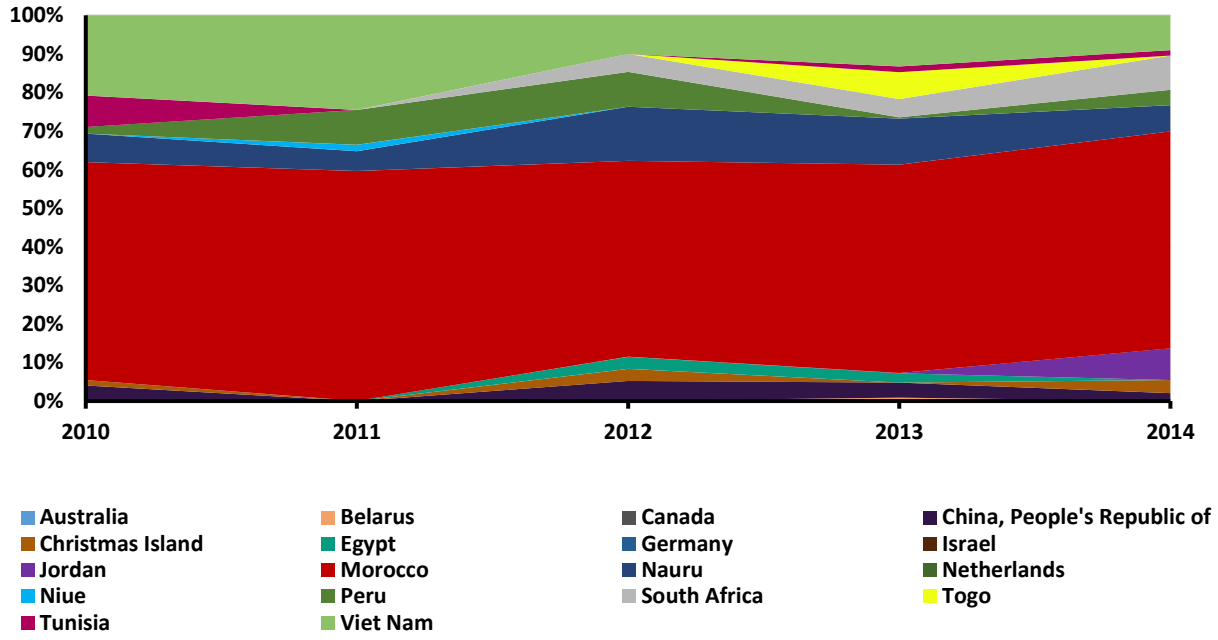

Figure 1-2: Percentage of Natural Rock Phosphates Imported into New Zealand by Country of Origin: 2010-2014. Data from Statistics New Zealand (2014).

Agriculture is one of New Zealand's largest industries with a direct contribution of 4.5% to the GDP (Gross Domestic Product) (The Treasury, 2014), thus phosphate rock import is directly affected by the state of both the world and local economy. A drought in 2007/2008 severely impacted the dairy industry, as a result, rock phosphate imports dropped significantly in 2008/2009 (Figure 1-3) (The Treasury, 2010). Low import of rock phosphate also coincides with recessions, most notably those of 1988, 1991, and 2008, with 2008 being comparatively the most severe (The Treasury, 2013).

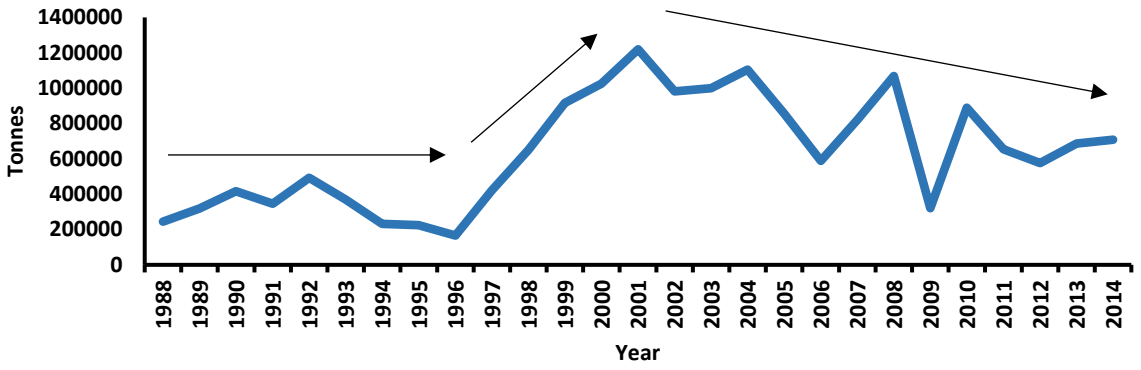

Figure 1-3: Yearly Import of Natural Rock Phosphate into New Zealand: 1988-2014. Data from Statistics New Zealand (2014).

One of the main issues with heavy application of fertilizers is the trace metals incorporated in the phosphate rock are also applied to the soils. Cadmium accumulation in New Zealand soils is a concern, as Cd is a biotoxic element and makes its way into the food chain via plant ingestion by livestock (McDowell et al., 2013). Historically, one of the main sources of phosphate rock imported into New Zealand was from Nauru, which is notable for its high Cd content (McDowell et al., 2013).

After the realisation that the fertilizers being applied in 1997/1998 were rich in biotoxic metals such as Cd, effort has been made to reduce the amount of fertilizer applied by switching from single to triple phosphate, and using lower Cd sources (Fertiliser Matters., 2005; Schipper et al., 2011). This has coincided with an overall decrease in rock phosphate imports since 2001 (Figure 1-3).

Commercial quantities of phosphorite nodules were identified on the Chatham Rise in the 1970's, following the realization that Nauru and other ocean island phosphate sources were in decline (Kudrass & von Rada, 1984; Mackay et al., 1980). The most recent phosphorite resource estimate is 23.4 Mt along Chatham Rise (RSC Consulting Ltd, 2014), enough to maintain New Zealand's rock phosphate demand for the next 20 years (Chatham Rock Phosphate Limited, 2014). This would allow New Zealand to be independent from other countries, as currently there is heavy reliance on Morocco for rock phosphate imports (Figure 1-2).

1.6 Mining of Chatham Rise Phosphorite Deposits

Exploiting natural resources can result in financial benefits for the local economy. It has been estimated that mining of the Chatham Rise phosphorites could contribute up to $280 million NZD to New Zealand's GDP per year with the follow on effect of contributing up to $120 million dollars towards New Zealand's local economy (Golder Associates (NZ) Limited, 2014a). Conversely, the EPA contested that the financial gain proposed by Chatham Rock Phosphate Ltd (CRP) would not have s higher impact on the economy as claimed (Environmental Protection Agency, 2015).

CRP currently holds prospect and mining permits for the Chatham Rise phosphorite deposits. In 2014 their application for Marine consent to begin mining was declined by the Environmental Protection Agency (EPA) (Environmental Protection Agency, 2015). CRP have since appealed and intend to reapply for marine consent (Chatham Rock Phosphate Limited, 2016a).

CRP were set to be the first company in the world to begin a mining operation at deep ocean depths (300-400m); however, a Namibian company has since been given clearance to mine seafloor phosphorite deposits off the Namibian coast (Chatham Rock Phosphate Limited, 2016b). Namibian Marine Phosphate (Pty) Ltd (NMP) intend to initially begin dredging at 225 m water depth (Namibian Marine Phosphate (Pty) Ltd, 2011).

Chapter 2. Phosphorite Formation: A Review

2.1 Introduction

The process for phosphorite formation is inherently complicated, with many mechanisms and factors involved, giving way to an equally complicated nodule chemistry. This chapter provides an overview of the mechanisms for phosphorite formation relevant to New Zealand marine phosphorites.

2.2 Marine Phosphorus Cycle

2.2.1 Sources

For phosphogenesis to occur, there must firstly be a source of phosphorus available in the marine environment. There are multiple pathways that phosphorus (P) can take to enter into the oceans. The most significant flux is from river transport (Benitez-Nelson, 2000; Froelich et al., 1982), followed by atmospheric/aeolian dust, and seafloor volcanism (Benitez-Nelson, 2000).

In the terrestrial environment phosphorus can be bound to clays, soils and organic matter as oxides of aluminium and iron, as well as particulates from weathered crustal rocks, and P dissolved directly into water runoff, eventually reaching the ocean through river transportation (Benitez-Nelson, 2000; Bennett & Schipanski, 2013; Filippelli, 2011). The total pre-anthropogenic river associated fluxes into the ocean are estimated to be ~ 10×10^{-9} mol P / cm^2 of the ocean surface y^{-1} (Froelich et al., 1982).

Approximately 140×10^{10}g y^{-1} of atmospheric phosphorus is deposited directly into the oceans, based on sources of P bound to sediment particles, industrial sources (e.g. from the fertilizer industry and combustion sources), and as dust carried by wind from continents, specifically the Sahara Desert (Graham & Duce, 1979).

Estimates of volcanic P flux into the oceans are difficult to directly measure, and thus have been derived from laboratory experiments using both artificial basalt/phosphate powder mixtures, and condensates from fumaroles (Yamagata et al., 1991). Yamagata et al., (1991) discovered that water soluble phosphate could be formed from condensing high temperature (1340°C) volcanic gasses. However, the total hydrothermal flux of P into the oceans is an

apparently minor contribution centred at the site of the associated hydrothermal activity (Benitez-Nelson, 2000).

2.2.2 Sinks

For P to be available for phosphogenesis, it needs to be incorporated into a sink which delivers P to marine sediments (Benitez-Nelson, 2000). There are multiple sinks in the marine environment, of which the most important is the burial of organic matter (Benitez-Nelson, 2000), with an estimated flux of 32 x 10^{10} mol P yr^{-1} (Delaney, 1998). The second most important recognised sink of P in the marine environment is P complexed with iron oxyhydroxide phases in the water column (Delaney, 1998). It has been proposed that P scavenging by oxidised Fe derived from local hydrothermal fluids is also an effective sink of P into marine sediments with an estimated flux of $1.43x10^{10}$ mol P yr^{-1} (Wheat et al., 1996).

2.3 Phosphogenesis

2.3.1 Types of phosphate deposits

Marine phosphorite formation occurs primarily in seafloor sediment pore water rather than by direct precipitation from seawater (Froelich et al., 1988; Jarvis et al., 1994). There are three main classifications of phosphorite deposits characterised by their mechanisms of formation (Walsh, 2009 and references therein).

1. Diagenetic replacement nodules, hardgrounds, and crusts which form on continental slopes, shelves, banks, and seamounts whereby an existing carbonate precursor undergoes dissolution and is replaced by apatite.
2. Bedded deposits of pelloids, siltstone, and wackestone.
3. Insular or guano type phosphate deposits formed from bird droppings.

New Zealand marine phosphorite deposits are characterised by type 1 diagenetic replacement deposits, and their mechanisms of formation are explored in the following sections.

2.3.2 Mechanisms of phosphorite formation

Phosphogenesis typically occurs in marine continental shelf environments that are characterised by nutrient rich deep water upwelling, high primary biological production causing high organic material deposition, and very low detrital sediment input e.g. modern Peru shelf (Filippelli, 2011; Froelich et al., 1988).

The formation of pelletal (Type 2) phosphorites follows a two-step process, as determined by Froelich et al. (1988) through direct pore water measurements of modern apatite producing sediments on the Peru Shelf:

1. The concentration of P reaches a critical threshold, and the precipitation of a metastable calcium phosphate precursor (struvite [$NH_4MgPO_4.6H_2O$]) occurs in the upper few cm of the sediment.
2. F^- and CO_3^{2-} present in the sediment pore water is taken up by the precursor phase, leading to the formation of CFA (carbonate–fluorapatite) or francolite [$Ca_{10-a-b}Na_aMg_b(PO_4)_{6-x}(CO_3)_{x-y-z}(CO_3.F)_y(SO_4)_zF_2$].

In diagenetic replacement (Type 1) phosphorites, the precursor does not precipitate from the sediment pore water, but rather is a pre-existing mineral phase e.g. carbonate rock (Starinsky et al., 1982). The exact mechanisms are still not fully understood, but it is thought that an existing carbonate matrix, or calcite, is first partially dissolved, possibly with some bacterial influence, and then reprecipitated as francolite (Lamboy, 1993).

2.3.3 Mechanisms of Concentrating Phosphorus in Interstitial Pore Water

Both authigenic and diagenetic phosphorite nodules require supersaturation of phosphate PO_4^{3-} in sediment pore water to form CFA. In order to facilitate the formation of apatite, there has to first be a sufficiently high source of P in the sediment pore water. In areas with high productivity the main sources of dissolved P are sourced from deposited organic particulate matter and fish bones (Froelich et al., 1988; Schenau et al., 2000).

However, these simple processes are sometimes not enough to explain the high saturation of P required, or the occurrence of accessory minerals such as glauconite. Froelich et al., (1988) proposed an iron redox model, based on the “phosphate pump” model by Shaffer (1986) as

another mechanism behind P supply and saturation in sediments on the Peru Margin (Figure 2-1). FeOOH when freshly precipitated and released into the water column can scavenge high quantities of P from seawater and decomposing organic matter to form $FeOOH.PO_4^-$ (Froelich et al., 1988; Shaffer, 1986). When it is sufficiently buried below the sediment-water interface to reach the suboxic zone Fe^{3+} is reduced to Fe^{2+} and PO_4^{3-} is released (Froelich et al., 1979) (Figure 2-1).

Figure 2-1: Schematic representation of the iron pump mechanism. Modified after Froelich et al. (1988), and Jarvis et al. (1994).

The iron pump model also explains the association of glauconite type minerals with phosphorites, e.g. hardgrounds from the Cenomanian of Devon, southwest England (Carson & Crowley, 1993). Glauconite formation requires burial within the sub oxic zone, at the interface between the oxic and anoxic areas of the sediment profile, where Fe^{2+} and Fe^{3+} can occur simultaneously (Figure 2-1) (Froelich et al., 1988; Glenn & Arthur, 1988). To form glauconite, the sediment pore water must be a semi-closed system with minimal oxygen availability, otherwise, FeOOH species are likely to dominate (Carson & Crowley, 1993). Pyrite formation is also explained by deeper burial into the suboxic section of the sediment profile (Glenn & Arthur, 1988).

Whilst the iron pump model seems to explain the mechanism facilitating apatite precipitation, it has been suggested that SEM images of diagenetic apatite display evidence of microbial activity as the catalyst for apatite precipitation (Lamboy, 1993). Further studies have also found environments of phosphogenesis where the iron pump is not operating for example in the Arabian Sea Oxygen Minimum Zone (Schenau et al., 2000), where P is concentrated from solely the degradation of organic matter and dissolution of fish bone debris, and re-incorporation of material that had previously undergone phosphogenesis.

2.3.4 Deposit formation processes

The formation of marine phosphate deposits was once thought to be solely a global process at times of high P input from high P weathering and biological production due to variations in climate and tectonic regime (Filippelli, 2011). It is now understood that phosphorite formation consists of two processes that simply need to occur in the same place, at approximately the same time; phosphogenesis and strong current winnowing (Filippelli, 2011).

First, phosphogenesis needs to occur, with local environmental conditions as outlined above, coupled with the migration of currents interacting on the seafloor, to enable the deposition and build-up of organic matter without disturbance (Filippelli, 2011). This ensures that there is a source of P, and minimal amounts of terrestrial detritus to dilute P in the sediments to encourage the precipitation of apatite.

Once phosphogenesis has occurred, and there is a build-up of apatite and associated minerals in the suboxic section of the sediment profile, they need to be concentrated to form a deposit which involves winnowing by currents to remove light grains of surrounding sediment (Filippelli, 2011). This is the same process that has led to the formation of Chatham Rise phosphorite nodules (Kudrass & Von Rad, 1984a; Von Rad & Rosch, 1984).

2.4 Incorporation of trace metals

Other than the grade of the deposits (wt% P_2O_5), one of the most important aspects to consider when intending to mine phosphate rock as an economic resource is the degree of potentially toxic elements the deposit could contain. As such, an understanding of metal species that could be associated with, or incorporated into apatite phases is invaluable.

The apatite phase in phosphorites contains three main constituent ions; Ca^{2+}, PO_4^{3-}, and F^-. Ag^+, $Mg^{2+,}$ Sr^{2+}, Ba^{2+}, Cd^{2+}, Mn^{2+}, Zn^{2+}, REE^{3+} (Rare Earth Elements), Sc^{3+}, Y^{3+}, and U^{4+} are readily substitutable into the Ca^{2+} site. CrO_4^{2+}, AsO_4^{3-}, and VO_4^{3-} are able to substitute into the PO_4^{3-} site (Jarvis et al., 1994). However, trace elements can also be adsorbed onto the apatite crystal faces (Jarvis et al., 1994), scavenged or supplied by organic matter in the case of U (Starinsky et al., 1982), or contained in minerals associated with phosphorites such as Rb, Zr, Ni, Zn, and Y in glauconite (Cullen, 1980; Von Rad & Rosch, 1984). Two trace metals that appear to be commonly incorporated into phosphorite deposits have drawn particular attention: U and Cd.

Uranium is typically highly enriched in marine phosphorite deposits, but the degree of enrichment varies markedly between deposits from only 4 ppm (Ilyin pers.comm., 1993 cited by Jarvis et al., 1994) to over 600 ppm (This study) with an average of 120 ppm (Altschuler, 1980 cited by Jarvis et al., 1994). Phosphorites that have undergone a higher degree of diagenesis tend to have higher U concentrations, due to prolonged take up of dissolved U in interstitial pore water from more organic matter degradation (Starinsky et al., 1982).

Radioactivity resulting from the high enrichment of U in phosphorite nodules should be taken into consideration should be deposit be mined for application fertiliser. In the context of the Chatham Rise phosphorite deposit it has been concluded that the decay products of ^{238}U, which includes ^{210}Po, ^{226}Ra, and ^{210}Pb, could be as risk to local biota and more research is required (Environmental Protection Agency, 2015).

Cadmium is another element commonly associated with phosphorite deposits and has the unwanted side effect of concentrating in pastures because of phosphate fertilizer application (Section 1.5). The average Cd concentration in phosphorites in known phosphorite deposits is 20 ppm, 66 x higher than average shale (Jarvis et al., 1994). The exact reason for the strong enrichment of Cd in marine phosphorites is still unknown and heavily debated (Jarvis et al., 1994), but some suggest Cd simply substitutes directly into the apatite crystal lattice in the place of Ca^{2+} (Gnandi et al., 2009).

Chapter 3. Geological Setting and Palaeoceanography

3.1 Introduction

Global and regional events such as glacial cycles, tectonic uplift, and subsidence, have contributed to create optimal conditions required for phosphorite formation in certain marine environments in offshore New Zealand. This chapter reviews the geological and palaeoceanographic history, stratigraphy, and topographical features associated with phosphorite nodule deposits.

3.2 Topographical Features

Chatham Rise is approximately 150 km wide and extends west of South Island, New Zealand, for ~1000 km (Von Rad & Rosch, 1984). The major topographic features (Figure 1-1) of Chatham Rise include: Mernoo Bank, formed by local uplift (Herzer & Wood, 1988); Reserve Bank, and Matheson Bank; formed by a basement high; and Veryan Bank, which is composed of volcanics (Falconer et al., 1984).

The crest of Chatham Rise is separated from the continental shelf offshore of Banks Peninsula by Mernoo Gap, a narrow saddle ~ 570 m deep (Pasho, 1976). The northern slope of Chatham Rise is steeper than the south, with both slopes deepening to ~ 1000-3000 mbsl (Nodder et al., 2012).

Bollons Seamount is located to the east of Campbell Plateau, and south of the Chatham Islands (Figure 1-1). The seamount is ~1000 m below sea level. Pukaki Saddle is a depression that sits between the high points of Bounty Plateau, and Pukaki Rise on Campbell Plateau. Snares Depression is a low point situated between Snares High and the Auckland Islands.

3.3 Chatham Rise Surficial Stratigraphy and Nodule Distribution

The surficial stratigraphy includes only the first 50 cm of the sediment profile, and a typical profile from Chatham Rise is shown in Figure 3-1. A base layer of phosphorite nodules is overlain by 20 cm of "white ooze burrows" (Cullen, 1980). A second layer of phosphorite deposits occurs, which is then overlain by ~30 cm of glaucony bearing sandy mud.

Despite a "patchy surficial distribution", phosphorite layers on Chatham Rise can be continuous, but can be overlain by up to 0.7 m of foraminiferal ooze and glauconitic sandy muds (Cullen, 1980). Small (<0.5 mm) nodules can be observed from areas where there is

no apparent nodule coverage on the surface of the sediment, hypothesised to have been carried upwards by bioturbation, indicating the possibility of larger nodule deposits beneath (Cullen, 1980). It has also been hypothesised the scouring from ice burgs has influenced the distribution of the Chatham Rise phosphorite deposit (Cullen, 1987).

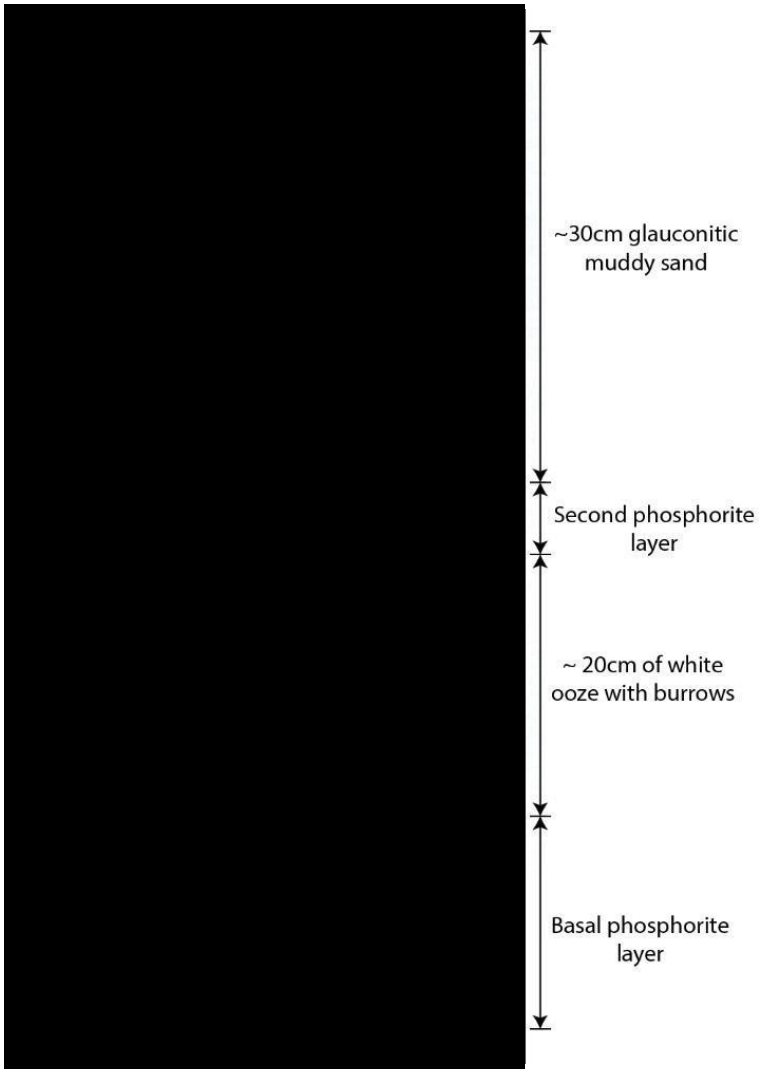

Figure 3-1: Piston core H638; the most complete piston core recovered from Chatham Rise. Scale is in meters. Modified after Cullen (1980).

3.4 Geological and Palaeoceanographic History

After the major Rangitata orogeny forming event throughout New Zealand, Chatham Rise and Chatham Island areas experienced intense fault related activity throughout the rest of the Cretaceous (Wood et al., 1989), where faulted schists and greywacke basement formed east-west trending grabens along Chatham Rise (Cullen, 1965; Falconer et al., 1984). There was widespread subsidence in Chatham Rise, Campbell Plateau, and Bounty Trough regions (Figure 1-1) due to thermal contraction of the crust (Wood et al., 1989).

At ca. 85 Ma major rifting began from the centre of Bounty Trough which resulted in the eventual separation of Bollons Seamount from Campbell Plateau (Davy, 2006). The Middle Cretaceous Chatham Rise was a terrestrial mountainous area of widespread alluvial, fluvial, deltaic, and lacustrine environments (Wood et al., 1989), whilst the Chatham Islands were populated with forests (Stilwell et al., 2006).

Sedimentation throughout the Cretaceous was influenced by active faulting, resulting in the deposition of mainly graben infill (Figure 3-2) (Falconer et al., 1984). By the Late Cretaceous, faulted basement highs that created mountain ranges had been eroded down to peneplains (Wood et al., 1989).

Shallow marine sedimentation dominated during the Paleogene for both Chatham Rise and Chatham Island areas (Figure 3-2) (Wood et al., 1989). This was a period of stability with little or no fault related activity for Chatham Rise indicated by the absence of Palaeocene sediment infill in fault bound basins (Figure 3-2) (Herzer & Wood, 1988).

Extensive faulting activity that defined the Cretaceous period for Chatham Rise and Chatham Island regions had restarted by the Eocene, resulting in further regional subsidence (Wood et al., 1989). This resulted in up to 400 metres of sediment accumulating in half grabens on western Chatham Rise (Figure 3-2) (Herzer & Wood, 1988; Wood et al., 1989).

By the Middle Eocene, a second major volcanic episode occurred on the Chatham Islands (Panter et al., 2006). The oldest known seafloor eruptions on Chatham Rise occurred in the Early Palaeocene (63±0.6 Ma) on central Chatham Rise, and in the Early Eocene (56 ± 0.5 Ma) south of the Chatham Islands (Timm et al., 2010). Volcanism on the Chatham Rise throughout Early Oligocene is characterised by multiple small eruptions (Timm et al., 2010). The widespread and long lived volcanism on and near Chatham Rise resulted in volcanic material being incorporated into sediments from the Palaeocene to the Middle Eocene (Figure 3-2) (Wood et al., 1989).

Subsidence in the Chatham Rise region continued into the Early Eocene, and by this stage Chatham Rise was in a deep water environment (Wood et al., 1989). This resulted in the deposition of deeper water facies such as chalks and chert, as well as some local erosion (Figure 3-2) (Wood et al., 1989).

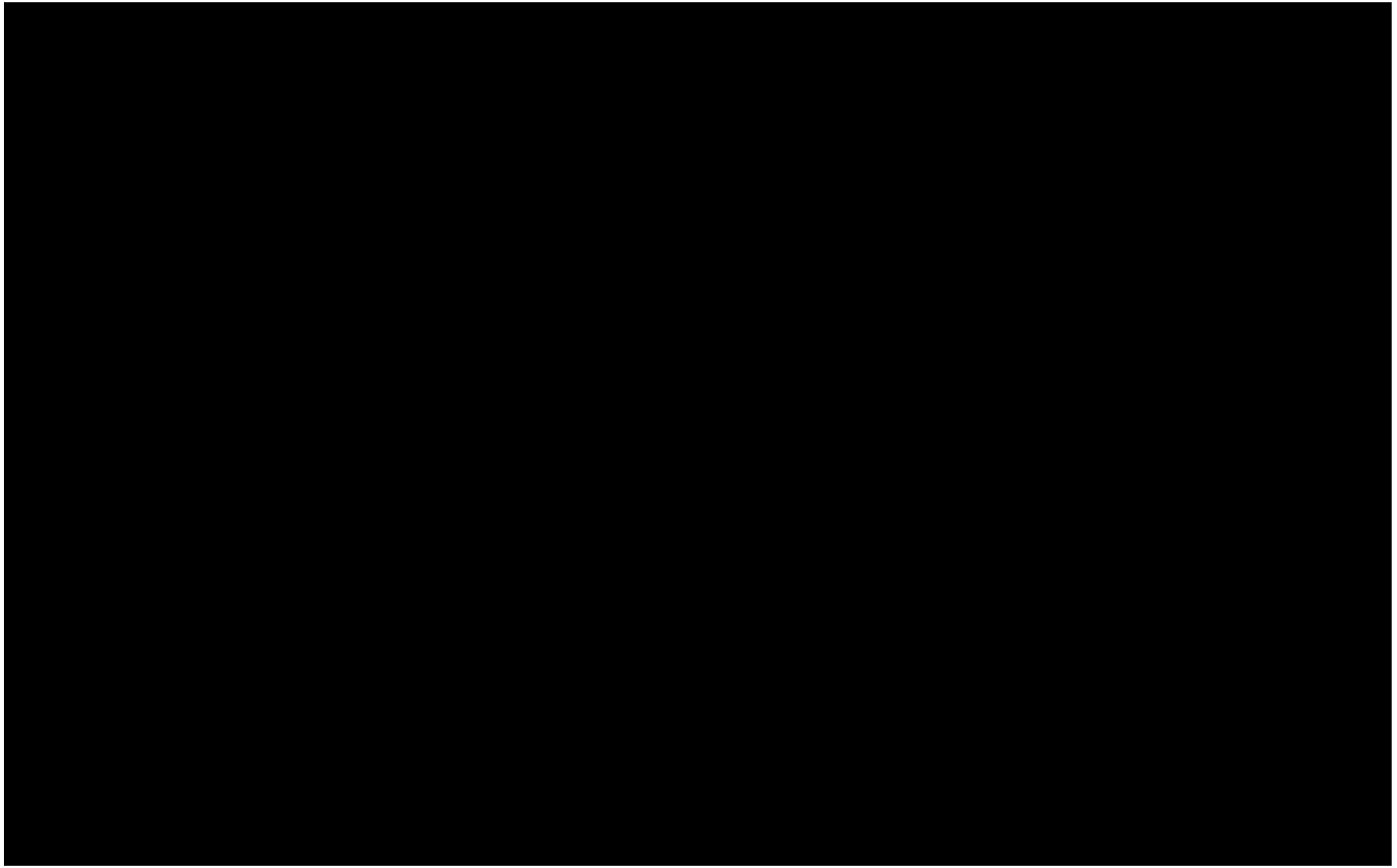

Figure 3-2: Chronostratigraphic panel of the Chatham Rise and Chatham Islands.
Modified after Lawless (2012). Chatham Rise stratigraphy interpreted from seismic unit descriptions by Falconer et al. (1984) and Wood et al. (1989). Chatham Islands stratigraphy from James et al. (2011). Geological timescale modified after Cooper and Agterberg (2004).

During the Oligocene global climatic conditions had dramatically changed. For the first time Antarctica had formed small ice sheets (Zachos et al., 2001). Coupled with the tectonic separation of Antarctica and Australia, the climatic changes had the follow-on effect of creating stronger proto-Antarctic Circumpolar current (ACC) (Nelson & Cooke, 2001) and the Deep Western Boundary Current, which flowed around the Chatham Rise topography causing widespread erosion and non-deposition around the entire region (Carter et al., 2004). The increased circulation of cooler water masses around New Zealand also caused surface ocean temperatures to drop as low as 2-6 °C (Nelson & Cooke, 2001). This increase in erosional currents led to a 2 - 4 Myr non-deposition hiatus also known as the Marshall Paraconformity (Carter, 1985; Fulthorpe et al., 1996).

The Marshall Paraconformity is widespread and is recorded offshore on the north Chatham Drift (Carter et al., 2004), and in Bounty Trough (Horn & Uenzelmann-Neben, 2015). Early Oligocene chalks on the Chatham Rise were eventually eroded by these strong currents, leading to the formation of the Oligocene – Miocene unconformity surface (Figure 3-2) (Wood et al., 1989).

New Zealand during the late Oligocene to Early Miocene was at a sea level high stand and terrigenous sedimentation was comparatively low (Carter et al., 2004). Phosphatised and glauconitised fragments of the remaining early Oligocene limestone, including thin (<300 m) glauconitic sands and silts, marls, and foraminiferal oozes (Figure 3-2) were deposited on the Oligocene-Miocene erosional unconformity surface of Chatham Rise (Figure 3-2) (Wood et al., 1989). Conversely, the Chatham Islands experienced periods of erosion and non-deposition throughout the Middle to Late Oligocene (Wood et al., 1989).

The Early Miocene saw warmer climatic conditions (Nelson & Cooke, 2001). During the Middle Miocene, surface ocean primary biological productivity was increasing (Weedon & Hall, 2004), coeval with the northward migration of the Sub Tropical Front to its present location over Chatham Rise (Nelson & Cooke, 2001) (Figure 1-1). The presence of the Sub Tropical Front over the Chatham Rise combined with the increase in biological activity would have provided substantial organic matter, aiding in enabling phosphogenesis processes to occur in the surficial sediments.

From the Middle to Late Miocene, climatic conditions around New Zealand cooled dramatically affected by global changes in the climate (Nelson & Cooke, 2001). A new permanent ice sheet was established on East Antarctica (Zachos et al., 2001) resulting in a more extensive and stronger ACC (Nelson & Cooke, 2001) and erosive Deep Western Boundary Current flows (Carter et al., 2004). These erosive flows, further enhanced by the additional establishment of the West Antarctic ice sheet (Carter et al., 2004) likely caused extensive winnowing which helped to concentrate the phosphorite nodule deposits (Figure 3-2) (Falconer et al., 1984).

In the Late Miocene terrigenous sedimentation in the Canterbury Region increased dramatically due to the active Alpine Fault (Barnes & Shane, 1992; Wood et al., 1989), resulting in the deposition of clastic, fault related sediments towards the west of Chatham Rise region (Figure 3-2) (Wood et al., 1989). Basalts also erupted on the seafloor until the Latest Pliocene along the crest of the Chatham Rise, forming the Urry Knolls Seamounts (Herzer et al., 1989). The last major volcanic episode on the Chatham Islands followed, occurring in the Early Pliocene (Panter et al., 2006).

At the climax of the Pleistocene Glacial Period, with sea levels at their lowest, ice bergs were large enough to scour the seafloor of Chatham Rise (Kudrass & Von Rad, 1984b). From the Pliocene-Pleistocene until present, the character of sedimentation on Chatham Rise has changed dramatically with a notable decrease in carbonate deposition (Figure 3-2) (Wood et al., 1989).

3.5 Age of New Zealand Seafloor Phosphorite Nodules

Knowing the age of phosphorite nodules can give insights into the processes operating at the time of formation, hence an understanding of the formation conditions required for phosphogensis. Age determination has been attempted for Chatham Rise, Bounty Plateau, and Campbell Plateau nodules using foraminifera, nannofossils, strontium isotopes, and potassium argon radiometric dating.

Foraminifera in the sediments associated with Chatham Rise phosphorite nodules, based on key species *Sphaeroidinellopsis seminulina,* indicates a mixed age of approximately half Early Miocene, and half Middle Miocene, with a few ages as young as the Late Miocene

(Zobel, 1984). Conversely, Burns (1984) documented the presence of the nannofossil *Reticulofenestra bisecta*, in phosphorite material, indicating a Middle to Late Oligocene age. Lower Oligocene (Lower Wh) foraminiferal species, of *Chiloguembelina* and *Globigernia* cf. *angiporoides*, have also been found in phosphorite nodule material (Cullen, 1980).

Both the foraminifera and nannofossil specimens were not preserved well, making age determination difficult (Burns, 1984; Zobel, 1984). Zobel (1984) suggested that the Oligocene aged nannofossils and foraminifera in chalks and limestones were re-worked, and that the phosphorite nodules are more likely to be of Early to Late Miocene age. This would be consistent with the Late Miocene and younger phosphatised cetacean bones found amongst the phosphorite nodules (Fordyce, 1984).

Strontium isotopes were used to obtain phosphorite formation age constraints on the basis that the francolite phase in the phosphorite nodules is a replacement mineral and that the francolite would not therefore, inherit strontium from the pre-cursor carbonate material. Strontium ($^{86}Sr/^{87}Sr$) isotopes used to date the replacement francolite in the Chatham Rise phosphorite nodules, produced ages of ca. 4.9 Ma (McArthur et al., 1990). More recently it has been shown that francolite Sr ratios continuously re-equilibrate with the sediment pore water (Rao et al., 2008). Since the sediment profile during phosphogenesis is not a totally closed system the Sr ratios are not a reliable method for age determination.

A few studies have determined Ar –Ar and K- Ar dates for glauconite associated with the phosphorite nodules. As glauconite coating the phosphorite nodules is a replacement mineral (Lawless, 2012), its age can give an approximation of the age by which phosphogenesis was complete. The phosphorite nodules contain two distinct types of glauconite minerals: mature pelletal and immature glauconite, which are incorporated in the internal phosphorite material, and rims respectively (Kreuzer, 1984)**.** Kreuzer (1984) obtained an age range of 10 - 25 Ma on the central phosphorite material. The outer rim glauconite layer returned an age cluster of 6.7 - 8.4 Ma (Late Miocene), with the full range from 4 - 11 Ma.

Argon-argon dating of mature, dark black pelletal glauconite contained in surficial sediments of Chatham Rise produced an average age of 5.75 Ma (Late Miocene) (Lawless, 2012). Although Lawless (2012) suggests the true ages could be older, due to argon inheritance effects after crystal lattice closure, the age obtained is consistent with previous ages. It was

concluded by Lawless (2012) that most importantly the combination of lowered sea level, and deep ocean current upwelling from an established Sub Tropical Front over Chatham Rise lead to the conditions required for glauconite formation in the Miocene.

In summary, it has been determined that the precursor material of the Chatham Rise phosphorite nodules is Oligocene – Miocene in age based on foraminiferal and nannofossil ages (Burns, 1984; Kudrass & von Rad, 1984a; Zobel, 1984). Phosphogenesis was active from the lower Late Miocene to the Late Miocene (Kudrass & von Rad, 1984a). The cessation of active phosphogenesis is marked by the formation of a glaucony rim on the nodules in the Late Miocene (Kreuzer, 1984; Kudrass & von Rad, 1984a), coeval with glauconite formation in the surficial sediments of Chatham Rise (Lawless, 2012).

Phosphorite nodules from Campbell Plateau have not been as thoroughly studied. However, Summerhayes (1967) obtained an Upper Miocene-Pleistocene foraminiferal age for Pukaki Saddle nodules, and an Eocene to Lower Miocene age for nodules from Snares Depression. Phosphorite nodules from Bounty Plateau are manganese encrusted, with the phosphorite nodules acting as nuclei for the 0.5 cm crusts (Summerhayes, 1967). Considering a 1 mm per 100 kyr accumulation rate for manganese crusts, Summerhayes (1967) estimated the manganese crust on nodules to be at least 500 ka old. These nodules have been interpreted to have undergone phosphogenesis at the same time as Chatham Rise phosphorite nodules, but that at ca. 500 ka a change in environmental conditions likely to be associated with seafloor volcanic activity favoured the formation of Mn crusts over continued phosphogenesis (Summerhayes, 1967).

Chapter 4. Geochemistry

4.1 Introduction

This chapter aims to characterize the chemistry of New Zealand marine phosphorites. Bulk analyses of major and trace elements were collected using inductively coupled mass spectrometry (ICPMS) and X-ray fluorescence (XRF). The key investigations in this chapter focus on the rare earth element (REE), trace, and major element geochemistry. The analyses investigate chemistry relative to nodule type, contents of potentially ecotoxic trace elements, spatial patterns and insights into the diagenetic processes of some New Zealand offshore phosphorites.

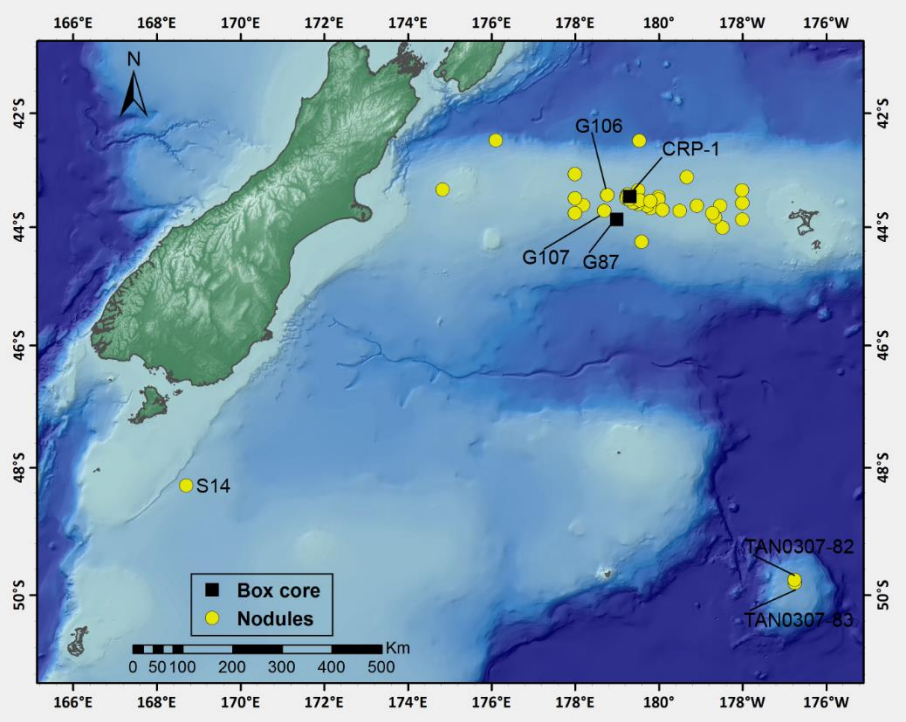

Figure 4-1: Locations of samples analysed in this study. Map courtesy of NIWA

.

Samples used for geochemical characterisation were chosen to represent as many sites as possible to give a robust indication of spatial differences in bulk chemistry. Nodules from 47 sites were sampled, in addition to two box core samples and seawater samples collected on the *R.V. Tangaroa* voyage TAN1503 (Figure 4-1).

4.2 Mineralogy

4.2.1 Phosphorite Nodules

The Chatham Rise phosphorite nodules vary greatly in size, ranging from 1-2 mm to larger than 150 mm, with the most common size range of 20-40 mm (Cullen, 1980). A defining feature of the Chatham Rise phosphorites is their heavily bored and burrowed surfaces, resulting in irregular sub rounded to sub angular shaped nodules, which are assumed to have been formed before the nodules became highly indurated (Cullen, 1980). Chert nodules up to 800 mm in diameter have also been recovered from ooze sediments on the Central Rise between 179°05'E, 43°25'S and 179°10' E, 43°30' S (Kudrass & Cullen, 1982).

Typical Chatham Rise phosphorite nodules consist of five zonal layers (Figure 4-2); a glaucony outer rim, a crystalized apatite zone (collophane), a goethite zone, an outer phosphatized chalk zone and a weakly phosphatized chalk core. Pyrite spherules can be found in the glaucony and crystalized apatite zones (Cullen, 1980; Von Rad & Rosch, 1984).

The rim is typically a smooth, "vitreous" black coating of variable thickness (~1-2 mm) (Cullen, 1980; Von Rad & Rosch, 1984). The rim glaucony is a pigment type and in many nodules can be seen to grade inwards into a khaki green colour in the crystallised apatite zone (Lawless, 2012).

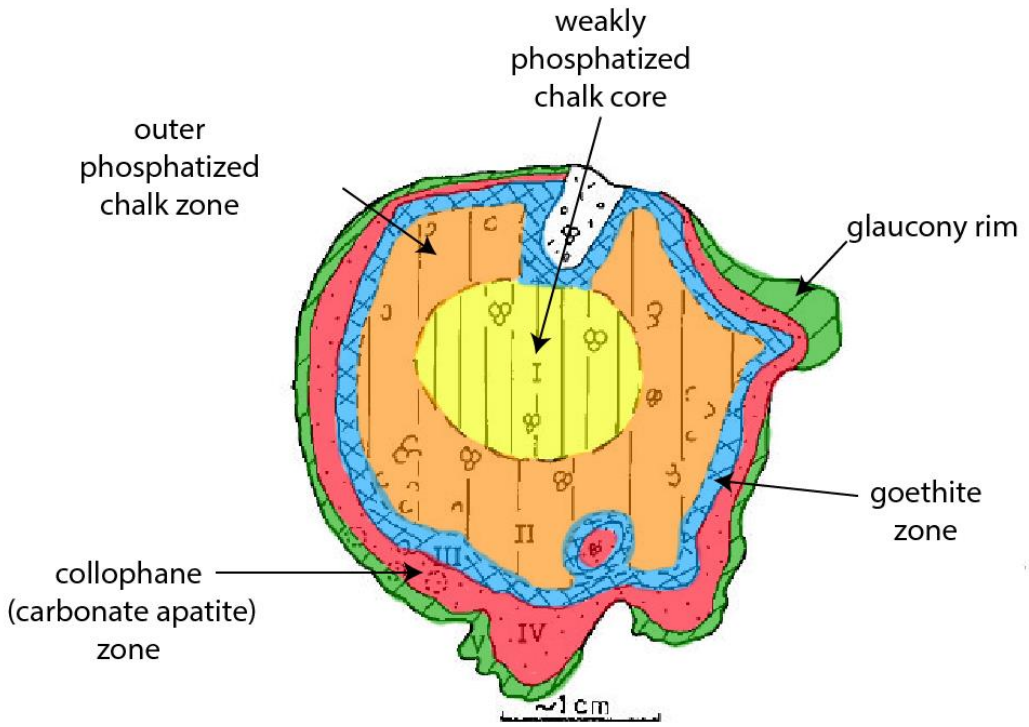

Figure 4-2: Schematic cross section of a typical Chatham Rise phosphorite nodule.
Modified after Von Rad and Rosch (1984). V= glaucony rim, IV= collophane/ apatite zone, III= goethite zone, II= outer phosphatized chalk zone, I weakly phosphatized chalk core

The black rim coatings that characterize Chatham Rise nodules have previously been described as glauconite (Cullen, 1980; Kudrass & Cullen, 1982; Pasho, 1976; Von Rad & Rosch, 1984); however, the minerals analysed have too low a content of MgO (< 2.2%), Al_2O_3 (<6 %), K_2O (<3.5 %) and FeO (<5 %) (Walsh, 2009). More recent X-ray diffraction analyses show the nodule rims consist of nefedovite ($Na_5Ca_4(PO_4)F$) + an unnamed mineral ($Ca_2(Mn,Fe)_7(PO_4)_6(OH,H_2O)_4$), with minor amounts of wicksite ($NaCa_2Fe_5Mg(PO_4)_6.2H_2O$) (Walsh, 2009). Hence, the rim minerals will be referred to as glaucony rim minerals throughout this thesis. Walsh (2009) defines this rim type as "type 1". The Chatham Rise nodules also contain mature, dark green pelletal glauconite throughout the interior zones of the nodule (Kreuzer, 1984).

The interior of the nodules is comprised of a "yellowish-grey" to "yellowish-brown" phosphatized chalk (Cullen, 1980; Von Rad & Rosch, 1984). Infilling, bioturbation structures are a common feature of Chatham Rise phosphorite nodules. Dark orange-brown lenses contain iron oxyhydroxides (goethite) (Von Rad & Rosch, 1984). Foraminifera tests replaced by glauconite, or by iron oxides such as goethite or limonite are abundant throughout the interior of the nodules (Von Rad & Rosch, 1984).

4.2.2 Bone texture and duricrust nodules

In this study, bone texture type nodules are nodules whose precursor was cetacean bone, rather than carbonate or chalk. Bone textured nodules were recognised by Von Rad and Rosch (1984), and confirmed as whale bone by Fordyce (1984) most likely of Miocene age. The bone texture nodules are coated in the same black, vitreous glaucony rim minerals as typical nodules. They maintain the bone shape, and the porous bone texture can still be observed in the interior of the nodule. The pores are infilled with a tan mineral. Bone texture nodules only make up ~1 % of the Chatham Rise phosphorite nodules (Von Rad & Rosch, 1984).

Figure 4-3:Examples of bone textured nodules from Chatham Rise.
Left: Bone texture nodule from site G112. Right: Bone texture nodule from site I613.

Duricrust type clasts in this study refers to phosphatized carbonate that did not have a pebble shaped precursor. The term "duricrust" was used to describe Chatham Rise hardgrounds by Cullen (1987). The vitreous black glaucony rim minerals only occur on the top side of these samples (Figure 4-4).

Figure 4-4:Duricrust sample type E79-4-Lge.
Left: Top of sample showing vitreous black glaucony mineral. Right: Underside of sample.

4.2.3 Sediments

The nodules lie upon a matrix of bottom sediments comprised of poorly sorted, gravelly, muddy-fine sands (Von Rad & Rosch, 1984). The sediment typically comprises of 20-40% silt, 30-60% very fine sand, abundant foraminifera tests and sand sized glauconitic grains (Cullen & Singleton, 1977; Von Rad & Rosch, 1984). Detrital feldspar and volcanic glasses also make up a minor component of Chatham Rise seafloor sediments, as well as pebble and cobble sized glacial erratics (Kudrass & Cullen, 1982).

4.3 Analytical Methods

4.3.1 Sample Preparation

Samples used for the bulk geochemical characterization were selected from previously collected material from cruises spanning from the 1960's to 2003. The samples were stored in dry, ambient temperature conditions. Nodules were selected based on rough size fractions, as well as how many were left from each site. Care was taken to collect representative size fractions of nodules from each site; however, some sample sites were reduced to one nodule size fraction as they had previously been processed. The distribution and number of sample sites was also limited to the samples available in storage.

Nodules were gently rinsed with distilled water to remove any sediment cover, and allowed to air dry. Samples were then crushed using a sledge hammer. Samples were placed between thick sheets of paper, and fragments contained within plastic snap lock bags to prevent any metal contamination from the hammer. Any sample that appeared to have contacted the hammer was discarded.

A few of the more indurated and larger nodules were crushed using a hydraulic press. These samples were covered in paper and crushed between the tungsten carbide plates, with any material that had contacted the plates discarded. All samples were rinsed with distilled water and dried at 50 ° C.

The sample sizes were small, 10-15 grams in most cases, therefore powdering of the samples had to be done manually using a ceramic mortar and pestle. Blanks of the aluminium silicate mortar pestle were taken by grinding silica sand to assess any potential contamination (Appendix A-7.). As powdering samples by hand cannot produce the same level of homogeneity that milling can, in every run of trace element analyses one sample was duplicated to assess the homogeneity of the powders. Prior to analysis all samples were dried at 110 °C overnight

4.3.2 Bulk major element analysis

All samples were fused into glass disks, that were then analysed on a Panalytical Mini-Pal 4 XRF Spectrometer at NIWA. Calibration curves for the analytical procedures were established using up to five phosphate standards for analysis of nodules, and eleven sediment and rock standards for sediment analysis.

The glass disks were made by weighing 1g of sample and 10g of lithium meta/tetra-borate powder into a platinum crucible. An ammonium iodide tablet was added to the mix to act as a fusion release agent. The powder mixture was stirred prior to heating with a Polytetrafluoroethylene (PTFE) rod. The mixture was then heated to 1100 °C in a Modutemp fusion oven for 20 minutes, with swirling of the crucible midway to prevent bubbles forming. The molten material was then poured into pre-heated platinum moulds to set at room temperature. Half of the disks were made at NIWA, and the other half by Spectrochem Analytical, CRL Energy Ltd, Seaview, Lower Hutt, using the same sample to flux ratio.

XRF Standards and sample analysis

The standards used for XRF calibrations should ideally be of similar matrix to the samples measured. As such, two calibration curves were used for sample analysis: one for phosphate samples and one for marine sediments. Four international phosphate standards were used to derive the calibration curve for phosphate nodule analysis. As Chatham Rise sediments are a mixture of continent derived sediment, calcareous material and micro- phosphate nodules the calibration curve for sediment analysis was a mixture of eight sediment, dolomite and phosphate standards.

Due to a lack of suitable certified reference material for phosphate nodule analysis, measurements for MnO and Na_2O were beyond the limits of the calibration curves i.e. nodule compositions were outside of the ranges of standard values for these elements. The calibration curves for Al_2O_3, K_2O and P_2O_5 were not well defined, again due to a sparsity of suitable standard material, so analyses of these elements by Inductively Coupled Plasma Mass Spectrometry (ICPMS) were preferred over XRF analyses. CaO wt% measured by XRF was as an internal correction for ICPMS analysis for sample loss during sample transfer.

Loss on ignition (LOI) was taken as the difference between 100% and the sum of elements measured. As LOI was generally high (Appendix A-6), all XRF data was normalised to an anhydrous basis for use in plots, but both original totals and anhydrous values are given in Appendix A-2.

National Institute of Standards and Technology (NIST) standards 120c (Florida Phosphate), and 694 (Phosphate Rock, Western), which were used as two of the standards for the phosphate calibration, were measured together with samples as secondary standards to assess the accuracy of the calibration curve. Standard reference materials from the Unites States Geological Survey (USGS) SCO-1 (Cody Shale) and SDC-1 (Mica Schist) were used as secondary standards for sediment sample analysis. A comparison of results for these standards measured by XRF compared to their certified reference values is given in Appendix A-3.

4.3.3 Bulk trace element analysis

Bulk trace element contents were determined on dissolved samples using ICP-MS, on the ThermoScientific Element 2 sector field ICP-MS at Victoria University of Wellington. The USGS standard reference material (SRM) BHVO-2 was used as the primary calibration standard, and NIST120c, a standard reference phosphate rock, was used as the secondary standard. For each analytical sequence, standards were run first, followed by five samples. The standards were then repeated followed by five more samples. The standards were then run again to bracket the sequence. Backgrounds were measured every four analyses. The background counts per second (CPS) were subtracted from sample CPS. Element concentrations in the samples were calculated using the standard-sample bracketing method using the following equation:

Equation 1. $Concentration_{sample} = (CPS_{sample} / CPS_{BHVO\text{-}2}) \times (Dil_{sample} / Dil_{BHVO\text{-}2}) \times reference\ value,$

Where CPS_{sample} and $CPS_{BHVO\text{-}2}$ are the background subtracted counts per second for the sample and BHVO-2, respectively, Dil_{sample} and $Dil_{BHVO\text{-}2}$ are the dilution factors for the sample and BHVO-2, respectively. Reference values used for BHVO-2 are from Jochum et al. (2005). XRF Ca content was used as an internal correction to correct for sample loss resulting from the wetting behaviour of the samples in 1M and 3M HNO_3 solutions.

The element concentrations were corrected using Equation 2:

Equation 2. Corrected Concentration$_{sample}$ = Equation 1. x (Ca $_{XRF}$ / Ca $_{ICPMS}$)

A 1 ppb multi element solution was used for tuning the ICPMS instrument prior to analysis, and to monitor oxide and double-charged ion generation by measuring BaO/Ba^{+} (0.1 - 0.3%), Ba^{++}/Ba^{+}(4 - 4.9%), and UO^{+}/U^{+}(5.1 - 6.6%). Most of the elements were measured in low resolution. Ca, Mg, Al, P, Sc, Ti, V, Cr, Mn, Co, Ni, Cu, Zn, and Ga were measured in medium resolution. Analyses for Sb, Sn, Zr, and Tl were discarded for all samples due to high RSD% and reproducibility issues. Arsenic was also measured; however, there is currently no BHVO-2 reference value for As, and the compiled value for NIST120c was not reliable, therefore As contents are not reported in this study.

ICP-MS Standards

Ideally, standards for calibration are closely matrix matched to the sample – in this case, phosphorite. Two Standard Reference Material (SRM) phosphates were trialled: NIST120c, a phosphate rock from Florida, and BCR-32, a Moroccan phosphate rock. BCR-32 had issues staying in solution, and thus was not used. NIST120c is not well characterized for trace elements, and therefore could not be used as the primary standard, for calibration.

Instead, BHVO-2, a Hawaiian basalt, was used as the calibration standard as it is very well characterized for most trace elements (Jochum et al., 2005). This standard was used for all major and trace elements. Samples and SRMs are run at dilutions of 70,000 x, greatly minimising any matrix effects.

Trace elements in the secondary standard (NIST120c) are not very well characterized. Compiled values are available from GeoReM (Jochum et al., 2005), and were generally acquired using XRF. Standard addition methods were used to determine values for a suite of trace elements in NIST120c, which span across the transition and lanthanide group elements (M. Handler & A. Albot, unpubl. Data).

Duplicate analyses of samples were run to monitor reproducibility (external precision) (Appendix A-5.). Most Elements reproduced within 10%. In four analytical sessions,

instrument conditions led to BaO spectral interferences on Eu that produced inaccurate, high Eu concentrations, observed clearly in duplicate analyses of sample G224-1-Med (Appendix A-5.), which were run in each analytical session. Eu values for samples processed in these sessions were not used.

Beaker cleaning procedure

Savillex 23 ml beakers were batch cleaned, before being transferred to the ultra-clean laboratory at Victoria University of Wellington for final cleaning. Batch cleaning involved sub-boiling sequentially in HCl and HNO_3. The beakers were first rinsed with tap water, wiped with ethanol both inside and out, then rinsed with 18.2 Ω MilliQ water. The beakers were then sub-boiled (80°C) in analytical grade half concentrated HCl for 24 hours. The beakers were then rinsed three times with 18.2 Ω MilliQ water, before being sub-boiled again overnight in analytical grade half concentrated HNO_3. The beakers were then rinsed three times with 18.2 Ω MilliQ water and transferred to the ultra clean laboratory to dry.

The batch cleaned beakers were then refluxed on a hotplate at 120°C overnight with ~ 5 ml of 6-7M double sub-boiled analytical grade HNO_3. The beakers were then rinsed three times with 18.2 Ω MilliQ water, and refluxed again overnight with ~5ml of 6-7M optima grade HNO_3. After being rinsed again three times with 18.2 Ω MilliQ water and dried, the beakers were ready for samples.

Acid digestion procedure

The acid digestion procedure is modified from that of McCoy-West (2009). 50-100 mg of sample was weighed into the clean 23 ml Savilex Teflon beakers. Samples were then treated with an initial aqua regia oxidising step consisting of a ratio of 2 parts concentrated HCl to 1 part concentrated HNO_3. All acids used for sample processing were optima grade. The samples were then capped and left cold for one hour. The aqua regia was then evaporated off at 120°C. Approximately 2 ml of concentrated HF, and ~1 ml of concentrated HNO_3 was added to the samples. The beakers were capped and refluxed on a hotplate at 120°C for 2-3 days to digest the silicate phases. After this time the samples were taken off the hotplate to cool down, then the acid was evaporated to incipient dryness, so as to not form any insoluble fluoride phases or lose sample due to electrostatic build up from the beakers. Enough HNO_3

to just cover the sample cake was then added and evaporated at 120°C to convert the samples to nitric form and ensure all HF had been removed. This step was repeated again and evaporated at 120°C to dryness. Next, ~ 4 ml of 6-7 M HCl was added to each sample, capped, and refluxed on a hotpate at 120°C overnight to dissolve the sample cake. Samples were cooled down and examined visually for precipitates. If precipitates or undissolved residues were observed, the samples were treated to 10 minutes in an ultrasonic bath. If the precipitates were simply colloid aggregates, the ultrasonic bath would break them down. If the precipitates did not break down, the samples were evaporated down, and treated to HF and HNO_3 overnight to ensure complete digestion, and the HNO_3 and HCl steps repeated. Once all samples were in solution, the HCl acid was evaporated off at 120°C to dryness. Concentrated HNO_3 was applied to cover the sample cake, and evaporated off to convert the sample back to HNO_3.

Finally, the samples were brought back up into solution with 9 ml of 1M nitric acid, and refluxed overnight. Samples were transferred into 10 ml centrifuge tubes, which had been pre-cleaned in dilute optima grade nitric acid, and centrifuged for 10 minutes at 2400rpm. Samples were then diluted ~70,000 times in 1% optima grade nitric acid ready for analysis using the ICPMS. Sample powders and aliquots used for dilution were weighed on a high precision balance (±0.00001 g). If any precipitate was observed after the sample had been centrifuged, the sample was not run for analysis as the underlying assumption of solution sample analysis is that the sample must be fully dissolved.

Method Development

Relative to the igneous standard reference material used, BHVO-2, the behaviour of the dissolved phosphorite samples in 1M HNO_3 differed noticeably. The phosphorite solutions displayed wetting to the Teflon beaker, whereas the BHVO-2 solution did not. This was of concern as the wetting behaviour meant that 100 % sample transfer from beaker into centrifuge tube was not possible for all nodule samples. A small auto pipette was used to attempt to recover as much sample as possible. ICPMS data were internally corrected using anhydrous CaO wt % from XRF analysis to correct for any sample loss.

The beakers used are made of a commercial brand of PTFE, Teflon. PTFE has a carbon backbone, where the hydrogen atoms are replaced with fluorine atoms, a polymer of CF_2

(Leote et al., 2013). Replacing the hydrogen atoms with fluorine atoms lowers the surface tension of the material. CF_2 has a measured surface tension of between 15 mN/m (Leote et al., 2013) and 21 mN/m (Föllmi, 1996). Any solution with a higher surface tension (e.g. water with a surface tension of 72 mN/m) in contact with the PTFE surface will not spread out but repel, known as "non-wetting" behaviour (Leote et al., 2013). If a solution with a lower surface tension than the PTFE is in contact with the surface, then the solution will spread and stick or "wet" the PTFE surface. One method of measuring the degree of wetting is to measure the wetting angle of a drop of solution on the solid (PTFE) surface. Put simply, if Θ (wetting angle) = 0°, then the surface of the substrate is perfectly wettable. If $\Theta < 90°$ the substrate is wettable, and if $\Theta \geq 90°$, then the substrate is perfectly unwettable (Leote et al., 2013).

The nodule samples displayed wetting behaviour, with a visually approximated wetting angle of less than 90 degrees. This means that the surface tension of the dissolved nodule solution has a surface tension of below 15 mN/m. The major component of the sample solution at the stage where the wetting behaviour is observed is 1M HNO_3. This is roughly 3% HNO_3 and 97 % milliQ water. The dilution factor of the sample powder in the 9ml of 1M HNO_3 solution is already 100-150 times. Bringing up the solution in 3M HNO_3 instead of 1M HNO_3 in an attempt to dilute what was causing the wetting behaviour of the solution did improve the sample transfer, but did not completely resolve the problem. Interestingly, Bollons Seamount nodule samples consistently displayed less wetting behaviour than Chatham Rise sediment and nodule samples.

Another issue with sample preparation was that some samples produced a brown-black precipitate in the 1M HNO_3 dilution, once cooled down and centrifuged. The samples were completely in solution when inspected in 6M HCl, and again when transferred to the centrifuge tubes after being brought up in 1 – 3M HNO_3. The precipitate formation appeared to be time dependent. Some samples did not show any signs of precipitation immediately after being centrifuged, but did form precipitates after 24 hours had passed.

The sample types that precipitated were typically muddy fine-medium sand, glauconite sediments, and the standard reference material BCR-32. This precipitation was not random,

as both sediment sample G107 and SRM BCR-32 were digested in multiple batches with the same result of precipitation each time.

Since the samples that precipitated were observed to fully dissolve in 6M HCl, in an experiment, the solutions were brought up in 2.5 M HCl instead of HNO_3 to see if the HCl could stabilize the solution to prevent precipitation. The samples fully dissolved in the 2.5 M HCl; however, upon cooling and transferring the samples to the centrifuge tubes, which took less than 2 hours, the sediment samples had precipitated. Some samples (R6-b) precipitated in the Teflon beaker before being transferred into centrifuge tubes.

Considering that the samples dissolve well in HCl, but precipitate out just as easily, the precipitate is likely to be FeOOH (T. Seward, Pers. Comm. 2015). FeOOH, or goethite, is known to be a major mineral phase in Chatham Rise phosphorite nodules (Von Rad & Rosch, 1984). Once FeOOH polyhedra slowly nucleate and aggregate, they rapidly crystalize and fall out of solution (Grundl & Delwiche, 1993), which is consistent with the behaviour observed in this study. However, Fe_2O_3 wt% was not a reliable predictor for sample precipitation. This issue was not able to be satisfactorily resolved and therefore only 66 samples, out of the total of 96 were able to be analysed for trace element concentrations.

Micro X-Ray Fluourescence (µXRF)

µXRF maps were collected by Dr. Michael Gazley (CSIRO) using a Bruker M4 Tornado X-ray fluorescence spectrometer, which has a 50 kV Rh X-ray tube, at the Australian Resources Research Centre, CSIRO, Perth, Australia. A map is produced by moving the sample beneath a stationary beam with a nominal beam spot size of 25 µm, using a step-size also of 25 µm. At each point a full X-ray spectrum is recorded and can then be deconvolved to give elemental contents. Detection limits vary from ppm levels for transition series metals to sub wt % for light (Mg and Al) and heavy elements. Datasets collected using the Tornado were processed using Bruker Esprit software to produce grey-scale maps for each element which were then combined using a MATLAB graphical interface designed by Dr. Mark Pearce (CSIRO). The Scanning electron microscopy (SEM) elemental content maps were obtained using a Phillips XL40 scanning electron microscope, also by Dr. Michael Gazley at the ARRC.

4.4 Results

4.4.1 Bulk Major Elements

Selected major element bivariate plots show a negative linear relationship between K_2O, SiO_2, Fe_2O_3, Al_2O_3, and MgO and nodule size for Chatham Rise phosphorite nodules (Figure 4-5). Bollons Seamount nodules show the same general relationship, but do not plot on the same trend as Chatham Rise nodules. Conversely, smaller size fractions of Chatham Rise nodules have lower CaO wt% and P_2O_5 wt% than larger size fractions.

The composition of a sample of young cetacean bone was included in this analysis as an end member to observe how the chemistry changes during the phosphatisation of bone. The young bone sample was not completely pure as some lithified chalky sediments could not be washed out of the bone pores. The average CaO wt % and P_2O_5 wt % contents appear to have increased in the phosphatised bone relative to the young bone (Figure 4-5-a.).

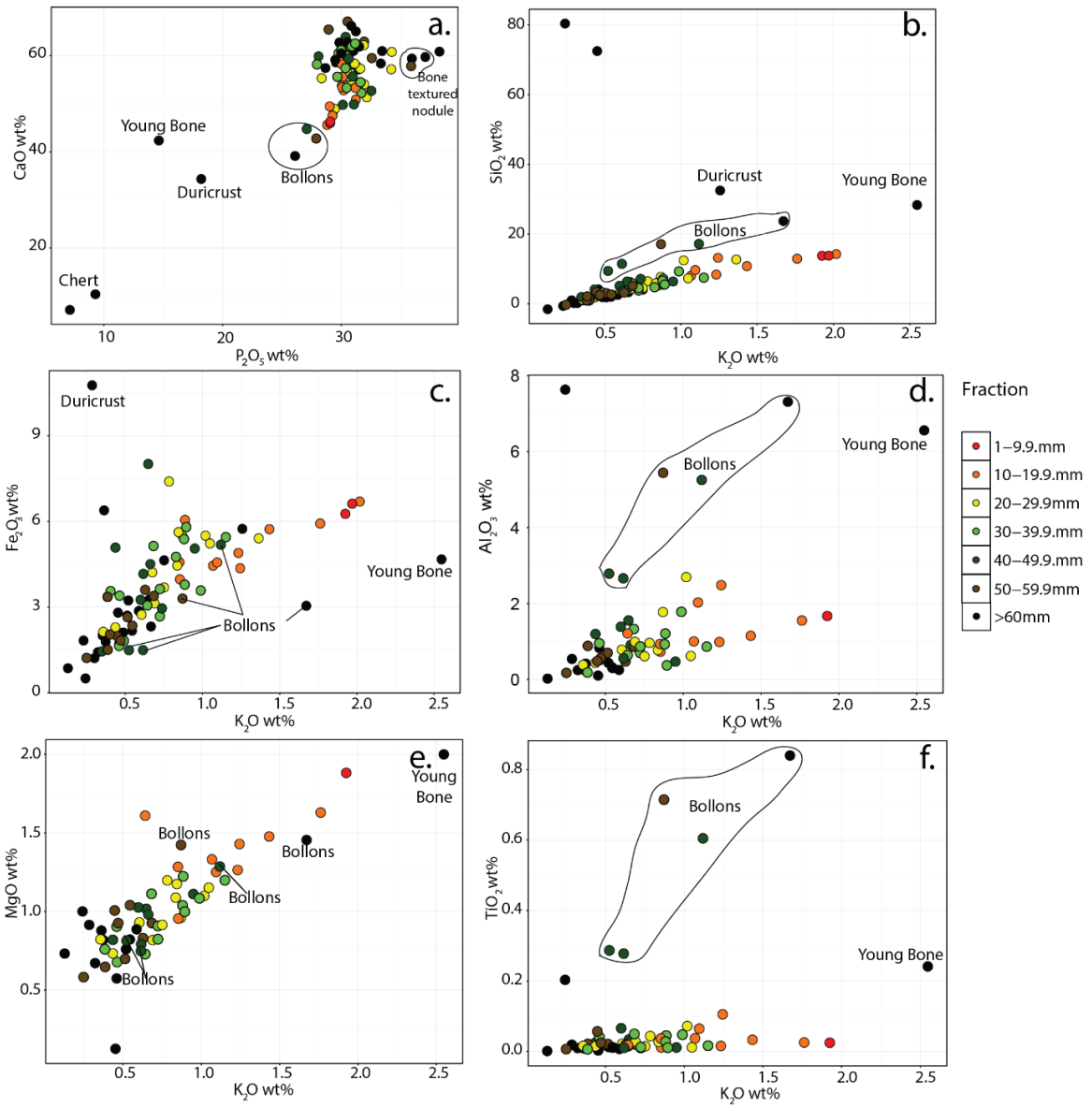

Figure 4-5: Selected major element bivariate plots.
TiO_2, P_2O_5, Al_2O_3 and MgO analyses measured by ICPMS (n=65). K_2O, Fe_2O_3, SiO_2, and CaO analyses measured by XRF (n=82).

Major element contents normalised to average upper crust (using recommended values from Rudnick and Gao, 2014) are shown in Figure 4-6. Relative to average upper crust, Chatham Rise nodule samples, and the offshore South Island nodule (S14-1-L) from site S14 (Figure 4-1), are depleted in SiO_2 TiO_2, Al_2O_3, MnO, MgO, FeO (total Fe measured as FeO), and K_2O, and enriched in CaO and P_2O_5 (Figure 4-6).

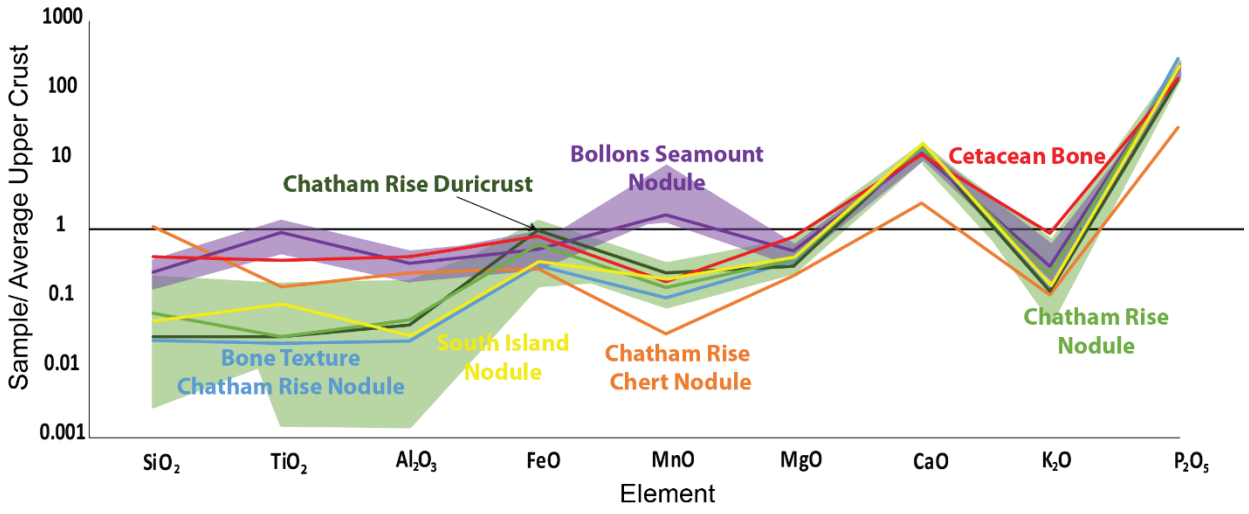

Figure 4-6: Phosphorite nodule major elements (wt %) normalised to average upper crust. Recommended upper crust values from Rudnick and Gao (2014). Solid lines = median, shaded area = range. SiO_2, FeO, CaO, and K_2O measured by XRF (n=82). P_2O_5, TiO_2, Al_2O_3, MnO, and MgO measured by ICPMS (n=65).

Bollons Seamount samples are depleted in SiO_2, Al_2O_3, FeO, MgO, and K_2O, and enriched in MnO, CaO, and P_2O_5 relative to the average upper crust (Figure 4-6). All Bollons Seamount samples are depleted in TiO_2, except for TAN0307-83-3. They also show variation in major elements compared to the continental shelf derived Chatham Rise phosphorite nodules, with higher enrichments in TiO_2, Al_2O_3, SiO_2 and MnO, but similar enrichment for FeO, MgO, CaO, K_2O and P_2O_5.

Surficial sediment fractions from two sites, G107 and G106 (Figure 4-1), were analysed (Figure 4-7). The same major element trends as seen in phosphorite nodules, are seen in the two sediment sites. The highest enrichments in SiO_2, Al_2O_3, and TiO_2 are seen in the smallest size fraction, and linearly decreases with increasing size fraction. Fe_2O_3, MgO and K_2O collectively display the same trend for the smallest fraction, <63µm containing the lowest wt % and the next size fraction up, 63µ – 2mm, the highest wt %. From 2-8mm there is a linear decrease in content with increase in fraction size.

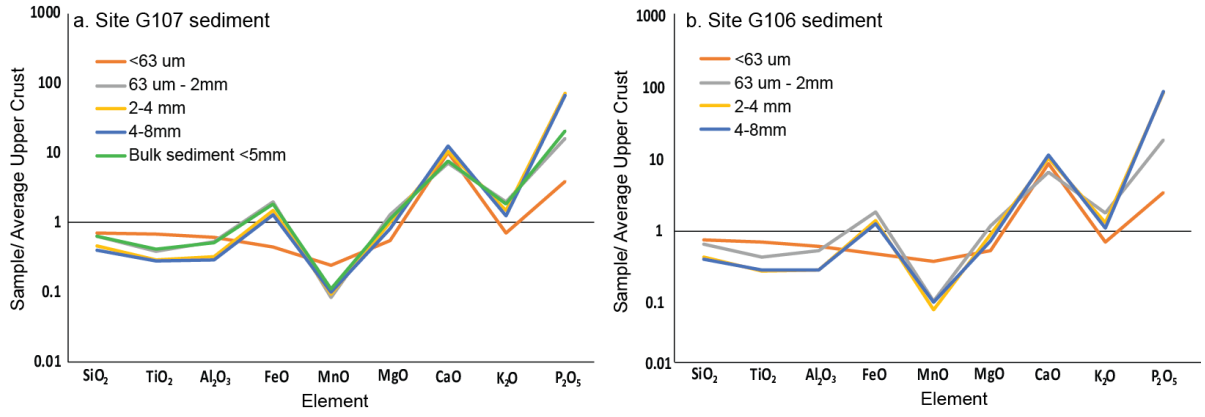

Figure 4-7: Sediment major elements by size fraction.
Normalised to average upper crust using recommended values from Rudnick and Gao (2014).

P_2O_5 enrichment increases with an increase in size fraction. MnO has a remarkably high enrichment in the <63 µm fraction, with contents in all other size fractions being similar across both sites. The <63µm and 2-4mm fractions have the same relative wt %, along with the 4-8 and >8mm fractions. The 63µm- 2mm fraction displays the lowest CaO enrichment across both sites.

Surficial sediments from sites G87 and G107 show enrichment in CaO, and P_2O_5, and depletion in SiO_2, TiO_2, Al_2O_3, and MnO relative to the average upper crust (Figure 4-8). Bulk sediment from site G107 displays higher enrichment in FeO. Chalk sediments are enriched and depleted in the same elements as surficial sediments. However, they show greater depletion in SiO_2, TiO_2 and Al_2O_3 (Figure 4-8). Bulk chalk sediment from site G244 displays higher enrichment in FeO relative to the average upper crust than other measured bulk sediments.

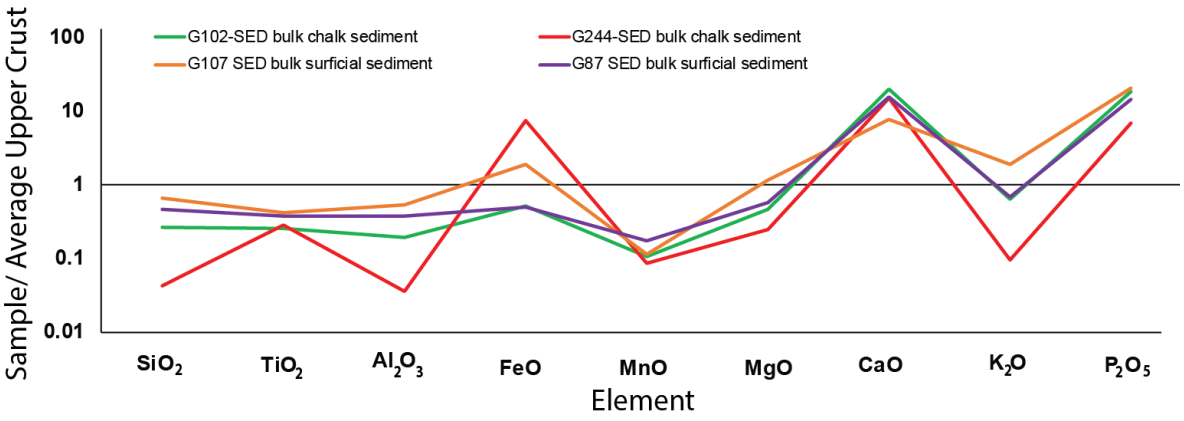

Figure 4-8: Bulk surficial and chalk sediments normalised to average upper crust using recommended values from Rudnick and Gao (2014).

4.4.2 Bulk Trace Elements

Relative to average upper crust, a common feature of the Bollons seamount nodules is enrichment in the first-row transition metals Co, Ni, Cu, Zn, in addition to Sr, Y, Mo and U, and depletion in Sc, Cr, Ga, Rb, Cs, Hf and Th (Figure 4-9). There is some variation in nodules from different sites. Site TAN0307-83 nodules display enrichment in V, Ta and Pb, whereas site TAN0307-82 shows depletion in these elements relative to the average upper crust.

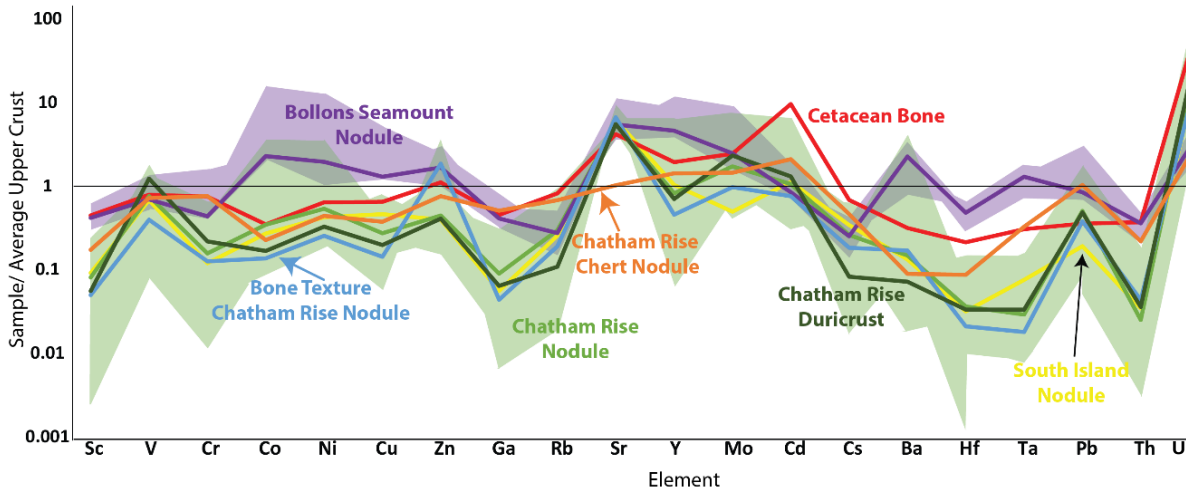

Figure 4-9: Phosphorite trace elements normalised to the average upper crust. Recommended values for the average upper crust from Rudnick and Gao (2014). Solid lines: median of the sample type. Shaded area: range of enrichment and/or depletion.

Chemical variation is also seen at the site scale in samples from Bollons Seamount. At site TAN0307-83, sample TAN0307-83-3 displays a higher enrichment in Co, Ni, Cu, Mo and Pb. Conversely, sample TAN0307-83-2 shows enrichment in Ba and Cr, whilst sample TAN0307-83-3 displays depletion in these elements. These differences most likely reflect the different nodule types: TAN0307-83-3 is a representative Bollons Seamount nodule, whereas sample TAN0307-83-2 is a conglomerate type (Figure 4-10).

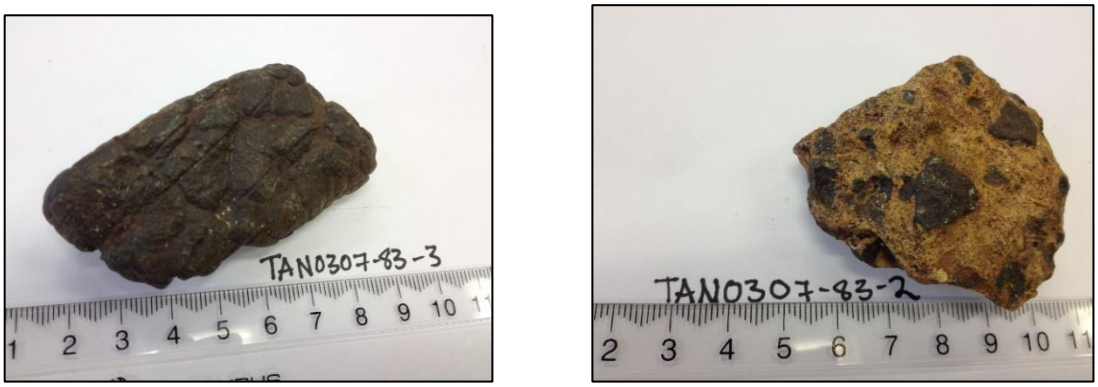

Figure 4-10: Sample images of samples Bollons Seamount nodules: TAN0307-83-3, and TAN0307-83-2.

Chatham Rise nodule samples, including duricrust and bone texture type nodules, in general display an average enrichment in Sr, U, Y and Mo relative to the average upper crust. Depletion is observed in Sc, Cr, Cu, Ga, Rb, Cs, Ba, Hf, Ta, Pb and Th (Figure 4-9). Young cetacean bone displays the highest Cd enrichment (10x), as well as higher enrichment in Cs, Hf, and Ta relative to typical Chatham Rise nodules (Figure 4-9). The offshore South Island nodule, S14-1-L, follows the same depletion and enrichment patterns as the median Chatham Rise phosphorite nodules.

Some nodules; however, display greater enrichment relative to the majority of Chatham Rise nodules when normalised to the average upper crust: V(nodule samples from sites G35, N829, N857, N845, H663, G121, I572 and N959.), Co (samples from sites G35, H959, G305 and E79), Ni (Samples from sites G35, G304, H959, E79, G121 and N839), Zn (Sites I613, N868, G112, G35, G244 and N857), Cd (Sites G35, H959, N829, N857, G227, and N839), and Pb (G304, I572, N824, and G35). Half of the samples show enrichment in Y, and half are depleted. The spatial relationships of key trace metals are further explored in section 4.5.1.

Bulk chalk sediment samples, G224-SED and G102-SED, with large phosphorite nodules removed, were analysed for trace elements. Due to analytical issues with sediment samples precipitating out of solution, only two samples were analysed for trace elements in this study. A typical muddy fine-medium glauconite sand, G106<2mm, has also been included. Two additional typical muddy glauconite surficial sand sediments are presented in Chapter 5, but were not included in this section as the analytical methods (partial digestion) did not yield comparable results.

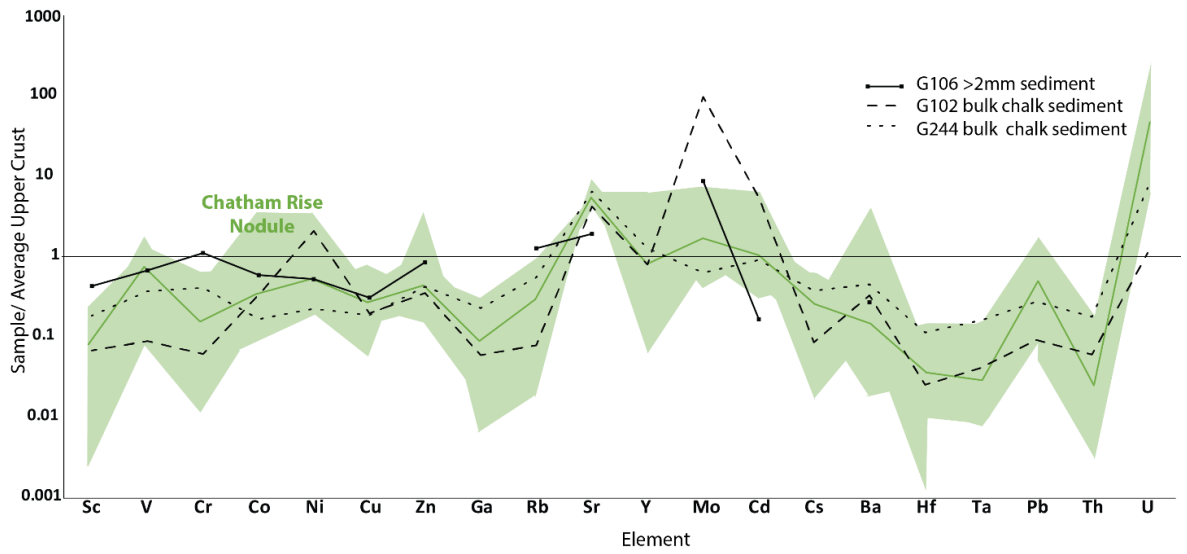

Figure 4-11: Bulk sediment trace elements normalised to average upper crust. Average upper crust values from Rudnick and Gao (2014). Shading represents the range in Chatham Rise phosphorite nodule samples.

In general, all the sediments are enriched in Sr and U, and depleted in Ba, V, Zn, Co, Cu, Sc, Ga and Cs relative to the average upper crust (Figure 4-11). Site specific differences in trace element enrichments and depletions are also observed. Surficial sediment from site G106 shows greater enrichment in Rb and Cr relative to the average upper crust, than chalk sediment from sites G102, and G244. Site G244 chalk sediment displays higher enrichment in Mo and Cd than bulk sediments from sites G106 and G102. Overall, with the exception of Mo, the trace elements in bulk chalk and surficial sediments show enrichment and depletion of trace elements within the range of Chatham Rise phosphorite nodules.

4.5 Nodule trace element correlations

Correlation matrices were used to identify strong correlations between major and trace elements in Chatham Rise nodules (Figure 4-12). Correlations were only calculated for typical Chatham Rise phosphorite nodules (n=51), as the sample size for Bollons Seamount was too small (n=5). The Pearsons method is not robust to outliers, and requires data to be as close to normally distributed as possible. Elements that are found in multiple mineral phases will display correlations that are only moderate or weak in strength. Only correlations with $p>0.05$ are used.

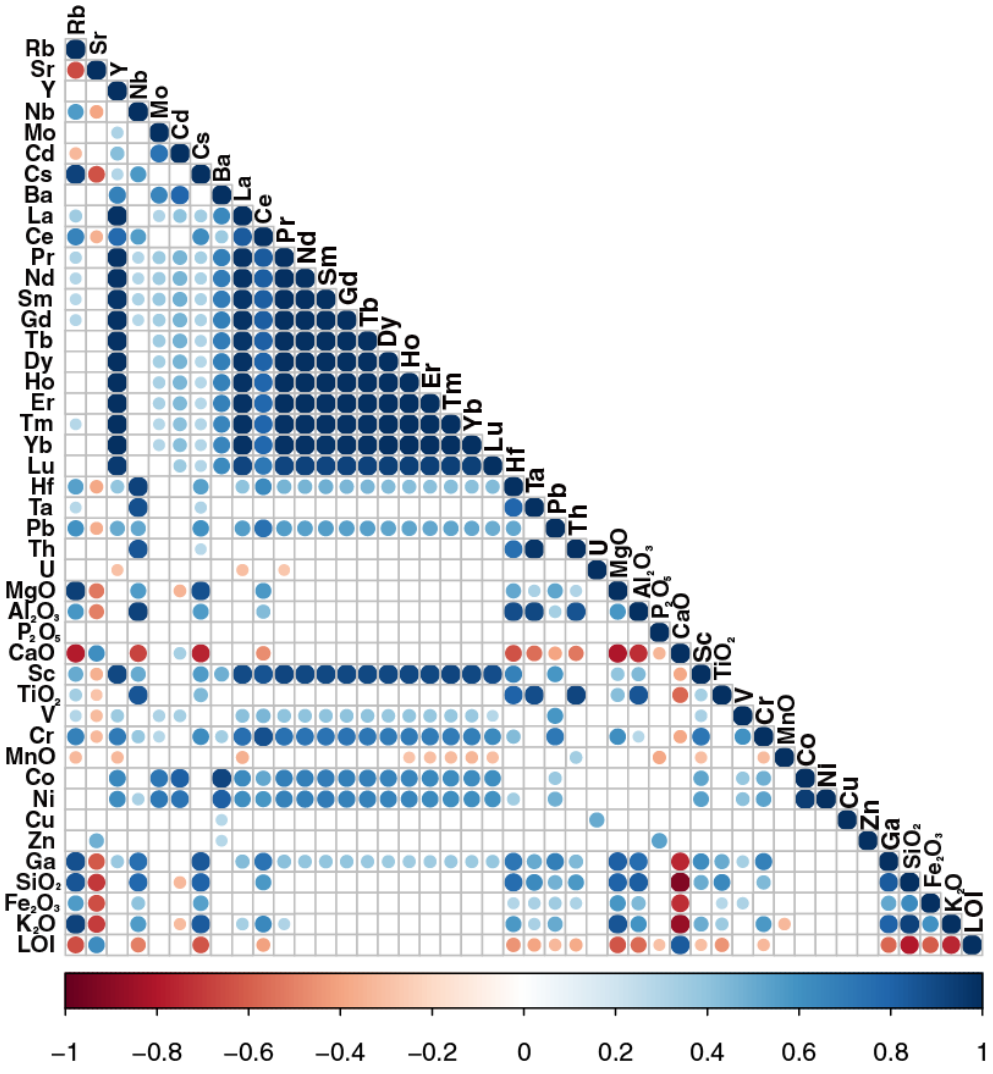

Figure 4-12: Pearsons correlation matrix for typical Chatham Rise phosphorite nodules (n=51). Bone texture, duricrust, chert, and cetacean bone samples are excluded. Only major and trace elements acquired by ICPMS are used except for Fe_2O_3, K_2O, CaO, and SiO_2. Colour scale indicates r_p value. Correlation calculations and image generated using corrplot, developed by Wei and Simko (2016).

Major elements K_2O and SiO_2 have strong positive correlations with Rb, Cs, MgO and Ga, and strong negative correlations with Sr, Ca and LOI. K_2O and SiO_2 also have moderate positive correlations with Ce, Hf, Sc and Fe_2O_3. TiO_2 displays strong positive correlations with Nb, Hf, Ta, Th and Al_2O_3, and moderate positive correlations with SiO_2 and Ga. Al_2O_3 also has strong positive correlations with Nb, Hf, Ta, in addition to TiO_2, Ga and SiO_2. Al_2O_3 has moderate positive correlations with Rb, Ce and Mg. Al_2O_3 also displays strong negative correlations with CaO. MgO has similar strong positive correlations to K_2O and SiO_2, in addition to Ta and Hf.

CaO displays a strong positive correlation with LOI. Strong negative correlations with CaO include Rb, Sr, Nb, Cs, MgO, Al_2O_3, Ga, SiO_2, Fe_2O_3 and K_2O, along with moderate negative correlations with Ce, Hf, Ta, Pb, Th and Sc. P_2O_5 does not display any strong correlation with any major or trace element, only a moderate positive correlation with Zn.

The suite of REE display strong positive correlations with Sc and Cr, and moderate correlations with Pb, Co and Ni. Ce is the only REE that displays moderate positive correlations with SiO_2, K_2O, Cr, Cs and Nb. Ce also displays a moderate negative correlation with Sr.

Ba does not show a strong correlation with any of the major elements. Ba has strong positive correlations with Cd, Y, Mo, Co and Ni, with moderate positive correlations with all REE except for Ce.

The positive correlations between K_2O, Ga, Nb, Hf and Ta are further explored in Figure 4-13. The contents of all of these elements increases with decreasing nodule size (Figure 4-13-a,b,c,d). Bollons Seamount nodules collectively contain higher contents of Ga, Nb, Hf and Ta, and similar K_2O contents relative to Chatham Rise nodules.

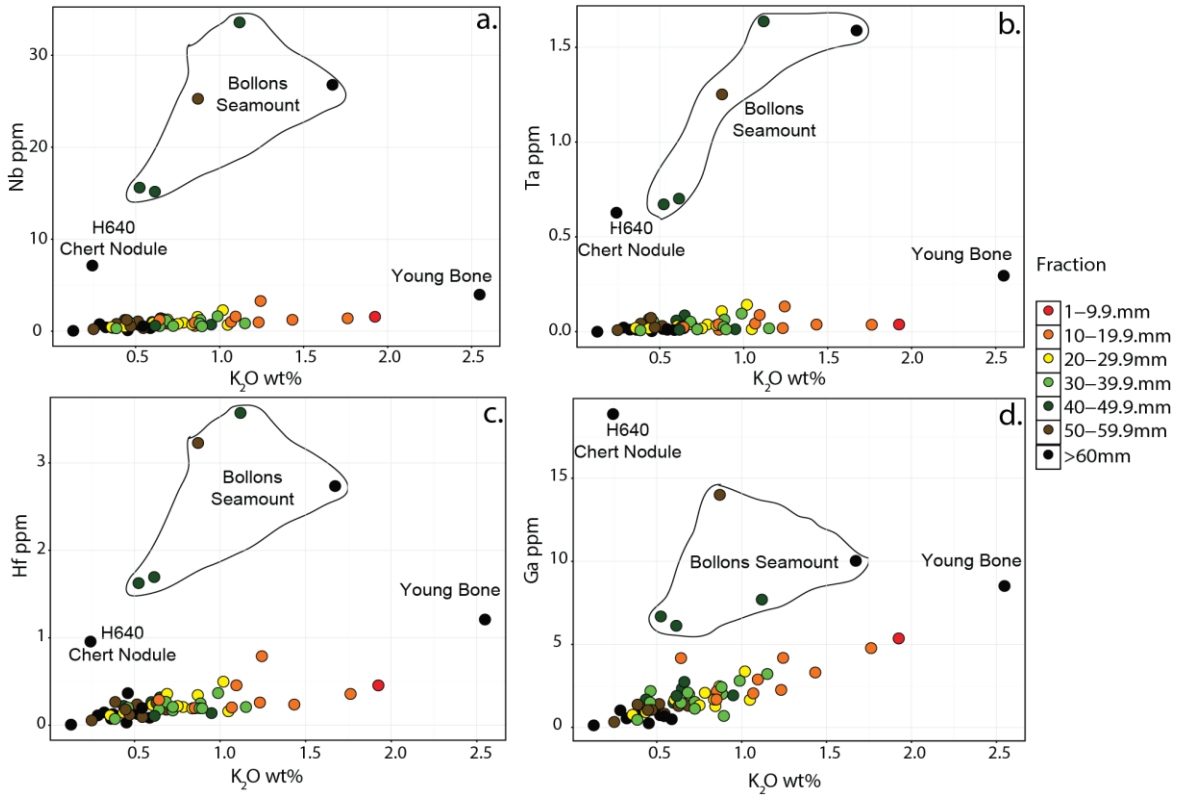

Figure 4-13: Selected bivariate plots of nodules by size fraction.
a: Nb and K_2O, b: Ta and K_2O, c: Hf and K_2O, d: Ga and K_2O. XRF analyses used for K_2O. Bollons Seamount and other sample types are included for reference.

Bivariate plots of Ba and Ni (Figure 4-14-a), and MnO and Ba (Figure 4-14-b) show that samples from sites G35, A904, G121, H959 and E79 are highly enriched in Ba relative to other Chatham Rise nodules. The enrichment of Ba in these nodules trends towards Bollons Seamount nodule values. Enrichment appears to be site specific, and not correlated with nodule size fraction. Ni and MnO variation relative to Ba is small. Co (Figure 4-14-d) and Cd (Figure 4-14-c) are enriched in samples from the same sites, with the addition of samples from sites N829 and N845. Enrichment of both elements appears to increase linearly with Ba. Again, enrichment in Ba, Co and Cd does not appear to be size fraction dependant. Contents of Ba, Co and Cd in sites displaying enrichment have similar contents as Bollons Seamount nodules.

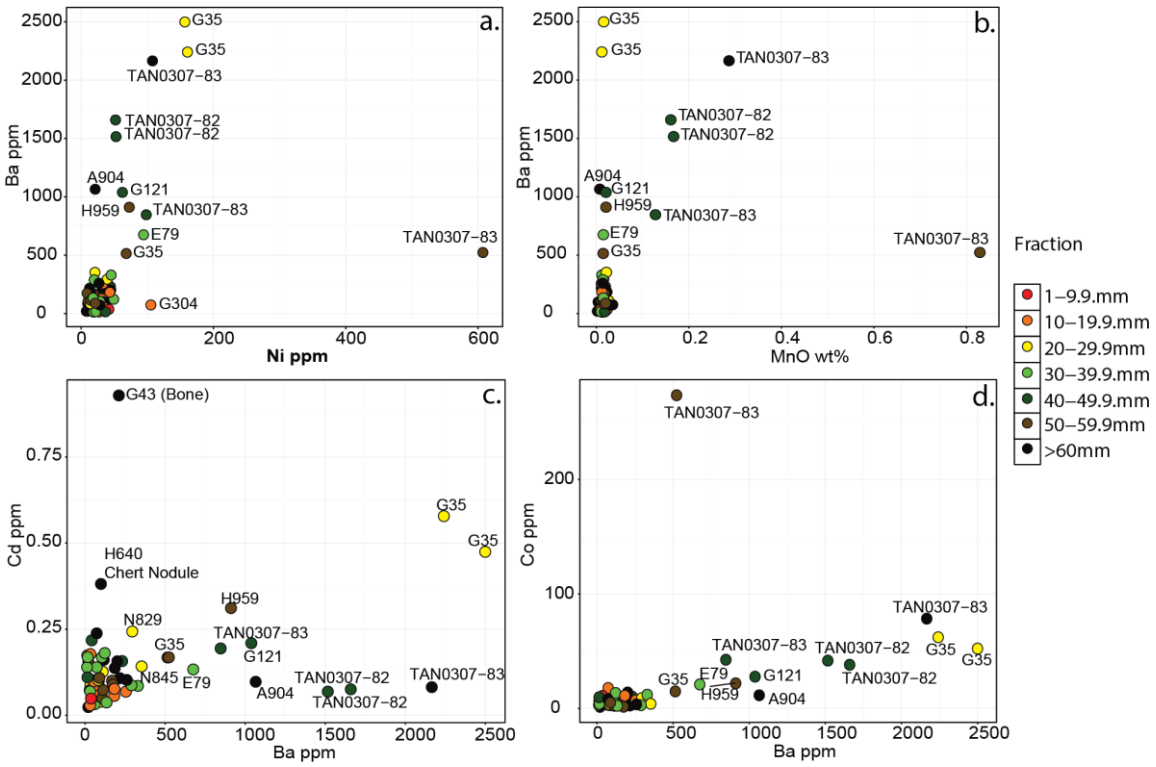

Figure 4-14: Selected bivariate plots of nodules by size fraction.
XRF analyses used for K_2O. Bollons Seamount and other sample types are included for reference. a: Ni and Ba, b: MnO and Ba, c: Ba and Cd, d: Ba and Co.

The moderate correlations with LREE and major elements K_2O, Al_2O_3 and SiO_2 are shown in Figure 4-15. There are two apparent trends regarding Ce and major elements: a high Ce and a low Ce trend. The same is seen for Pr. Smaller nodule size fractions have the highest Ce and Pr contents in each trend. Nodules from sites G35, H959, N839, and A904 display enrichments in both Ce and Pr, trending towards Bollons Seamount nodules.

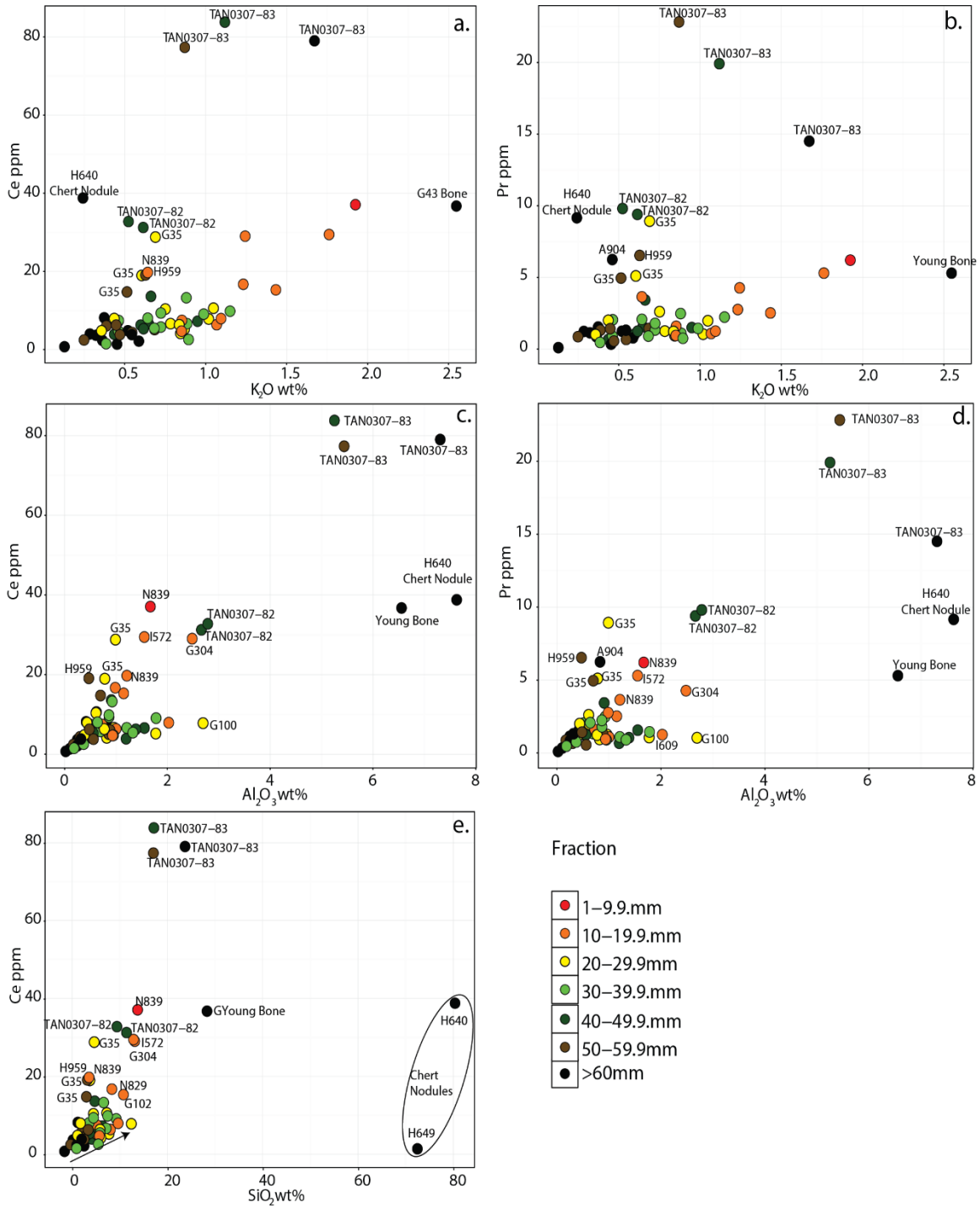

Figure 4-15: Selected bivariate plots of nodules by size fraction.
XRF analyses used for K_2O. Bollons Seamount and other sample types are included for reference. A possible size dependant trend is highlighted by an arrow in e.

4.5.1 Rare Earth Element Patterns

Post Archean Australian Shale (PAAS) values were used to normalise nodule REE for comparison to other studies. Normalised to PAAS, REE patterns (Figure 4-16) are characterized by negative Ce and Eu anomalies, and enrichment of the heavy REE (HREE) relative to light REE (LREE).

The majority of Chatham Rise nodules, including bone texture, recent cetacean bone, and duricrust types, are depleted in REE relative to PAAS. However, all samples from site G35, as well as samples H640-3-Lge, H959-2-Med, A904-1-Lge, N839-3-Sm and I572-3-Sm display middle REE (MREE) and HREE enrichment relative to PAAS. A chert nodule sample (H630-3-Lge) is also enriched in MREE and HREE. The offshore South Island nodule sample (S14-L) displays similar REE patterns to Chatham Rise nodules. Bollons Seamount samples are all enriched in REE, excluding Ce, relative to PAAS (1-4x).

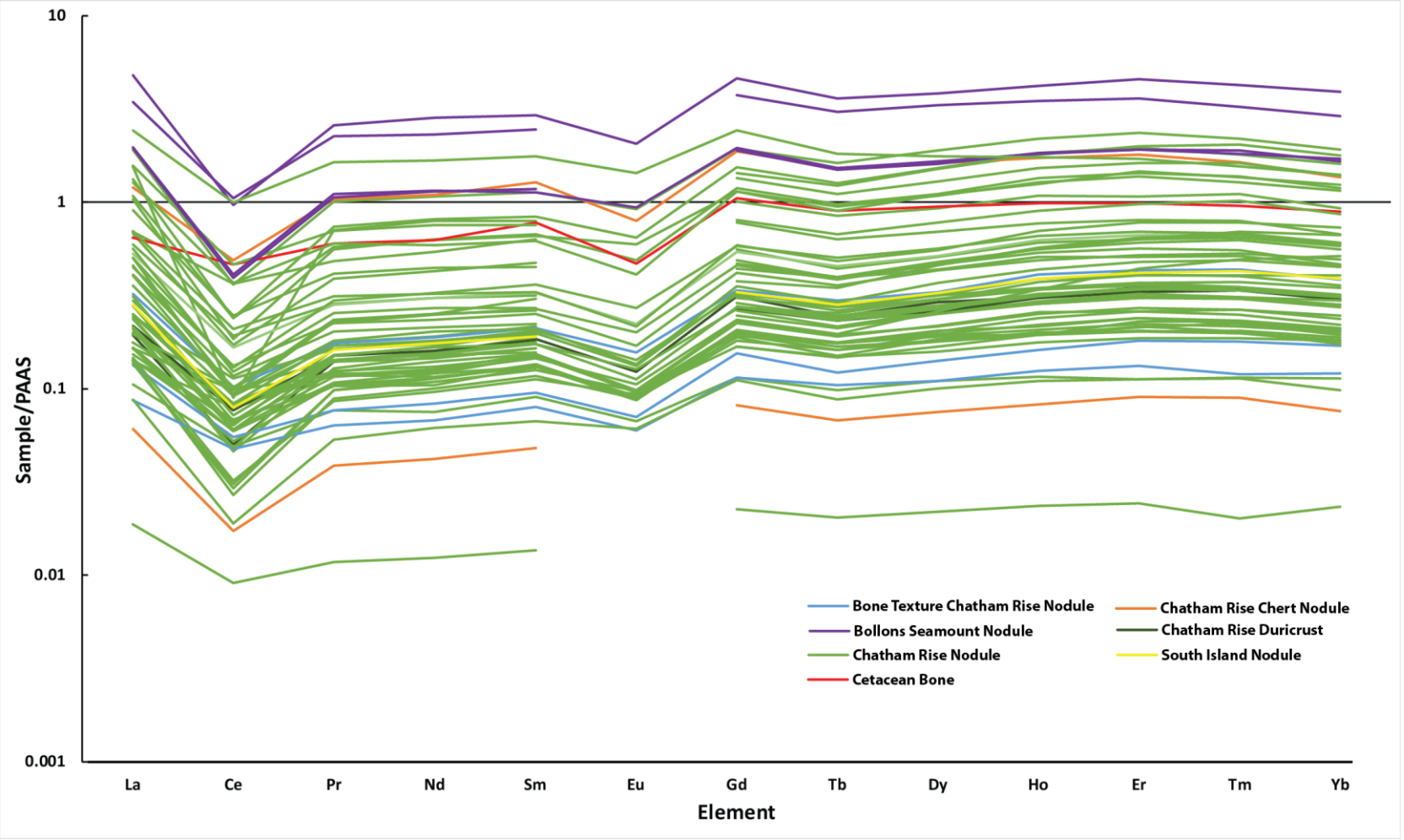

Figure 4-16:Sample REE normalised to Post Archean Australian Shale (PAAS). PAAS values from McLennan (1989).

In general, smaller sized nodules have higher contents of REE relative to larger nodules. Samples of different size fractions from the same site tend to have the same REE patterns, but at different relative contents (Figure 4-17). There are exceptions, such as nodules from site N824 (Figure 4-17-b), where the medium sized nodule (relative) has higher enrichment in REE than the smallest (relative) sized nodule. There was not enough contrast in nodule size fractions in Bollons Seamount samples to deduce any obvious size effects.

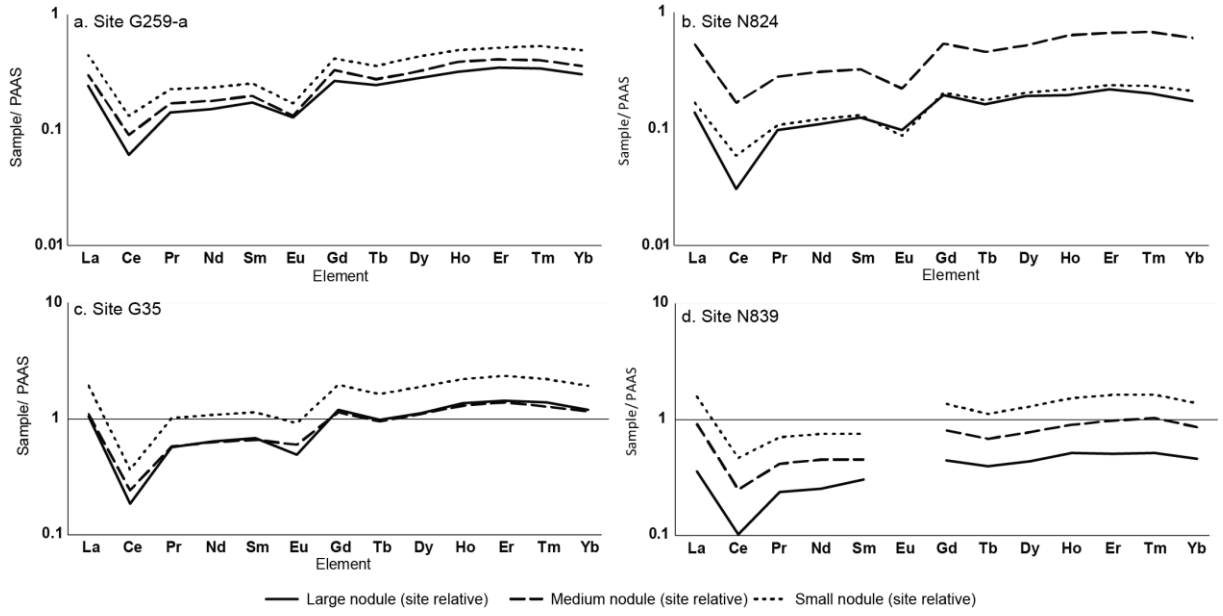

Figure 4-17: Selected REE plots of Chatham Rise phosphorite nodule samples by site. Normalised to PAAS using values from McLennan (1989).

Chatham Rise sediments are depleted in REE relative to PAAS (Figure 4-18), and are characterised by negative Ce and Eu anomalies, and HREE enrichment, similar to Chatham Rise phosphorite nodules. The chalk sediment from site G102 displays higher enrichment in REE relative to the chalk sediment from site G244.

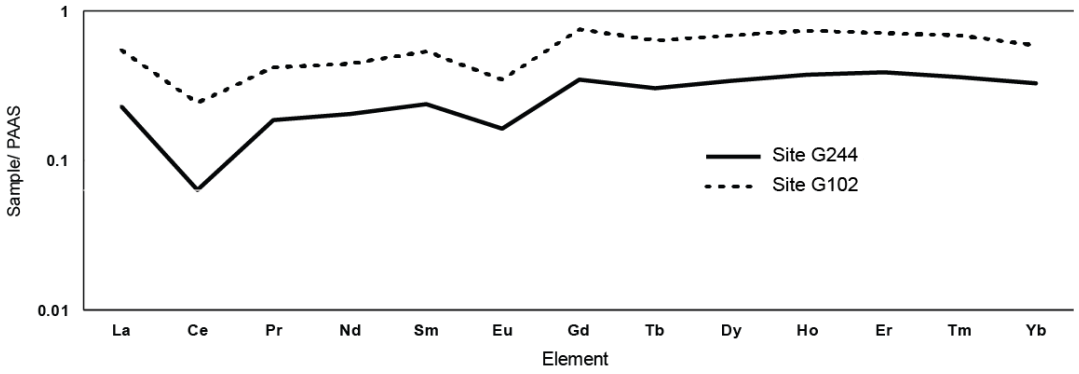

Figure 4-18: Chatham Rise sediment REE normalised to PAAS McLennan (1989). Both sediments are chalk sediments.

4.5.2 Spatial variation in nodule trace element contents

Unless specified, the mean of trace metal contents of all fractions analysed from each site are used to compare trace metal contents between sites. Where there is only one analysis from a site, the single analysis is used as a representative. Only Chatham Rise nodules and duricrust samples were used for comparisons, as the bone texture nodules display notably different chemistry, and only make up approximately 1 % of the phosphorite nodules on Chatham Rise (Von Rad & Rosch, 1984). In general, there does not appear to be any strong spatial trends in trace metal content in phosphorite nodules from Chatham Rise. The spatial patterns of selected potentially ecotoxic trace elements (Cd, Ni, U, Ba, and V) are explored in this section. Ba has shown high concentrations in some samples (Figure 4-14).

Uranium

No distinct and obvious geographic trends in U content could be observed across all Chatham Rise sites (Figure 4-19), although in general sites towards the east tend to have higher average contents of uranium relative to those in the west.

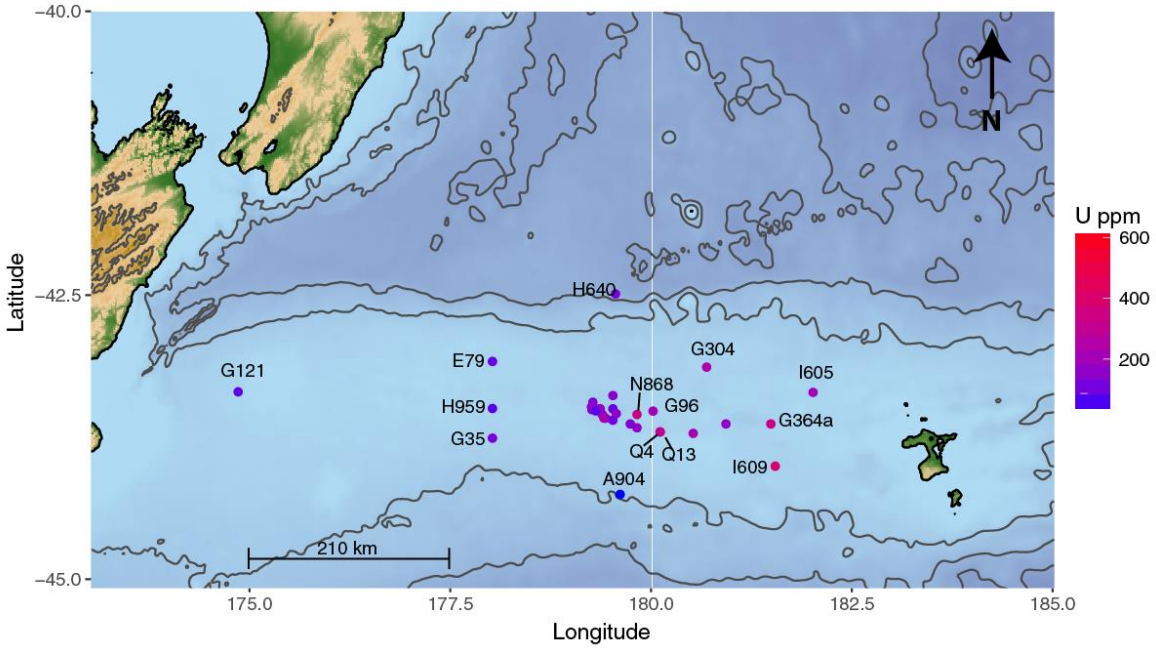

Figure 4-19: Map showing relative average concentration of uranium between sample sites. Map was created using marmap developed by Pante and Simon-Bouhet (2013) using bathymetry data from NOAA (National Oceanic and Atmospheric Administration) (Amante & Eakins, 2009; Aydin et al., 2010).

Vanadium

The contents of V in nodules appears to increase from the southeast to the northwest, with the highest content from site E79: the site closest to Reserve Bank (Figure 4-20).

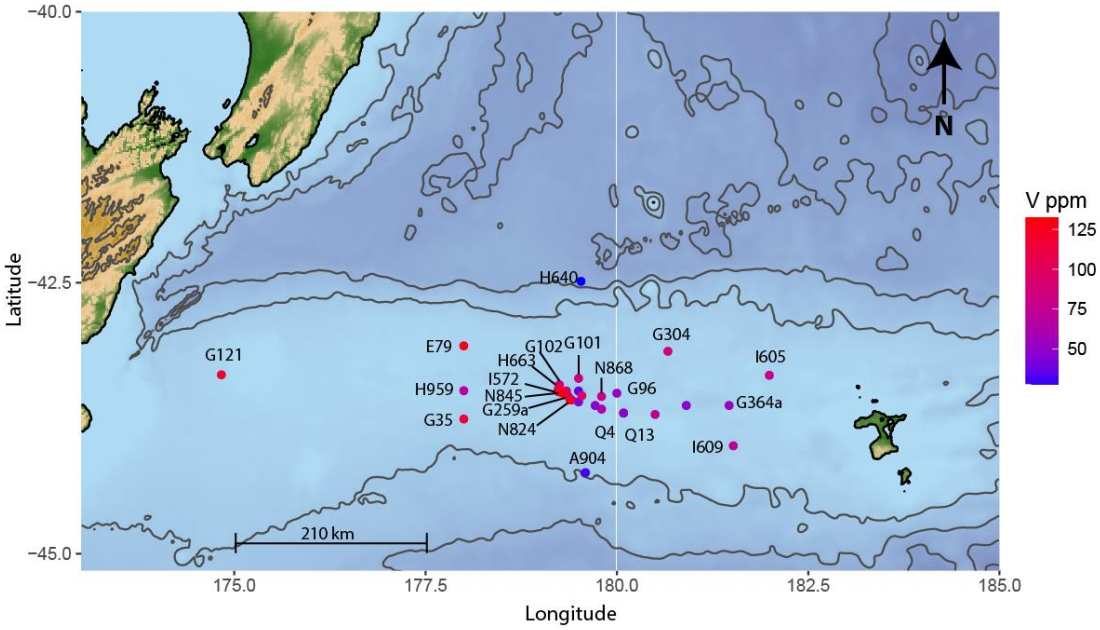

Figure 4-20: Map showing average content of vanadium between sample sites.
Map was created using marmap developed by Pante and Simon-Bouhet (2013) using bathymetry data from NOAA. (Amante & Eakins, 2009).

Barium

There is very little range in the average Ba contents between sites. The exception to this are sites G35 and A904, which show the highest Ba content. From site G35 to site E79 there is an apparent gradational decrease in V content (Figure 4-21).

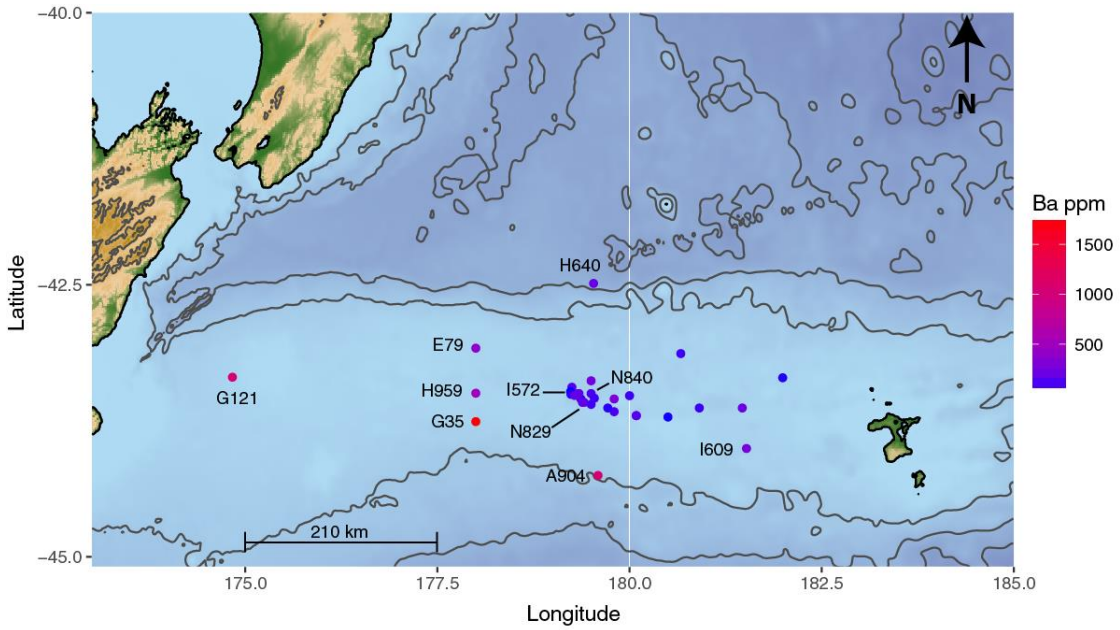

Figure 4-21: Map showing relative content of barium between sample sites.
Map was created using marmap developed by Pante and Simon-Bouhet (2013) using bathymetry data from NOAA (Amante & Eakins, 2009).

Cadmium

Overall, there is a small range in Cd content across all sites on the Chatham Rise. The highest mean content is found at site G35 (Figure 4-22).

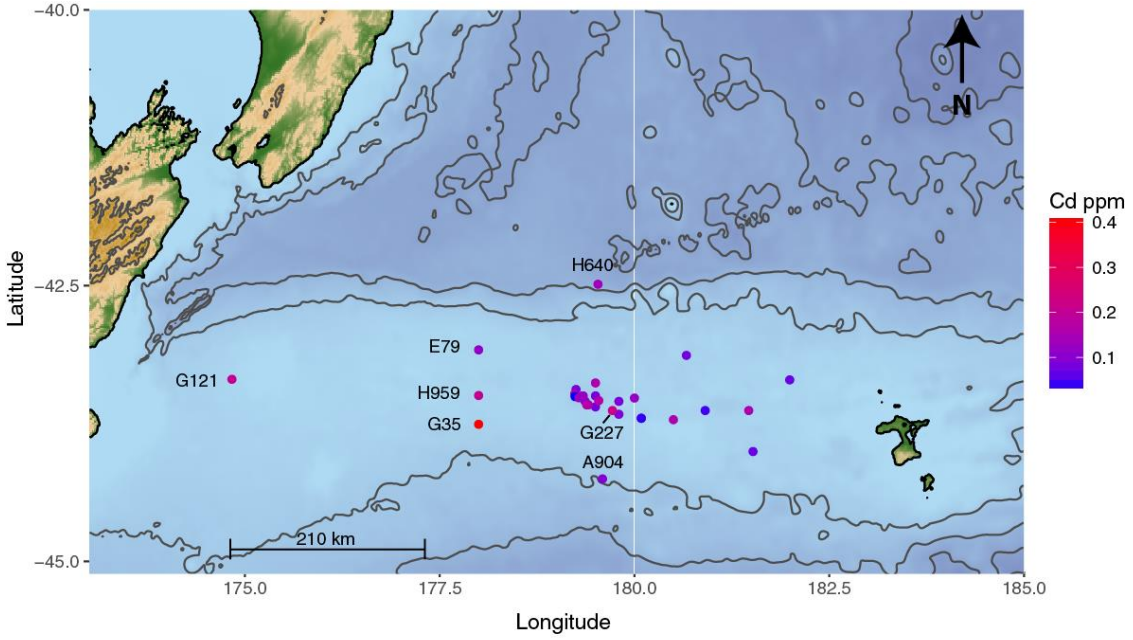

Figure 4-22: Map showing average content of cadmium between sample sites.
Map was created using marmap developed by Pante and Simon-Bouhet (2013) using bathymetry data from NOAA (Amante & Eakins, 2009).

Nickel

The average Ni contents are similar, except for two sites, G35 and G304, which have the highest contents (Figure 4-23).

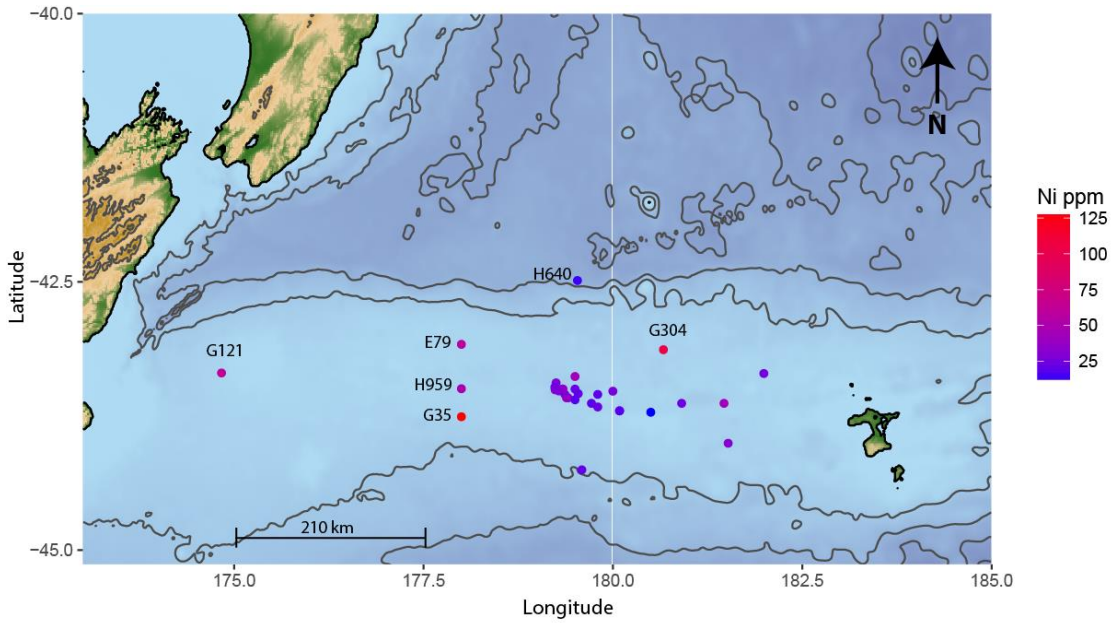

Figure 4-23: Map showing relative average concentration of nickel between sample sites. Map was created using marmap developed by Pante and Simon-Bouhet (2013) using bathymetry data from NOAA (Amante & Eakins, 2009).

4.6 The distribution of trace elements within nodules, determined by µXRF

Three of the most distinct varieties of phosphorite nodules from the sample set were chosen for µXRF mapping. Two are from Chatham Rise, and include a sample typical of Chatham Rise nodules (G221-Med, Figure 4-24) and a chert nodule (G100-1-L, Figure 4-25). The third is from Bollons Seamount (TAN0307-var-83-1). This enables a qualitative approach to identifying where elements are distributed within the nodules, and hence identify different phases and zones within the nodules.

The Chatham Rise nodule analysed consists of the concentric compositions previously described in Section 4.2.1. The glaucony rim phase contains the majority of the Si and K contained in the nodules (Figure 4-24-F, G, H, I). The interior of the nodules is mostly a Ca rich phase, with minor contents of P, K, and Si (Figure 4-24 The areas of high K and Si are most likely associated with sparse mature glauconite grains throughout the interior of the nodule. Areas high in P have a gradational contact with the central Ca rich phase (Figure 4-24-I). Figure 4-24-E shows another variation where the Fe phase is contained within the same zone as the crystalized apatite phase, in contrast to the typical model where goethite exists in a separate zone (Figure 4-2). In Figure 4-24-C some overlap of the S, P, and Fe channels can be observed. As observed in Figure 4-24-A the infill of these structures is a creamier yellow than the surrounding matrix.

The chert nodule (G100-1-L, Figure 4-25), unlike G221 which crumbles when broken, displays conchoidal fracturing. Additionally, this nodule was highly indurated relative to the other nodule samples from Chatham Rise and Bollons Seamount sites. Chert nodule G100-1-L has a similar exterior to the average Chatham Rise phosphorite nodule; dark –greenish vitreous black Type 1 rim, with abundant surface pitting. Nodule G100 is rounded, rather than the more common sub-angular or sub-rounded nodules found on Chatham Rise. The internal zoning of nodule G100 is far more complex than that of G221 (Figure 4-25). The rim minerals do not grade into another phase, it is a continuous, irregular zone. A dark grey-black mineral sharply separates the dark green rim from a thick zone of a yellowish tan mineral. The interior of the nodule is a medium grey, smooth mineral, with creamy white speckles <1 mm in diameter randomly scattered throughout. There are 5 borings, ~2-3 mm in diameter in the centre of the nodule. The sample was found already halved, thus it is unclear if this nodule has been bored post collection.

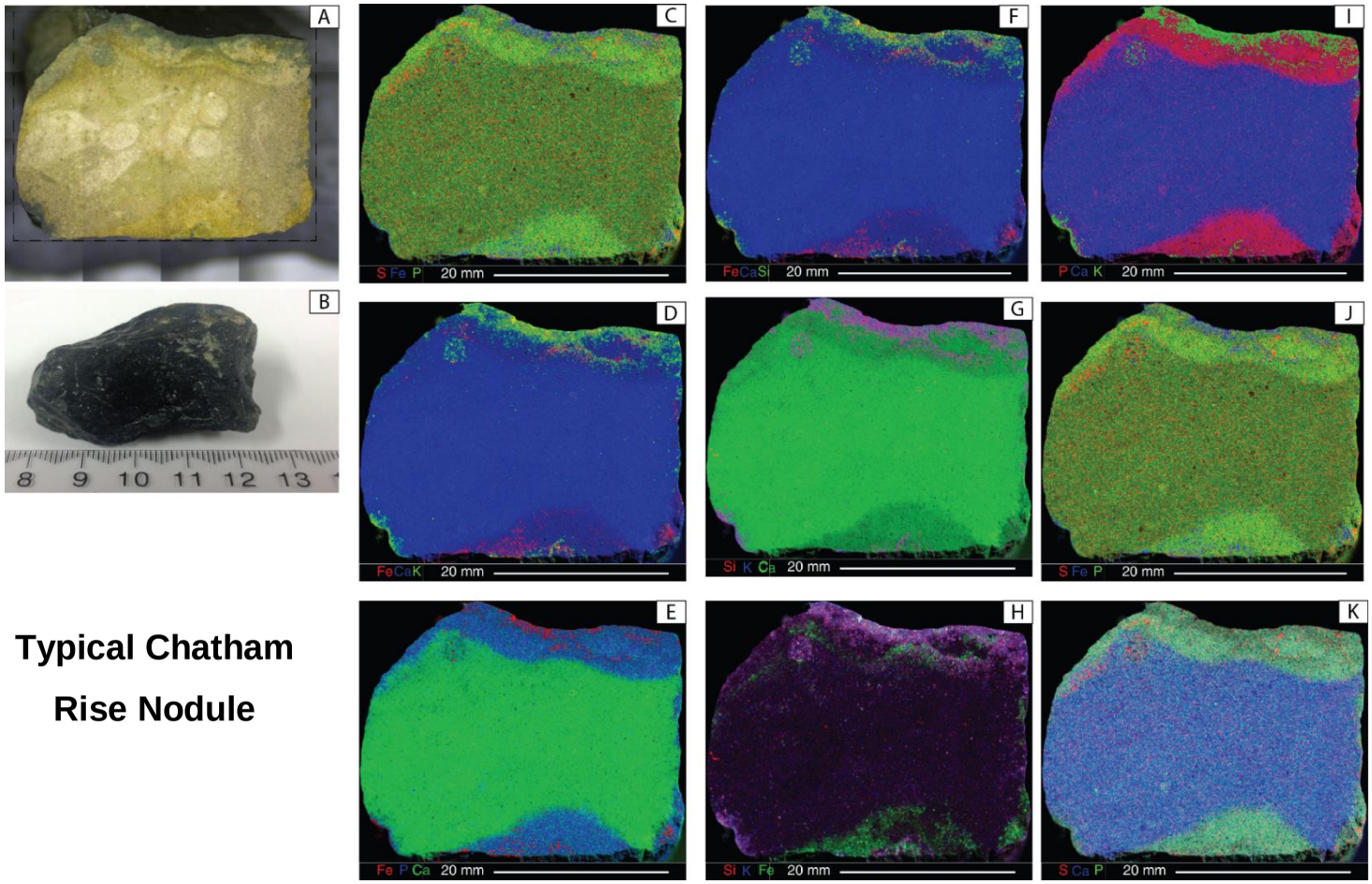

Figure 4-24: A: Mosaic of scanned G221- 2-L nodule. Compiled by Dr. Micahel Gazley (CSIRO). Dashed lines = scanned area. B: scale in cm. Image of the nodule exterior. C: uXRF map showing sulphur in red, iron in blue, and phosphorus in green. D: uXRF showing iron in red, calcium in blue, and potassium in green. E: uXRF map showing iron in red, phosphorus in blue, and calcium in green. F: uXRF map showing iron in red, calcium in blue, and silicon in green. G: uXRF map showing silicon in red, potassium in blue, and calcium in green. An overlap of silicon and potassium shows purple in the image. H: uXRF map showing silicon in red, potassium in blue, and iron in green. An overlap of silicon and potassium shows purple in the image. I: uXRF map showing phosphorus in red, calcium in blue, and potassium in green. J: uXRF map showing sulphur in red, iron in blue, and phosphorus in green. K: uXRF map showing sulphur in red, calcium in blue, and phosphorus in green. uXRF maps collected by Dr. Michael Gazley (CSIRO).

The core mineral is shown in the μXRF maps to be a Si rich phase, with Ca and P rich inclusions (Figure 4-25-E). The yellowish tan zone is a Fe rich Si phase (Figure 4-25-D). Ca and P channels overlap, indicating that they are both contained within the same phase, most likely apatite (Figure 4-25-E). This phase appears to be restricted to a couple of separate zones; the dark olive green zone directly beneath the rim, patches in the yellowish- tan zone, and within the white inclusions, and large white circular inclusion within the core Si rich phase.

Similar to sample G221, S channels somewhat overlap with the P channels indicating a relationship between the two elements. However, there is still a zone that is S rich that does not overlap with the P channel, possibly indicating a second S bearing phase separate to that of the P phase. This second sulphur bearing phase appears to be mostly separate to the yellowish- tan iron rich phase, indicating it may not be associated with pyrite.

Chert Nodule

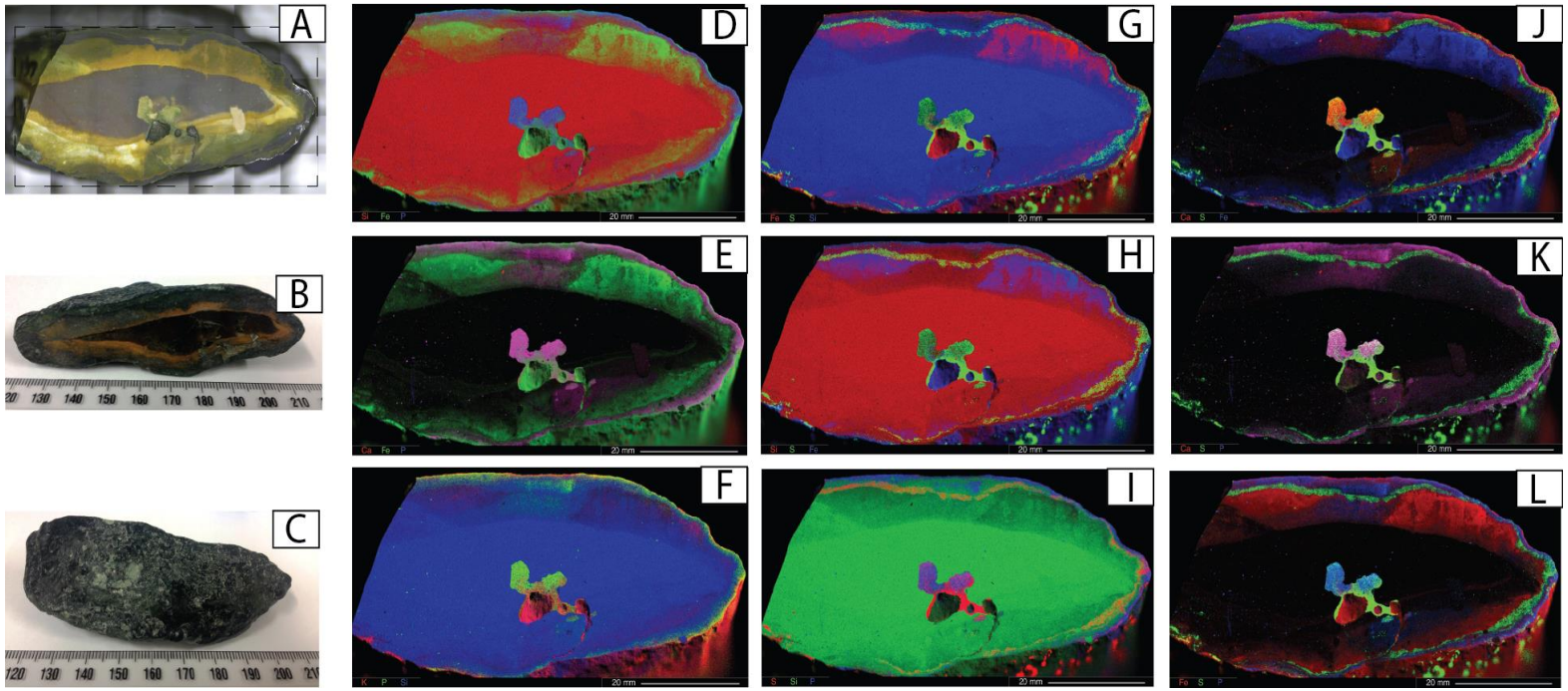

Figure 4-25:Compiled uXRF maps and images of nodule G100-1-Large.
A: Compiled mosaic image collected by Dr. Michael Gazley (CSIRO). Dashed lines = scanned area. B: Image of entire specimen. Scale in mm. C: Image of exterior of the nodule. Scale in mm. D: uXRF map showing silicon in red, iron in green, and phosphorus in blue. E:uXRF map showing calcium in red, iron in green, and phosphorus in blue. The overlap of calcium and phosphorus results in a purple colour. F: uXRF map showing potassium in red, phosphorus in green, and silicon in blue. G: uXRF map showing iron in red, sulphur in green, and silicon in blue. H: uXRF map showing silicon in red, sulphur in green, and iron in blue. I: uXRF map showing sulphur in red, silicon in green, and phosphorus in blue. J:uXRF map showing calcium in red, sulphur in green, and iron in blue. The overlap of calcium and sulphur results in an orange colour.K: uXRF map showing calcium in red, sulphur in green, and phosphorus in blue. The overlap of calcium and phosphorus results in a purple colour. L: uXRF map showing iron in red, sulphur in green, and phosphorus in blue. uXRF maps were collected by Dr. Michael Gazley (CSIRO).

Bollons Seamount phosphorite nodules contrast greatly to Chatham Rise nodules. Nodule TAN0307-var-83-1 is generally rounded, and flat in form. The rim consists of a smooth, vitreous brown mineral ~1-2 mm thick. The top surface has a rough, irregular and knobbly appearance with areas of creamy yellow and orange brown (Figure 4-26-b). Directly beneath the rough rim zone there is a 2-3 mm zone of a creamy yellow P and Ca rich mineral, with Fe-rich black inclusions (Figure 4-26-E). The core of the Bollons Seamount nodule is grey.

The internal structure consists of parallel laminations with gradational upper contacts, and sharp lower contacts. The interior is overprinted with Mn-Fe dendrites which radiate towards the interior of the nodule from the rim. The interior is also rich in P and Ca. SEM images show that the dominant assemblages in the interior are apatite + minor quartz + anorthoclase, and quartz + minor anorthoclase (Figure 4-26-F).

The apatite rich areas occur around the silicate rich areas, as seen in the top centre of the SEM image where a silicate grain has sharp edges, as do many of the silicate grains (Figure 4-26-F). The dendrites cross cut the silicate grains, as well as the apatite, indicating the dendrite formation is a later phase in the phosphorite nodule formation. An iron chloride/oxyhydroxide phase is observed to be randomly scattered on ~10-15 μm circular grains (Figure 4-26-F). This Fe phase is present either in contact with the Mn-rich dendrites, or within the apatite areas, rarely within the silicate rich areas.

A striking feature of sample TAN0307-var-83-1 in particular is the regular, parallel curved lines in the left of the nodule (Figure 4-26-A, C). This has only been observed in this nodule. This feature was not caused during the preparation of the sample, and the authenticity of this as a genuine feature is evidenced by dendrites propagating along the cracks.

Bollons Seamount Nodule

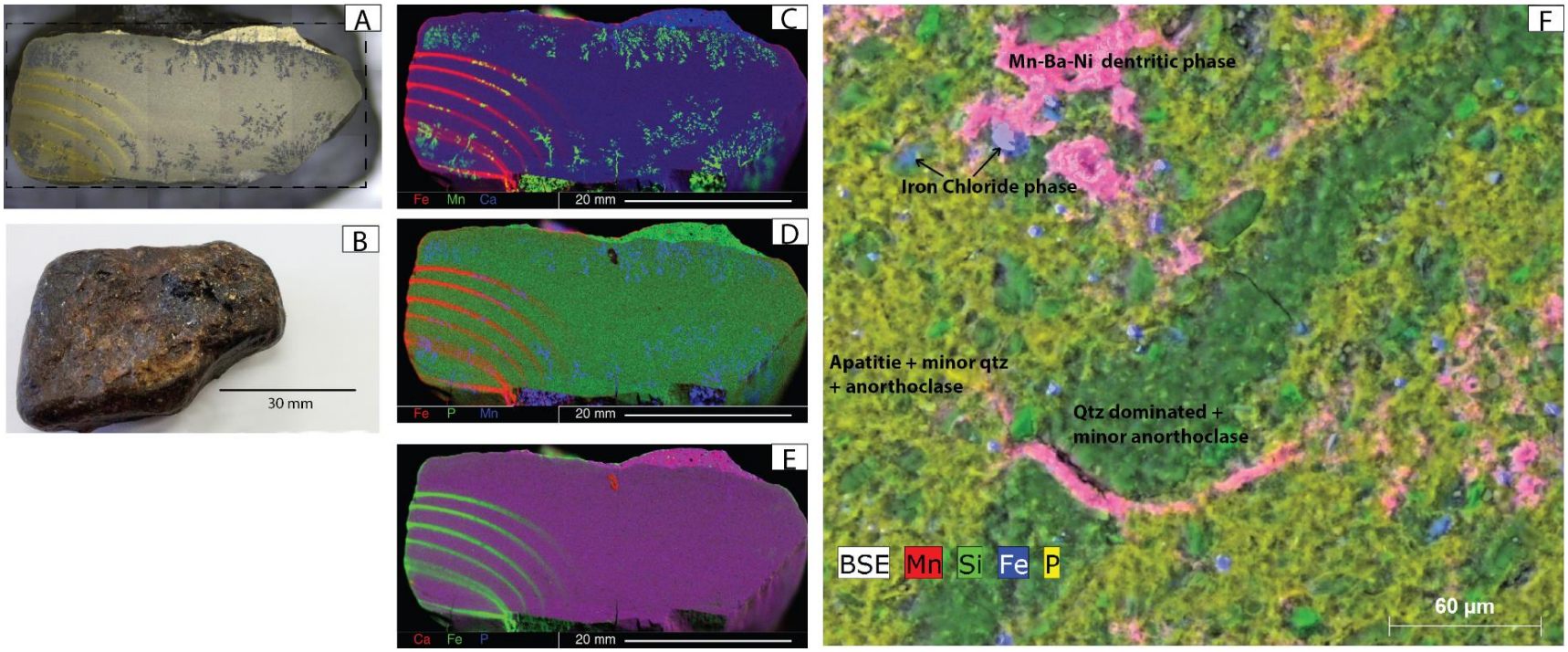

Figure 4-26 :uXRF maps and S.E.M. images of nodule TAN0307-var-83-1 .
A. Mosaic image of TAN0307-83-var1 collected by Dr. Michael Gazley (CSIRO). Dashed lines = scanned area. B: Photograph of the intact nodule exterior. C: uXRF map showing iron in red, manganese in green, and calcium in blue. D: uXRF map showing iron in red, phosphorus in green, and manganese in blue. E: uXRF map showing calcium in red, iron on green, and phosphorus in blue. The overlap of calcium and phosphorus results in a purple colour. F: S.E.M. image zoomed in on one of the dendrites. uXRF maps and S.E.M. images were collected by Dr. Michael Gazley (CSIRO).

4.7 Discussion

4.7.1 Phosphorite Formation

Two different models of phosphatisation processes leading to the formation of the Chatham Rise phosphorite nodules were proposed by Kudrass and von Rad (1984a); the direct uptake of P dissolved in seawater by the $CaCO_3$ component of the exposed chalk nodules, and the uptake of dissolved P by $CaCO_3$ pebbles buried in anoxic muds. The observation of minimal $\delta^{34}S$ fractionation, which would be expected if phosphogenesis occurred in reducing pore water with a high degree of bacterial activity, led Kudrass and von Rad (1984a) to favour a model of P uptake directly from seawater.

Since the 1980's more work has been done to understand the processes of phosphogenesis. The facilitation of phosphate deposit formation requires periods of minimal detrital sediment deposition, and high organic matter deposition between periods of strong current winnowing to concentrate the deposit (Section 2.3.4). Direct uptake of P from bottom seawater is highly unlikely to be the main mechanism of apatite precipitation, as supersaturation of P is unlikely to occur in these conditions (Section 2.3.3). Whilst the decomposition of organic matter, and the subsequent release of P has been accepted as the main mechanism behind P supersaturation in sediment pore waters, and hence apatite precipitation, this process is not exclusively associated with high Fe content e.g. glauconite mineral formation (Jarvis et al., 1994). Chatham Rise phosphorite nodules are considered to have high Fe content, with over 5x the content of average phosphorite (Li & Schoonmaker, 2014).

Froelich et al. (1988) proposed an iron pump model scenario to explain the mechanisms behind apatite precipitation. The iron pump model is based on direct sediment pore water measurements from the Peru continental margin where phosphogensis is active at present. In the iron pump model, there are three separate zones in the sediment profile where different chemical reactions result in the formation of different key minerals (Figure 2-1). μXRF maps of a selected typical Chatham Rise phosphorite nodule show the highest contents of K and Si reside in the rim zone of the nodule, along with some high contents of Fe. These elements are associated with glaucony and biogenic opal, previously described in petrographic studies (Kudrass & Cullen, 1982; Von Rad & Rosch, 1984).

In the iron pump model, glaucony and opal mineral formation is observed in the suboxic zone of the sediment profile, where Fe^{2+} and Fe^{3+} can co-exist, and biogenic opal can be dissolved and incorporated into glaucony minerals. A strong positive correlation between K_2O and SiO_2 (Figure 4-12, Figure 4-5-b) confirms their strong association. Mg^{2+} from seawater diffuses down the sediment profile and is also incorporated into glaucony minerals. Strong positive correlations between MgO and K_2O observed in Chatham Rise phosphorite nodules in this study support this mechanism (Figure 4-12, Figure 4-5-e).

Phosphorous is sourced primarily from the breakdown of organic matter, with minor amounts scavenged by iron oxyhydroxides from seawater (Figure 2-1). As FeOOH diffuses down from the oxic zone to the suboxic zone of the sediment profile, the P is released and supersaturation occurs, facilitating the precipitation of apatite.

The only moderate positive correlations of Fe with rim associated elements such as K_2O (Figure 4-5-c, Figure 4-12) indicates Fe could be associated with multiple mineral phases other than in the rim. The μXRF map of the typical Chatham Rise phosphorite nodule shows S channels overlap Fe in a few places in the apatite zone, and not in other places (Figure 4-24-C). S is also observed to overlap P in some places and not in others (Figure 4-24-K) indicating multiple phases incorporating S.

Petrographic studies have previously established that many Chatham Rise phosphorite nodules contain both goethite, an iron oxyhydroxide, and pyrite spherules in the outer zones of the nodules (Von Rad & Rosch, 1984). The iron pump model also explains the formation of pyrite whereby iron in the anoxic section of the sediment profile is reduced and reacts with H_2S to form pyrite. The formation of Fe oxyhydroxides, as goethite in Chatham Rise phosphorite nodules, is also explained by the oxic zone of the sediment profile migrating downwards. This would cause the oxidation of pyrite and precipitation of oxyhydroxides (goethite) (Morse, 1991), as previously suggested by Von Rad & Rosch (1984).

The iron pump model also proposes that the sediment profile is not a closed system. Seawater from the water column is still able to slowly diffuse through the different sediment layers. This could explain why Sr isotope ratios are not appropriate for age determination as the ratios are consistently reset (Rao et al., 2008), resulting in anomalously young ages e.g. ages for Chatham Rise phosphorite nodules from McArthur and Walsh (1984). This could also

explain the minimal $\delta^{34}S$ fractionation observed by Kudrass and von Rad (1984a); there was some dilution of sediment pore by diffusing seawater.

Bollons Seamount phosphorite nodules display evidence of a very different formation history relative to Chatham Rise phosphorite nodules. The core of the nodules show that the precursor material was eroded and re-deposited volcanic, anorthoclase rich (Figure 4-26) and possibly previously formed phosphorite nodules that had been eroded. This precursor was then lithified, and most likely broken up into smaller flat pebbles by similar erosional current processes as Chatham Rise phosphorite nodules were during the Oligocene-Miocene.

A primarily P rich mineral observed beneath the nodule crust indicates a period of phosphogenesis occurred between the erosion of the precursors, and the formation of the Mn-Ba rich crust and dendrites. Bulk REE analysis shows that Bollons seamount nodules are characterized by REE enrichment, and a negative Ce anomaly (Figure 4-16), in which case the Mn crust is most likely not a hydrogenous accumulation, as they are characterized by a positive Ce anomaly (Maynard, 2014), assuming the crust is the main contributor of REE to the bulk chemistry. Generally, negative Ce anomalies are characteristic of Mn crusts that have formed from hydrothermal fluids (Maynard, 2014). To fully decipher the conditions of Mn crust formation, and hence interpret the environment, the specific mineralogy and chemistry of the Mn crust and dendrites must be known (Maynard, 2014). This would require further study, including X-ray diffraction analysis and trace element analysis of the crust only, which is beyond the scope of this study.

4.7.2 Diagenesis of Phosphorite Nodules

Inferences from Rare Earth behaviour

Phosphorite deposit REE patterns can give insights into their redox and diagenetic conditions, which can aid in the understanding how trace metals are enriched, e.g. U.

Phosphorite deposits can display a variety of REE patterns. The two most characteristic are those with a similar pattern to seawater, and those with concave down patterns. In general, older, weathered phosphorites display a concave down pattern, whereas younger post Jurassic phosphorites tend to display seawater patterns (Jarvis et al., 1994; Shields & Stille, 2001). Weathering and diagenetic alteration causes the fractionation of MREE from LREE

and HREE resulting in a concave down pattern (Jarvis et al., 1994; McArthur & Walsh, 1984).

If a seawater pattern is observed, it suggests that either quantitative uptake of preconcentrated REE through biological input or adsorption and desorption from oxyhydroxides has occurred, resulting in minimal fractionation of REE, thus 'preserving' the seawater REE pattern (Gadd et al., 2016; Reynard et al., 1999), or that REE have been scavenged from other dissolved phases such as biologically derived calcite or silica (McArthur & Walsh, 1984). In type 1, replacement nodules, such as the nodules found on Chatham Rise, very low quantities of REE are inherited from the carbonate precursor (McArthur & Walsh, 1984).

All phosphorite nodules in this study display seawater patterns (Figure 4-16) as previously observed in Chatham Rise nodules by McArthur and Walsh (1984). The lack of a concave down pattern also supports the conclusion by Cullen (1987) that Chatham Rise phosphorite nodules were not subjected to subaerial weathering, as previously suggested by Pasho (1976). Thus, incorporation of REE is most likely to have occurred early in diagenesis, mostly from adsorption to crystal faces, with only minor substitution into the crystal lattice of mineral phases present in the nodules. Light to middle, and heavy REE ratios normalised to the North American Composite Shale (NASC) also support this interpretation.

$(La/Yb)_{SN(NASC)}$ ratios are relatively unaffected by REE substitution into crystal lattices, and display values similar to that of modern seawater, where adsorption is the main mechanism of REE incorporation (Reynard et al., 1999). $(La/Yb)_{SN(NASC)}$ ratios are; however, fractionated by the preferential adsorption of LREE relative to HREE to crystal faces (Reynard et al., 1999). $(La/Sm)_{SN(NASC)}$ ratios are unaffected by adsorption, but greatly altered and increased.

All nodules in this study display $(La/Sm)_{SN(NASC)}$ values greater than >1 (Figure 4-27). $(La/Sm)_{SN(NASC)}$ values <0.3 indicate intense fractionation during prolonged diagenesis whereby MREE are preferentially substituted into the crystal lattice (Lécuyer et al., 2004), resultant in concave down REE patterns (Reynard et al., 1999). The high $(La/Sm)_{SN(NASC)}$ ratios in this study indicate very little alteration via substitution of REE has occurred (Lécuyer et al., 2004).

The majority of nodule samples have $(La/Yb)_{SN(NASC)}$ values >1 (Figure 4-27-a), i.e. enrichment of LREE compared to HREE (Gadd et al., 2016). However, all samples have $(La/Yb)_{SN(NASC)}$ ratios below 2.5, which indicates only minor adsorption during early diagenesis (Reynard et al., 1999).

A combination of both adsorption and substitution mechanisms of REE incorporation are therefore required to explain the full variation observed by nodules studied here, with adsorption being the most dominant mechanism, especially for Bollons Seamount samples (Figure 4-27-a). However, the ratios are still close to modern seawater and the REE display seawater patterns, indicating the REE signature has been preserved with very little diagenetic alteration and fractionation. Excluding Bollons Seamount samples, there appears to be a very weak size dependant trend (Figure 4-27-b).

The majority of large sized nodules have lower $(La/Yb)_{SN(NASC)}$ and $(La/Sm)_{SN(NASC)}$ ratios, whereas nodules from smaller size fractions cluster around higher $(La/Yb)_{SN(NASC)}$ and $(La/Sm)_{SN(NASC)}$ ratios. Smaller Chatham Rise nodules have a higher relative ratio of glaucony rim minerals to core minerals and vice versa. This indicates that both LREE and HREE could both be enriched in the rim minerals relative to core minerals with a higher degree of adsorption and substitution.

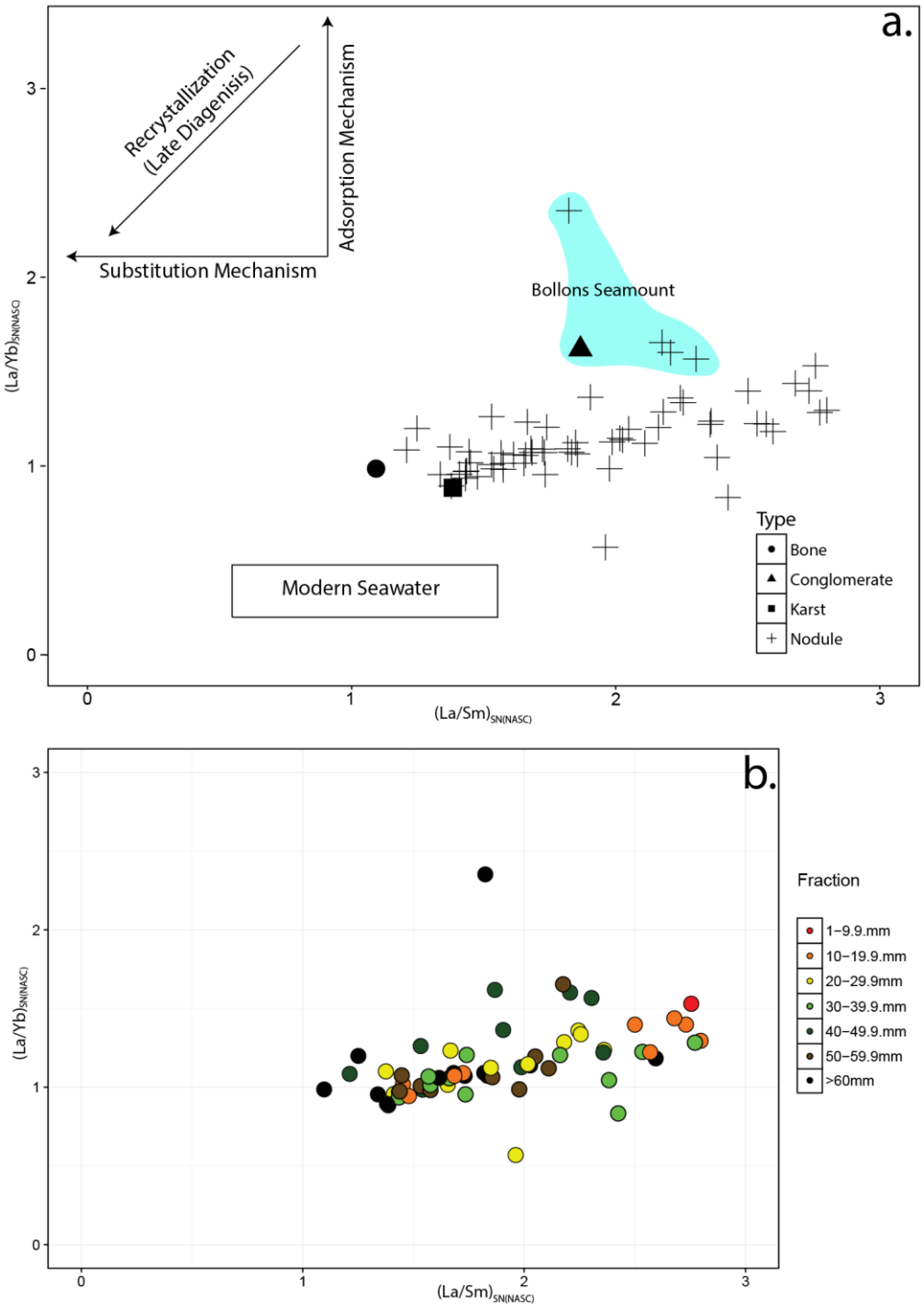

Figure 4-27: La/Sm versus La/Yb ratios.
Samples were normalised to NASC to maintain consistency with Lécuyer et al. (2004), Gadd et al. (2016), and Reynard et al. (1999) to aid in interpretation. NASC values from Gromet et al. (1984). Mechanism trajectories after Reynard et al. (1999) and Gadd et al. (2016). a: Substitution mechanism trajectory represents substitution of MREE into the apatite crystal lattice. Adsorption trajectory represents adsorption of LREE in preference to HREE during early diagenesis. Recrystallization trajectory is representative of late diagenetic recrystallization.

Cerium and europium anomalies as paleo-redox indicators

Every phosphorite sample in this study, irrespective of location, displays a negative Ce anomaly (Figure 4-16). This is similar to seawater, which has a negative cerium anomaly due to the oxidation of Ce^{3+} to the insoluble Ce^{4+} state in the upper, oxygenated water column. Ce^{4+} is readily scavenged from the water column by sorption to Fe and Mn oxyhydroxides (Elderfield & Greaves, 1982).

Even though all samples display negative Ce anomalies when normalised to PAAS, they also display various degrees of La enrichment. The accepted convention of calculating anomalies, that is, the relative difference between the actual and calculated theoretical value, is to use the geometric mean of the two nearest neighbours, which for Ce includes La. The underlying assumption is that those neighbouring elements are not anomalous. In this case, this assumption may not hold true.

A method has been developed by Bau and Dulski (1996) to validate Ce anomalies using $(Ce/Ce^*)_{SN(PAAS)}$ and $(Pr/Pr^*)_{SN(PAAS)}$. This method has been applied to sedimentary apatite by Gadd et al. (2016). Generally, Pr and Nd are not expected to be fractionated by any reasonable process in the marine environment. A negative Ce anomaly will result in $(Pr/Pr^*)_{SN(PAAS)}$ being >1. If a positive La anomaly is responsible for an apparent negative Ce anomaly, then $(Ce/Ce^*)_{SN(PAAS)}$ will be <1, and $(Pr/Pr^*)_{SN(PAAS)}$ will be close to 1.

$Ce/Ce^*)_{SN(PAAS)}$ and $(Pr/Pr^*)_{SN(PAAS)}$ in this study were calculated using the geometric mean of PAAS normalised data in order to make the plots comparable to Bau and Dulski (1996), using the following equations from Gadd et al. (2016):

$$Equation\ 3.\ Ce/Ce^* = Ce_N/(La_N * Pr_N)^{0.5}$$

$$Equation\ 4.\ Pr/Pr^* = Pr_N/(Ce_N * Nd_N)^{0.5}$$

All of the nodule samples from this study fit within the IIIB field, indicating that the Ce anomaly calculated is not a result of anomalously enriched La (Figure 4-28-a). A very weak trend with size fraction, $(Ce/Ce^*)_{SN(PAAS)}$, and $(Pr/Pr^*)_{SN(PAAS)}$ is observed in Figure 4-28-b.

Larger nodules in the 40-60 mm fractions generally display higher $(Pr/Pr^*)_{SN(PAAS)}$ and lower $(Ce/Ce^*)_{SN(PAAS)}$ anomalies. However, samples from the larger size fractions are also observed to have low $(Pr/Pr^*)_{SN(PAAS)}$ and higher $(Ce/Ce^*)_{SN(PAAS)}$. The degree of fractionation of Ce, and hence how negative the anomaly is, depends on the degree of oxidation of Ce. Smaller nodules display a weak trend of less fractionation of Ce relative to the larger nodules fractions. For Chatham Rise nodules there is a higher relative quantity of rim minerals relative to core minerals in smaller size fractions. This indicates that Ce associated with the glaucony rim minerals was exposed to an environment with less oxygenation than the core minerals. This supports the finding from section 4.7.1 that the glaucony rim minerals formed in more suboxic conditions.

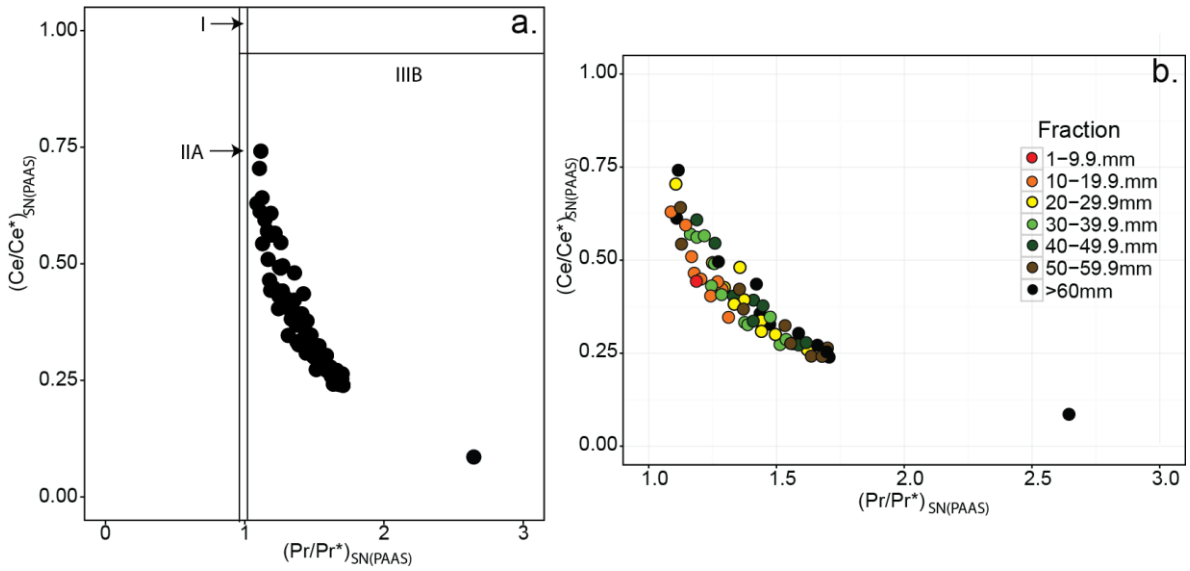

Figure 4-28:Nodule Pr and Ce anomalies normalised to PAAS.
a: Determination of the influence of La in Ce anomaly calculations. Fields from Bau and Dulski (1996). B: Ce and Pr anomalies by sample size fraction.

Previous studies have used negative Ce anomalies to interpret the paleo-redox conditions of local diagenesis, where negative anomalies indicate oxygenated interstitial sediment pore water (e.g. (Gadd et al., 2016; Joosu et al., 2015; Pattan et al., 2005; Shields & Stille, 2001)). However, other studies conclude that a negative Ce anomaly is simply inherited from the seawater when pore waters are in equilibrium during early diagenesis, preserving bottom

water signatures (e.g. (Pattan et al., 2005; Shields & Stille, 2001)). Ce can also be released into interstitial sediment pore waters by the dissolution of calcite and silica of a biogenic origin, which can result in negative Ce anomalies independent of the redox state of the sediment (McArthur & Walsh, 1984). Additionally, Ce may also be sourced from multiple mineral phases, as observed by moderately strong correlations between TiO_2, Al_2O_3, K_2O and Ce, which also display two different trends (Figure 4-15), indicating Ce may indicate different processes in different samples from different localities.

Strong correlations occur between Al_2O_3, K_2O, SiO_2 and Ce in Chatham Rise phosphorite nodules (Figure 4-15). The size dependant trend between K_2O, and Ce and Pr indicates that REE are strongly associated with the glaucony rim minerals. Further, smaller phosphorite nodules have a higher enrichment in REE than larger nodules (Figure 4-17), reflecting their higher ratio of glaucony minerals to core minerals. These observations suggest that for the majority of phosphorite nodules on Chatham Rise, REE are associated with the glaucony rim minerals. There are; however, some exceptions. There is a second, minor trend whereby samples from sites G35, H959, A904, and H959 are more enriched in Ce and Pr than other sites. Despite the high REE enrichment, it is demonstrated that nodules from site G35 still follow a nodule size dependant trend whereby the smallest nodule has the highest enrichment of REE, and vice versa (Figure 4-17). Diagenesis in the suboxic zone of the sediment profile could have persisted longer at these sites, leading to higher enrichment in REE during rim mineral formation or material previously enriched in REE could have been incorporated into the nodule precursor material.

Thus, it is the rim minerals that are most likely influencing the Ce contents of the bulk of Chatham Rise samples. These rim mineral phases have 50 times more Ce content than the core of the phosphorite nodules (Walsh, 2009). In the case of Bollons Seamount samples, bulk REE contents are influenced by the Mn rim, which is very effective at REE scavenging (McArthur & Walsh, 1984).

The formation of glaucony minerals require a suboxic environment and low sedimentation rates (Section 2.3.3). Therefore, the conditions of formation could not have been purely oxic during formation of the rim minerals, but were more likely to have been suboxic. REE have also been found to be enriched in reducing or suboxic sediment pore waters (Elderfield &

Sholkovitz, 1987), which could potentially explain why the rim of the nodule is far more enriched compared to that of the core. It is suggested then, that the glaucony rim of the Chatham Rise phosphorite nodules formed in the suboxic zone of the sediment profile (Section 4.7.1), where oxygenated seawater is still able to diffuse. In this environment, the negative Ce anomaly of seawater could be preserved during diagenesis.

The New Zealand offshore phosphorites all exhibit negative europium anomalies ($Eu/Eu^*_{SN(PAAS)} < 1$) (Figure 4-29) where $Eu/Eu^*_{SN(PAAS)}$ is calculated using the following equation from Gadd et al. (2016):

$$Equation\ 5.\ Eu/Eu^* = Eu_N / (Sm_N^{0.33} \times Tb_N^{0.67})$$

After Ce, Eu is the only other redox sensitive REE. It can exist in either a divalent or trivalent state in nature. The 3^+ trivalent state is the most stable in seawater. However, Eu^{2+} has a similar ionic radii to Sr^{2+} and can readily substitute into mineral phases in place of Sr (Shields & Stille, 2001). Seawater inherently has a negative Eu signature, with the strongest negative anomalies observed at depths of 100-600 mbsl (Elderfield & Greaves, 1982; Shields & Stille, 2001). Positive Eu anomalies in seawater can result when the sediment pore waters are reducing, or under the influence of highly acidic and high temperature (>200°C) hydrothermal activity causing the reduction of Eu^{3+} to Eu^{2+} (Joosu et al., 2015).

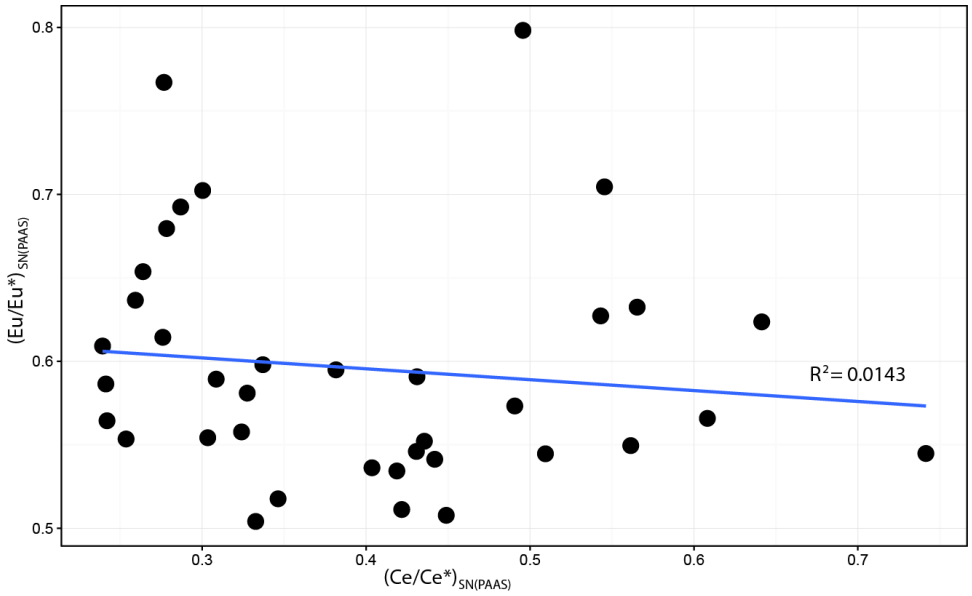

Figure 4-29: Ce vs Eu anomalies.

Phosphorite nodules can acquire negative Eu anomalies from inheriting the seawater signature whilst sediment pore water was still in equilibrium with the water column, or from the dissolution of minerals with existing negative Eu anomalies during diagenesis (Shields & Stille, 2001). In very rare and exceptional cases negative Eu anomalies can result from hydrothermal fluids: Eu anomalies of phosphorite nodules are therefore unreliable proxies for hydrothermal input during formation (Shields & Stille, 2001).

Eu and Ce anomalies in NZ phosphorites show no systematic relationship (Figure 4-29), indicating that the cause of the anomalies for these elements were not coeval secondary processes (Shields & Stille, 2001). The simplest explanation for the observed negative Eu anomalies in Chatham Rise and Bollons Seamount samples is preservation of the Eu signature from the sediment pore water, which inherits its anomalies from the water column. This is consistent with the overall seawater REE pattern observed in all samples in this study.

Other paleo-redox markers

The enrichment of other elements in marine phosphorite nodules can be indicative of redox conditions at the time of deposition. Additional ones include U, V, Ch and Cu.

Authigenic U content can be used as a paleo-redox proxy. In oxic water uranium exists as the highly soluble species U^{6+}, conversely in anoxic conditions U predominates in the U^{4+} state. U^{4+} is highly particle reactive, and will sorb to sediments and organic particulates within the sediment profile (Pattan et al., 2005; Wignall & Myers, 1988). If authigenic U is < 5 ppm, then deposition/ diagenesis occurred in an oxic environment (Jones and Manning (1994). Authigenic uranium content can be calculated using an equation by Wignall and Myers (1988):

Equation 6. Authigenic U= total U-Th/3

Chatham Rise nodules, including bone texture and duricrust samples, have calculated authigenic U contents between 17 – 639 ppm, indicating anoxic conditions during uranium enrichment. This is consistent with previous studies where 60-86 % of the total uranium in each individual Chatham Rise phosphorite nodule is U^{4+} (Kolodny & Kaplan, 1970), supporting anoxic conditions of U enrichment (Kudrass & Von Rad, 1984a).

It is possible that nodules at different localities spend different periods of time in the anoxic zone of the sediment profile, resulting in the wide range of calculated authigenic U contents. Another possibility is a higher supply of organic matter at different localities. This could result in different concentrations of U available in the interstitial pore water (Starinsky et al., 1982). Cullen (1987) suggested that the oxic zone of the sediment profile on Chatham Rise migrated downwards below the depth of the *in situ* phosphorite nodules, causing active phosphogenesis to cease. Therefore, it is likely that if the anoxic area of the sediment profile migrated upwards, the phosphorite nodules within this section of the sediment profile would experience U enrichment.

Uranium does not show any correlation with major or trace elements, or nodule size fraction in Chatham Rise phosphorite nodules (Figure 4-12). Geographically, there is no strong pattern to U enrichment in the Chatham Rise phosphorite nodules. Nor do different size

fractions from the same site display a clear trend of U enrichment relative to nodule size in this study, despite Von Rad and Rosch (1984) observing a higher median U content in nodules > 8 mm. One reason for this observation could be that U is associated with multiple mineral phases and organic material, or has adsorbed onto the crystal faces (Jarvis et al., 1994).

As enrichment depends on localized diagenetic conditions, areas that had nodules for longer periods of time in the anoxic zone of the sediment profile would have extended periods of time to incorporate U from the pore water. Since the phosphorite formation requires phosphogenesis and winnowing processes to occur repeatedly (Filippelli, 2011), conditions across the Chatham Rise would have changed regularly, and local conditions may have resulted in some areas being suited for U enrichment in some cycles, and not during others, which could add to the perceived random distribution of U enrichment. Indeed, Kudrass & von Rad (1984a) previously concluded that multiple episodes of phosphatisation had occurred in the Late Miocene on Chatham Rise, evidenced by the varying degree of phosphatisation of nodules found at the same site, as a result of new chalk pebbles being phosphatised each episode.

In contrast, Bollons Seamount nodules have a lower authigenic U content range of 5- 19 ppm at site TAN0307-83, and 11-12 at site TAN0307-82. Therefore, according to the interpretations of Pattan et al. (2005) and references therein, U enrichment in Bollons Seamount nodules is likely to have occurred in more suboxic conditions. This estimation; however, may not be reliable, as the formation history of the Bollons seamount nodules is complex as evidenced by uXRF and SEM mapping (Section 4.6). The authigenic U could have been inherited from another phase, rather than authigenically formed in their present environment.

A major limitation that could lead to inaccurate estimates of authigenic U is that *Equation 6* is developed for the use in mud rock sediment types (Wignall & Myers, 1988), not phosphorite nodules, despite Pattan et al. (2005) applying this method to sediments containing a substantial amount of authigenic phosphate.

The use of V/Cr, and Cu/ Zn ratios to determine paleo-redox conditions in sediments, examined by Pattan et al. (2005), were not applicable to this study. Only very weak or no

correlations of V and Cu with major and other trace elements indicates these elements most likely exist in multiple phases (Figure 4-12), leading to highly variable and unreasonable results. Therefore, the application of these paleo-redox indicators on the bulk contents of these elements is inappropriate, as it is evident that the nodules have experienced a variety of redox conditions during their formation history.

4.7.3 Detrital components in nodule formation

Chatham Rise phosphorite nodules show very low contents of Al_2O_3 and Th (Figure 4-30). These elements are enriched in detrital sediments, thus low contents of these two elements suggests very little detrital input into the carbonate precursors to the Chatham Rise phosphorites (Rao et al., 2008), consistent with previous observations by Von Rad and Rosch (1984) and Pasho (1976). By contrast, Bollons Seamount nodules have higher Al_2O_3 and Th contents than Chatham Rise nodules, bone texture nodules, and duricrust nodules (Figure 4-30).

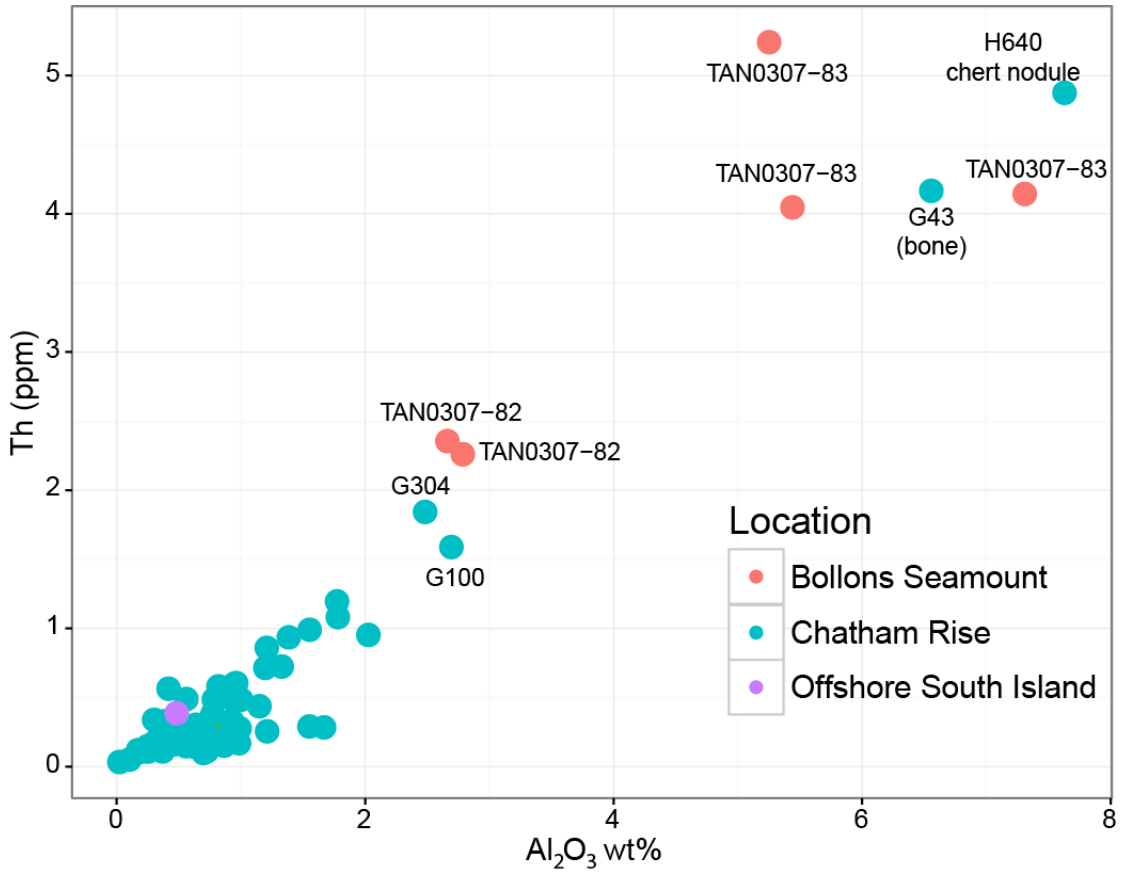

Figure 4-30: Bivariate plot of Al_2O_3 and Th to determine detrital sediment content.

The Bollons Seamount nodules do not contain a glaucony rim like the Chatham Rise nodules, which is where Al_2O_3 is concentrated in the Chatham Rise nodules. The Bollons Seamount nodules do; however, have anorthoclase present, as observed on SEM images (Figure 4-26).

Bollons Seamount K_2O and Al_2O_3 ratios trend towards anorthoclase composition, whereas the Chatham Rise nodules K_2O and Al_2O_3 ratios trend towards that of glauconite (Figure 4-31). This further indicates that when the precursor sediments to Chatham Rise phosphorite nodules were deposited, there was very little input from terrigenous sedimentation, whereas Bollons Seamount nodules may have had a significant influence from volcanic derived sediments, specifically the incorporation of anorthoclase into the nodule matrix.

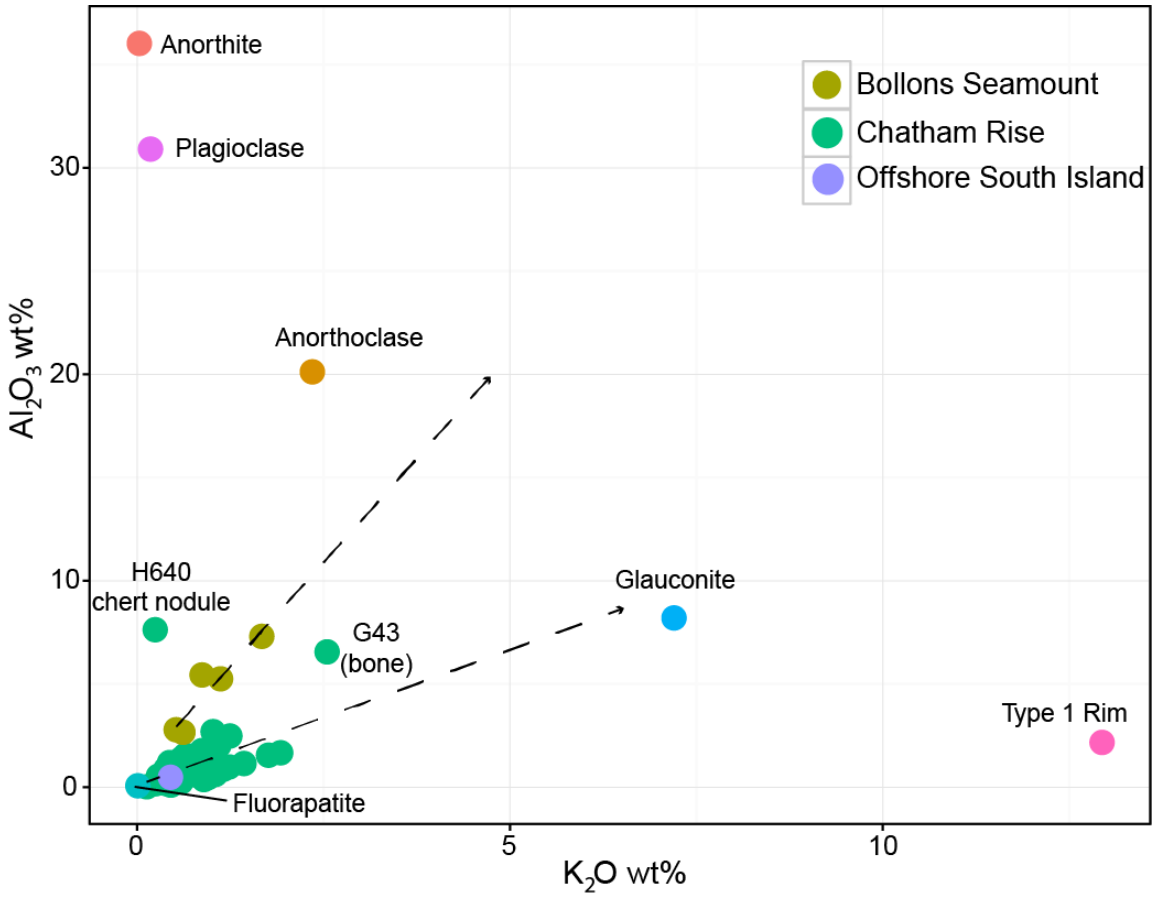

Figure 4-31: Al_2O_3 vs. K_2O for Chatham Rise and Bollons Seamount phosphorite nodules. Type-1 Chatham Rise nodule rim composition from Walsh (2009). Standard compositions for anorthite, anorthoclase, fluorapatite, and plagioclase from Jarosewich et al. (1980). Chatham Rise sediment glauconite composition from Lawless (2012).

4.7.4 The distribution of elements in nodules

Elemental distribution within nodules

The major element chemistry of the Chatham Rise phosphorite nodules varies with nodule size. Contents of K_2O, Al_2O_3, TiO_2, Fe_2O_3, SiO_2 and MgO decrease with an increase in nodule size. Conversely, MnO and CaO contents increase with increasing nodule size.

These trends have been observed previously by Von Rad and Rosch (1984). However, a key difference compared to this study is the size fractions of the samples analysed. Over half of the bulk samples analysed by Von Rad and Rosch (1984) were in the small 1-8 mm size fraction, whereas the majority of Chatham Rise phosphorite nodules analysed in this study are large from 10 mm to > 60 mm. Despite the difference, the relative major element chemistry trends are maintained between the two datasets, except for P_2O_5 and CaO.

The relationship between the nodule size and major element contents is due to the relative amounts of the main mineral phases stemming from the concentric mineral zonation (Von Rad & Rosch, 1984). In smaller nodules, there is a greater proportion of the glaucony rim mineral phases and crystalized apatite relative to the weakly phosphatized/ carbonate core of the nodule. Conversely, larger nodules have a smaller proportion of glaucony rim and apatite phases relative to the weakly phosphatized/ carbonate chalk core.

uXRF maps of typical Chatham Rise phosphorite nodule G221 show K_2O and SiO_2 dominate in the rim zone of the nodule (Figure 4-24). K_2O is observed to occupy some of the P rich zone as well. Fe is found dominantly from the rim of the nodule and part way into the P rich zone. Fe is also patchy in distribution. P_2O_5 is heavily concentrated in a zone between the rim and core of the nodule, along with Ca. Ca is heavily concentrated in the core with minor amounts of P_2O_5. The distribution of these elements in the nodule fits with the concentric zoning previously observed in Chatham Rise phosphorite nodules by Von Rad and Rosch (1984). The K_2O and SiO_2 zone is associated with the glaucony rim and biogenic opal, and grades inward into the apatite zone. Fe is associated with both goethite and the glaucony rim phases, as indicated by a patchier distribution between the rim and apatite zones. P is strongly associated with the apatite phase, which is observed to grade inwards towards the core, as

observed previously by Von Rad and Rosch (1984). The highest contents of Ca are found in the core of the nodules as a weakly phosphatized/ carbonate chalk phase.

Strong to moderate correlations between K_2O and SiO_2 were observed with MgO and Fe_2O_3 indicating they are also major phases incorporated into the glaucony rim minerals. Trace elements Rb, Cs, Ga, Ce, Sc, Nb and Hf have strong to moderate correlations with K_2O, and SiO_2 indicating they are also associated with the glaucony rim minerals. Previously, SiO_2, Al_2O_3, K_2O, Ni, Rb, MgO, Zn, Y, TiO_2 and Fe_2O_3 have been found to be associated with the rim minerals in Chatham Rise phosphorite nodules (Von Rad & Rosch, 1984).

The positive correlations between CaO, Sr and LOI observed in this study are associated with the carbonate core of the nodule. LOI and CaO have previously been interpreted as being associated with calcite (Von Rad & Rosch, 1984). CaO displays negative correlations with elements associated with the rim minerals; Rb, Nb, Cs, MgO, Al_2O_3, Ga, SiO_2 and K_2O. This indicates that these elements are not found in the core of the nodules in any significant amount. P_2O_5 demonstrates a lack of correlations with all other major and trace elements, apart from a weak – moderate positive correlation with Zn. A lack of correlation with other elements can indicate that P_2O_5 exists in multiple mineral phases other than apatite in the apatite zone of the nodule. The μXRF maps did not indicate any other areas of the nodule with a strong P_2O_5 signal, apart from small spots in the core of the nodule.

Geographic distribution of elements in nodules

Samples from some sites display enrichment in metals such as Ba, V, Co, Ni, Cu, Zn, Y, Cd and Pb, relative to other phosphorite nodules sampled from Chatham Rise in this study. The physical appearance of these nodules does not give any indication of a cause for the higher contents of metals. Nodules from sites G35, E79, A904, G121 and H959 are enriched in Ba, Ni and Co relative to other Chatham Rise phosphorite nodules, and trend towards contents observed in the Bollons Seamount nodules (Figure 4-14). This enrichment coincides with clear spatial differences in chemistry from different sites. Differences in local diagenetic conditions, different precursor carbonate units, or site specific incorporation of different mineral phases could contribute to differing chemistry on a local scale.

The precursor carbonate pebbles may have spent different amounts of time at different levels in the sediment profile, there may have been differing quantities of organic matter available, differing contents of Fe which would have changed the effectiveness of the iron pump for elements other than P. Additionally, there may have been different quantities of erratics or volcanic material in the surrounding sediments, altering the dissolved metals available in the sediment pore fluids.

Volcanism was active on the Chatham Rise starting in the early Palaeocene and persisting through the Late Eocene to the Early Oligocene (Timm et al., 2010). Volcanic features have been observed across the entirety of the Chatham Rise (Wood et al., 1989), including, but not limited to, the Veryan Bank, Urry Knolls, the Graveyards, and Eastern Chatham Rise. Volcanic material has previously been found associated with recent Chatham Rise sediments, especially sediments from the Palaeocene to the Middle Eocene (Figure 3-2). Some nodules have been reported to contain phillipsite, a mineral formed from the alteration of basaltic glass in the marine environment, filling pitts in nodule rims (Von Rad & Rosch, 1984). Thus, it is possible that volcanic activity could have had a site-specific effect on bulk chemistry through either enrichment from dissolution of volcanic derived minerals in sediments, or incorporation into the nodule precursor chalk, e.g. Ba, Ni, Co, Cd and REE in samples from site G35 which is located approximately 150 km northeast of Veryan Bank (Figure 4-21).

If volcanic material was the cause for chemistry variation, it would be expected that the REE patterns would display a positive Eu anomaly, as Eu^{2+} stable and enriched in early magmatic minerals such as plagioclase (Shields & Stille, 2001). However, all samples in this study display seawater REE patterns with negative Eu anomalies, irrespective of site location or nodule type. The nodules with trace metal enrichment are generally more enriched in REE content as well, trending towards contents seen in nodules from Bollons Seamount.

A further potential control on nodule chemistry would be differences in nodule precursor substrate. For example, the core nodule material in typical Chatham Rise nodules is a mixture of Early to Late Oligocene limestone, reworked with some Eocene material (Section 3.5). In contrast, the Bollons Seamount phosphorite nodules display more enrichment in the transition metals relative to the average upper crust than the Chatham Rise nodules (Figure 4-9) most likely due to not only a Mn crust, but different precursor material, such as

anorthoclase incorporated into the core. Chatham Rise samples that are similarly enriched to Bollons Seamount nodules (e.g. in Co, Ni, Ba) could have incorporated similar material. An SEM image of the enriched samples would be required to confirm this.

High Ba contents >1000 ppm have previously been observed in phosphorites, and were attributed to high organic matter flux from high paleo productivity (Mazumdar et al., 1999). Cu and Zn are also essential metals in aquatic biota (Australian and New Zealand Environment Conservation Council, 2000b), therefore, a very high organic matter flux, coupled with lower erosive current action in some areas could allow higher contents of Cu and Zn to be released into the interstitial pore water, leading to enrichment in phosphorite nodules in certain localities.

4.8 Geochemical considerations for use as a phosphate fertilizer

The lack of a need for extensive processing is an advantage of Chatham Rise nodules over other phosphate fertilizer products currently used in New Zealand. Processing of phosphorite into fertilizer can concentrate potentially toxic metals such as Cu, Ni, U, and Zn (Abed et al., 2008). Previous glasshouse experiments have demonstrated that Chatham Rise phosphate in both powder and pelletized form break down and dissolve more slowly than single super phosphate, and performance was overall comparable to single superphosphate as far as P availability was concerned (Mackay et al., 1980).

Relative to other sources of marine derived phosphate rock (Table 4-1) Chatham Rise nodules have lower Cd and Th. Conversely, Chatham Rise phosphorites have much higher average Ni and U, and up to 2x the Zn content. All other trace metals for which comparative data is available show the average Chatham Rise nodule contents are within the same range of other deposits used as fertilizers.

Compared to previous trace element analyses by Von Rad and Rosch (1984) (Table 4-1) average Chatham Rise phosphorite contents from this study are within the same range (including data for both 1-8mm and >8mm size fractions) for Co, Cr, Cu, Mo, Pb, and V. The range for Co, Cr, Pb, U and V is higher in this study. Mo and U have lower averages than previous analyses. It is important to note that advancements in improved analytical

precision and lower detection limits for trace element analysis have been made since the 1980's.

The offshore South Island nodule has lower average Cd, Mo, Pb and Th contents compared to other phosphate deposits. Contents of Cs are higher relative to other deposits that data is available for (Table 4-1). All other metals compared are within the range of other global phosphate deposits. Currently, the extent and economic potential of the deposit from which the offshore South Island phosphorite nodule originates is unknown as this is the first reported sample from the area. This could be part of a larger deposit associated with Snares Depression phosphorite deposits reported by Summerhayes (1967).

Bollons Seamount nodules have on average 12x less U than Chatham Rise nodules whilst containing similar P content. However, they are far more enriched in transition metals (Table 4-1). The Bollons Seamount nodules have lower contents of Mo, Cd and U relative to other comparable deposits (Table 4-1), but much higher contents of Co, Cs, Cu, Ni and Pb. All other trace metal contents compared are within the ranges of other phosphorite deposits. Co and Cu are essential trace elements for both plants and animals, and are currently deficient in New Zealand soils (Fert Research & AgResearch, 1999). The enrichment of Cu and Co, coupled with low U contents in Bollons Seamount nodules could be an advantage if the deposit were to be considered economically.

The low Cd content of Bollons Seamount, offshore South Island, and Chatham Rise phosphorite nodules is favourable for the potential use as a direct application fertilizer (Chatham Rock Phosphate Limited, 2014), as the application of Cd rich fertilizer and their subsequent enrichment in New Zealand soils is a known issue limiting current fertilizer use (Section 1.5). U contents in Chatham Rise nodules are highly variable, but on average much higher than other phosphate sources (Table 4-1).

Like Cd, U has also been accumulating in New Zealand soils following the repeated application of phosphate fertilizers. The majority of phosphate fertilizers applied to New Zealand soils from 1950 – 1980 originated from insular deposits from Nauru and Christmas Island, and contained U contents ranging from 31-121 ppm (Taylor 2007, and references therein). The U in the phosphates applied to acidic soils in New Zealand strongly sorbs to clays, carbon, and oxyhydroxides, thus is not significantly taken up by plants or leached into

waterways, resulting in very low risk of elemental uranium entering the human food chain (Taylor, 2007).

Taylor (2007) concluded that U accumulation was less of a concern at present than in the 1950's- 1980's as the U content of fertilizers had decreased. However, Chatham Rise phosphorite nodules are relatively high in U without processing (average U content in fertilizers measured in Taylor (2007) was 22 ppm versus 152 ppm average in the Chatham Rise nodules in this study), therefore could cause further long-term U accumulation in soils. The timeframe of U build up is, however, very slow. Phosphate applied to New Zealand soils from 1954-1975 had a U content of 42 ppm (Taylor, 2007). The highest accumulation rate measured in New Zealand soils, 0.047 $\mu g\ g^{-1}\ a^{-1}$, would theoretically take up to 563 years to exceed the United States Nuclear Regulatory Commission guideline of 30 ppm according to Taylor (2007). Soil leach testing using Chatham Rise phosphorites would be required to confirm this.

Country	As	Cd	Co	Cr	Cs	Cu	Mo	Study
Algeria	4.0	-	0.4	208.0	-	-	-	Pantelica et al (1997)
Aqaba, Jordan	5.0	3.0	-	15.0	-	3.0	-	Al-Hwaiti et al (2010)
Bayovar–Sechura ,Peru	14.3	17.3	15.4	134.0	-	17.0	30.4	Bech et al (2010)
Eshidiya, Jordan	9.0	1.0	-	8.0	-	4.0	-	Al-Hwaiti et al (2010)
Florida (NIST120c)	5.0	8.8	8.0	68.0	-	13.0	13.3	Jochum et al (2005)
Israel	4.8	-	0.4	56.0	-	-	-	Pantelica et al (1997)
Morocco	12.4	-	0.48	291	-	-	-	Pantelica et al (1997)
Morocco (BCR-32)	10.0	10.8-20.3	1.0	260.0	0.5	35.0	2.0	Jochum et al (2005)
Pakistan	-	7.2	9.4	17.0	-	5.5	-	Sabiha et al (2009)
Russia	-	-	2.1	23.3	-	-	-	Pantelica et al (1997)
Sokoto, Africa	11.1	-	19.8	28.0	0.4	-	76.0	Ogunleye et al (2002)
Syria	3.9	-	0.4	136.0	-	-	-	Pantelica et al (1997)
Togo, Africa	9.7	-	1.2	75.0	-	-	41.0	Ogunleye et al (2002)
Tunis	4.1	-	0.7	161.0	-	-	-	Pantelica et al (1997)
Turkey	-	7.7	0.2	-	-	62.1	-	Aydin et al (2010)
USA	12.4	-	0.4	142.0	-	-	-	Pantelica et al (1997)
Chatham Rise (Average)	-	0.15	9.15	20.46	1.48	8.70	2.45	This study
Chatham Rise (Range)	-	0.03-0.93	1.39-62.15	1.09-73.79	0.09-3.59	1.73-22.59	0.49-8.26	This study
Bollons Seamount (Average)	-	0.12	94.87	67	1.27	60.63	4.02	This study
Bollons Seamount(Range)	-	0.07-0.19	38.12-273.55	39.74-149.24	0.72-2.12	36.41-144.31	1.8-10.09	This study
Offshore South Island (n=1)	-	0.1	5.0	11.8	1.8	13.9	0.6	This study
Chatham Rise 1-8mm (Average)	38.3	-	15.4	9.0	-	13.7	7.0	Von Rad & Rosch (1984)
Chatham Rise 1-8mm Range	5-79	-	1-33	0.001-24	-	5-69	3-10	Von Rad & Rosch (1984)
Chatham Rise >8mm (Average)	13.3	-	13.8	2.7	-	13.8	6.6	Von Rad & Rosch (1984)
Chatham Rise >8mm (Range)	5-39	-	0.001-26	0.001-30	-	5-53	3-17	Von Rad & Rosch (1984)

Table 4-1: Comparison of phosphorites from this study to other phosphate deposits from around the world. Chatham Rise phosphorite values from this study exclude chert nodules

Country	Ni	Pb	Sc	Th	U	V	Zn	Study
Algeria	-	-	3.7	18.8	51.0	-	134.0	Pantelica et al (1997)
Aqaba, Jordan	-	-	-	-	-	-	29.0	Al-Hwaiti et al (2010)
Bayovar–Sechura ,Peru	16.8	5.8	-	2.2	44.9	49.2	65.4	Bech et al (2010)
Eshidiya, Jordan	-	-	-	-	-	-	23.0	Al-Hwaiti et al (2010)
Florida	31.0	28.0	-	-	114.0	90.0	72.0	Jochum et al (2005)
Israel	-	-	3.1	0.5	139.0	-	372.0	Pantelica et al (1997)
Morocco	-	-	8.7	3.4	127	-	345	Pantelica et al (1997)
Morocco	23.2	-	8.8	3.0	125.0	158.1-159	260.0	Jochum et al (2005)
Pakistan	28.0	89.0	-	-	-	-	67.2	Sabiha et al (2009)
Russia	-	-	0.07	20.4	85.0	-	-	Pantelica et al (1997)
Sokoto, Africa	-	-	11.8	3.2	65.0	65.0	59.0	Ogunleye et al (2002)
Syria	-	-	4.1	2.2	106.0	-	269.0	Pantelica et al (1997)
Togo, Africa	-	-	11.6	17.4	72.0	68.0	143.0	Ogunleye et al (2002)
Tunis	-	-	3.8	8.5	32	-	515	Pantelica et al (1997)
Turkey	4.4	6.3	-	18.1	-	-	14.9	Aydin et al (2010)
USA	-	-	6.4	7.6	80.0	-	403.0	Pantelica et al (1997)
Chatham Rise (Average)	35.61	10.26	1.42	0.50	152.06	78.95	59.75	This study
Chatham Rise (Range)	9.05-160.76	0.93-30.30	0.04-6.70	0.03-4.17	17.16-639.09	8.30-184.80	10.84-949.25	This study
Bollons Seamount (Average)	183.68	23.73	6.74	3.61	12.02	88.19	128.94	This study
Bollons Seamount(Range)	52.01-607.23	12.51-51.80	4.59-9	2.26-5.24	6.63-20.91	54.53-135.39	70.61-209.39	This study
Offshore South Island (n=1)	21.4	3.5	1.4	0.4	79.0	70.6	28.5	This study
Chatham Rise 1-8mm (Average)	31.5	14.3	-	10.6	172.3	75.6	-	Von Rad & Rosch (1984)
Chatham Rise 1-8mm Range	14-59	5-26	-	6-15	118-305	61-91	-	Von Rad & Rosch (1984)
Chatham Rise >8mm (Average)	16.3	7.4	-	11.8	242.1	59.3	-	Von Rad & Rosch (1984)
Chatham Rise >8mm (Range)	6-37	5-18	-	8-19	47-476	0.001-115	-	Von Rad & Rosch (1984)

Table 4-1 continued

Chapter 5. Ecotoxicity Experiments

5.1 Introduction

To determine the potential impact of seafloor sediment disturbance on local biota, the chemical release from sediments needs to be estimated. An extreme example of physical disturbance to the seafloor is the type of dredging proposed for the mining of deep sea mineral resources, such as phosphorites. The deep sea dredging method utilises a drag head (Figure 5-1), which loosens the seabed by using jet cutters, and mixes the nodules and surficial sediment (0.35 to 0.5 m) with water pumped to the surface through a vertical hydraulic suction system (RSC Consulting Ltd, 2014; Van Raalte. G. et al., 2013). After shipboard processing, tailings of <2 mm in size are then to be released back to the seabed by controlled diffusion ~10 metres above the seafloor (Environmental Protection Agency, 2015).

The discharge plume will contain chemical contaminants from the natural surficial sediments, largely from pore waters, and those desorbed from the mineral deposits. Once released from the discharge pipe the sediments and chemical contaminants will be diluted by dispersion of the sediment plume by ~200 x in surrounding waters (Golder Associates (NZ) Limited, 2014b). The time taken for the suction uptake, surface processing, and then discharge of the mineralised sediment is in the order of hours, but will differ depending on ocean depth for mining and the surface processing being used.

A simulation of the chemical effects of this seabed mining process can be done through sediment elutriate and column leaching experiments. The results from these experiments can then be used to evaluate the concentrations of chemical contaminants released, and their potential toxicity based on comparison with water quality guidelines and/or toxicity testing with sensitive marine species.

Elutriate is defined as separating fine particles and pore water from sediments (Hickey et al., 2014). Elutriate experiments are used to identify short-term near field effects of seafloor mining by simulating the conditions whereby the sediment is disturbed, collected, mixed with sea water, and dispersed back to the seafloor.

Previous ecotoxicity testing on Chatham Rise phosphorite-containing sediments, conducted independently on behalf of Chatham Rock Phosphate Ltd (Hickey et al., 2014), used sediment samples, which had been in frozen storage for a year before testing, leading to added uncertainty in the results (Environmental Protection Agency, 2015), In addition, the water used for the experiments was not collected from the Chatham Rise, but surface water from the Alderman Islands (Environmental Protection Agency, 2015; Hickey et al., 2014).

Figure 5-1: Deep Seafloor mining concept. Sediment is vacuumed up through the drag head for processing on board the ship.The tailings are released back to the seabed through the sinker and diffuser. From Schoute (2013).

Currently, there is a lack of baseline chemical data for the Chatham Rise, including background water quality measurements, specifically elemental composition (Environmental Protection Agency, 2015). For example, uranium raised some concerns because of elevated elutriate concentrations present in phosphorites and measured in the elutriate tests that used frozen sediment samples (Hickey et al., 2014). However, U has no Australian and New Zealand Environment Conservation Council (ANZECC) trigger value guideline for the marine environment (ANZECC, 2000a).

Environment trigger values are concentrations of known ecotoxic elements below which there is a low risk of toxic effects. If the trigger values are exceeded, then either monitoring or further investigation is needed (ANZECC,2000a). Hickey et al. (2014) used trigger values recommended for 99% species protection as the Chatham Rise is considered a pristine environment due to having a high water quality, thus the same criteria are used in this study. For metals and nutrients without water quality guidelines, concentration increases of 5x above background are used in place of trigger values to highlight potential concern (Hickey et al., 2014).

The Environmental Protection Agency (2015) Decision Making Committee for the Chatham Rock Phosphate Ltd marine consent hearing acknowledged that "While the mobilisation of heavy metals is possible, testing suggests that the concentration levels would not be sufficient to exert toxic effects on marine organisms, particularly after mixing with the surrounding seawater." (p. 150). The committee did; however, suggest that more testing be completed to further assess the baseline water quality of the mining area, and potential toxicity arising from the discharge of mining tailings due to concerns raised about the testing methods used, e.g. using frozen instead of fresh sediments (Environmental Protection Agency, 2015).

In this study, elutriate experiments were conducted on fresh surficial sediment, using seawater collected from near the seabed at the same site in order to more accurately quantify potential chemical release from disturbed sediments. Site CRP-1 is from within the Chatham Rock Phosphate Ltd mining permit area (Figure 4-1). The contaminants of potential concern include a suite of heavy metals, nutrients, and sulphides. Heavy metals are identified as stressors that are directly toxic to biota in excess concentrations (ANZECC, 2000a). Nutrients

are not usually considered directly toxic; however an excess above baseline concentrations can directly affect biota (ANZECC, 2000a).

Sulphide measurements can be used as an indicator of reducing conditions/anoxia present in the sediments. The release of anoxic sediment and sediment pore water into the oxygenated water column is of concern as minerals formed in anoxic conditions can dissolve in more oxygenated conditions releasing heavy metals, e.g. pyrite dissolution and re-precipitation as iron oxyhydroxides (Golder Associates (NZ) Limited, 2014b).

Whilst elutriate and leaching experiments allow the near field release of ecotoxic elements into the water column to be quantified, they do not give insight into the potential longer-term effects on the local biota. For this purpose, bioaccumulation experiments were conducted on biota, whose natural habitat closely resembles that of the mining site. Such experiments incorporate uptake from both dissolved contaminants and from dietary ingestion pathways and are commonly undertaken on whole sediments where pore water concentrations represent the highest potential exposure concentrations. The results of the bioaccumulation experiments are not intended to be critical body burden experiments, but rather indicators of potential suitability for further development.

Amphipods have been proven to be good bio-monitors for trace metals in their environment for both long term and short term exposures (Marsden & Rainbow, 2004). A surrogate amphipod species was used in this study to test bioaccumulation: *Chaetocorophium* c.f. *lucasi*, an estuarine amphipod species native to New Zealand, commonly found in estuaries in the North Island (Dewitt et al., 1999). Although this species is not native to the Chatham Rise; however, an amphipod species that is used routinely for ecotoxicity testing and thus provides a robust indication of possible metal bioaccumulation.

To assess the potential long-term chemical release and chemical equilibration from seafloor sediment disturbance, column leaching experiments were conducted. A prototype apparatus allowing dynamic elutriate experiments was custom built for this purpose (Appendix C.). The experiment consisted of three components running simultaneously: the dynamic column, a standard sediment elutriate experiment, and a seawater blank.

The standard elutriate experiment was used to evaluate any differences that the circulating water of the dynamic column could have on the total chemical release from the sediment, as well as to act as a comparison between the new methodology and standard elutriate tests conducted on shorter timespans. Prior this experiment, which was run for 168 hours (1 week), the longest elutriate test on Chatham Rise sediments had been 24 hours (Hickey et al., 2014). A week was used as a conservative length of time to observe if there are actually any long-term changes. If changes are still observed after a week of leaching, then even longer leaching experiments can be conducted.

5.2 Methods

5.2.1 Sample Collection

Sampling and subsequent preparation of samples for analysis were conducted on board the *R.V. Tangaroa* (voyage TAN1503), on the 12th and 13th of April, 2015. Sample collection consisted of two box cores deployed at sites CRP-1 and G87 (Figure 4-1), as well as two conductivity, temperature, depth (CTD) deployments for surface and deep water. Sampling protocols were provided by Dr. Chris Hickey, NIWA.

Upon collection, the box cores were split into five different zones which were used for subsampling (Figure 5-2). The first box core, G87, had very good recovery with 20 cm depth of sediment and no visible slumping of the surface (Figure 5-3). The high mud content (visual estimation) meant that the water was contained in the core box rather than washing through.

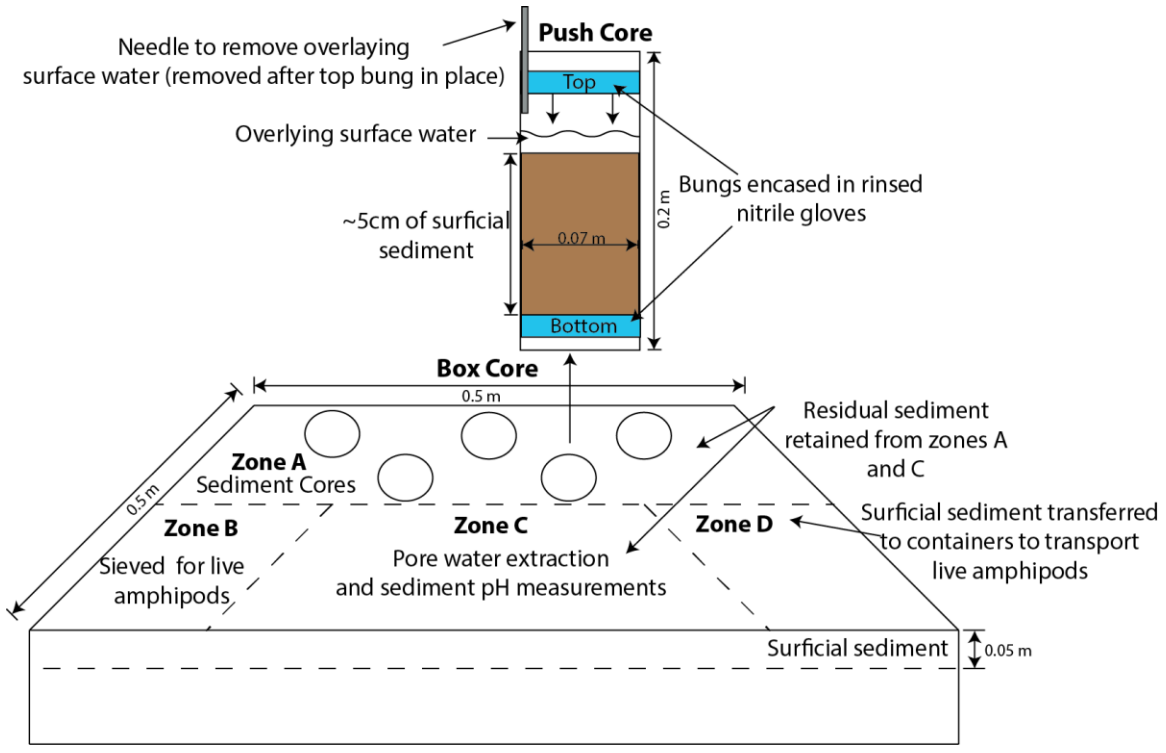

Figure 5-2: Schematic representation of the box core sampling zones and push cores.
Sampling zone and push core sampling diagram modified after protocols provided by Dr. Chris Hickey, NIWA.

Figure 5-3: Left: Box core from site G87 before water on surface was siphoned off. Right: Box core from site G87 after water had been siphoned off, and push cores inserted. Photos: Rob Stewart.

Surface water was siphoned using two ~50 cm long silicone tubes that were rinsed 3x with distilled water. Siphoned water was passed through a plastic 500 µm sieve to collect any invertebrates that were present in the surface water. Two amphipods were recovered from the G87 core using this method. The G87 core sediment surface had patchy concentrations of glauconite grains, and few (<20 %) ~2-10 mm phosphorite nodules.

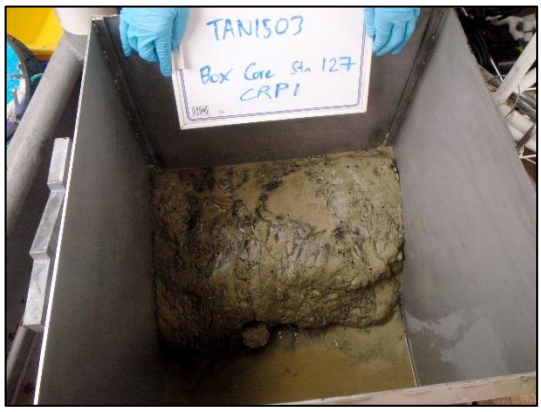

Figure 5-4: Box core sample from site CRP-1. Photo: Diana Macpherson.

The CRP1 box core was slumped, with almost half of the sediment disturbed (Figure 5-4). The surface of the slumped sediment also had patches of glauconite grains and phosphorite nodules ~ 2-10 mm in size covering ~30 % of the surface. The sediment was a muddy fine-medium sand. Despite the high degree of slumping, the core was still able to be split into zones to collect all required samples.

Five cores were recovered from each box core from zone A (Figure 5-2). Cores were inserted at a depth to retrieve the top 5 cm of surficial sediment (Figure 5-2). Core bungs were encased in a fresh nitrile glove and tied with a cable tie. The bungs were then rinsed with distilled water.

A bleed tube through the bung was required to release surface water from the core (Figure 5-2). A metal tube was used as a water bleed, as needles with plastic tubing could not be used – attempts to do so resulted in the tubing getting stuck and this method posed a health and safety hazard. Care was taken to ensure no contact between the metal tubing and sediment (Figure 5-2). Cores were then put in refrigerated (4 °C) storage. Pore water and pH was measured in zone C (Figure 5-2). Remaining surficial sediment was collected and refrigerated for column leaching experiments to be conducted onshore.

Seawater was collected from both the surface (9-11 mbsl) and near the seafloor (368-382 mbsl) using a CTD instrument equipped with Niskin bottles. A litre subsample of deep and surface seawater was collected from each site, along with 100 ml sub-samples for metals and nutrients. Water was also filtered into sample bottles provided by Hill Laboratories, Hamilton, using a 0.45 µm filter, preserved in optima grade HNO_3, and refrigerated (4 °C). Nutrient samples were unfiltered and immediately frozen. Sulphide samples were preserved in $ZnCl_2$, then refrigerated. pH was also measured. Residual seawater was transferred to chemically clean buckets that had been first rinsed with distilled water, then seawater from the site.

5.2.2 Elutriate Experiments

The method follows the U.S. Environmental Protection Agency (1991) toxicity leaching procedure for marine sediments. This method is a standardised procedure for the assessment of contaminated sediments in the open ocean. Elutriate experiments in this study were conducted using fresh surficial sediment and seawater from the Chatham Rise. Experiments were carried out during the *R.V. Tangaroa* voyage TAN1503 within a few hours of the samples being collected. Elutriates from site CRP-1 were conducted by the author. Elutriates from site G87 were conducted by Dr. L. Holland, a member of the TAN1503 science team.

A 100 ml subsample of sediment was added to 400 ml of deep seawater collected from the site. Nalgene bottles used were rinsed thoroughly with seawater from the site. One Nalgene bottle was used as a seawater blank, and was reused at site CRP-1, after extensive rinsing with distilled water and rinsing with deep seawater from the site. Both bottles were inverted every 5 minutes for 30 minutes to simulate surficial sediment disturbance. Photographs were taken after 30 minutes agitation, and after 1 hour of settling (Figure 5-5, Figure 5-6). The settling period aims to simulate the settling of a sediment plume.

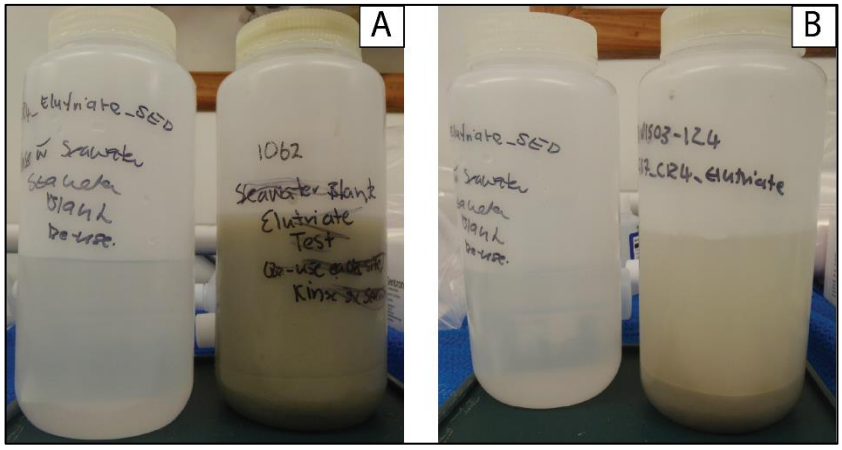

Figure 5-5:Elutriate experiment photographs for site G87.
A: Elutriate experiment after 30 minutes of agitation. B: Elutriate experiment after 1 hour of settling. Photo: Lyndsey Holland.

Water samples for metal analysis were filtered through both a 25 mm Whatman filter and a 0.45 µm filter. Distilled water was also processed through the same filter method to prepare a filter blank. Water samples were then transferred to pre-cleaned Hill Laboratory supplied sample bottles with samples for metal analysis preserved in HNO_3, for sulphide analysis in $ZnCl_2$, and nutrient samples were frozen. Samples were sent to Hill Laboratories, Hamilton, for analysis. Analysis reports outlining the methods used to obtain dissolved metals and nutrient analyses, along with analysis methodology, are presented in Appendices B-1 and B-2 .

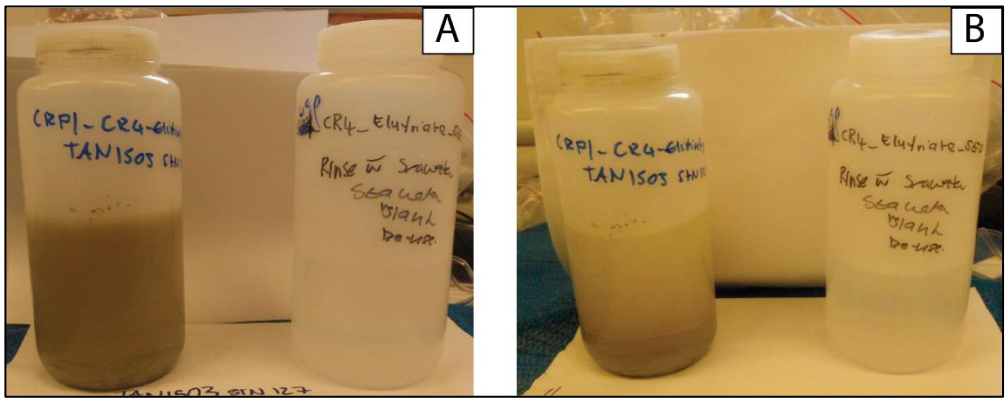

Figure 5-6: Elutriate experiment photographs for site CRP-1.
A: Elutriate experiment after 30 minutes of agitation. B: Elutriate experiment after 1 hour of settling.

A 100 ml subsample of fresh sediment from each site was also collected for geochemical analysis. The pH was measured for surface and bottom site seawater samples, and at the completion of the elutriate experiments. Before each measurement, the pH probe (Sentron SI series Lance FET 2270-010 probe with Sentron SI line pH meter) was calibrated and rinsed thoroughly with distilled water. The calibration slope of the probe was consistently 100 %, despite probe degradation warnings on the meter.

For pore water extraction, a Rhizosphere Research products (EUR) Rhizone sampler (0.15 µm pore size, 5 cm porous part, 12 cm tubing, 2.5 mm diameter) and 3 ml syringe were rinsed 3 times with distilled water, as was a 0.45 µm filter. In box core G87, water was siphoned off until ~1 cm depth remained. The Rhizone sampler was pushed through Parafilm, ~3 cm by 5 cm, as deep as the full length of the tubing on a 45° angle (Figure 5-7), and held on the sediment/water interface surface in zone C (Figure 5-2). Pore water could not be extracted from the box core sample from CRP-1 as the box core had been disturbed on retrieval, allowing all water to easily drain.

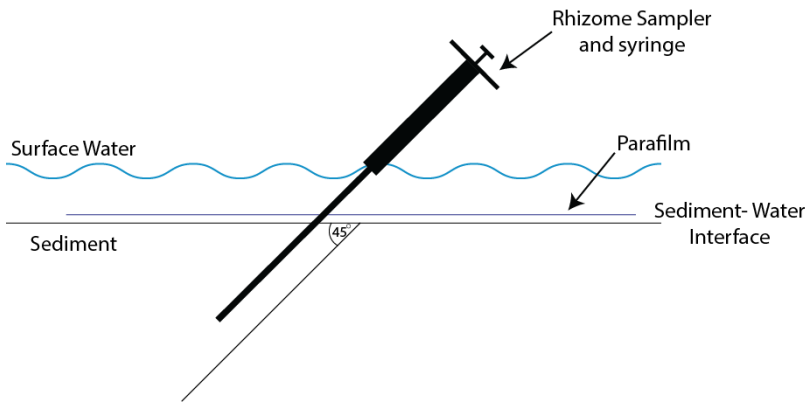

Figure 5-7: Schematic illustration of the sampling procedure for collected sediment pore water from the box core samples. Diagram not to scale.

The Rhizome sampler was left in situ whilst samples were transferred to vials to avoid creating space that could be filled in with percolating surface water. pH readings were also taken by pushing the pH meter into the sediment at 0.5 cm, 2 cm and 5 cm depth in both cores in zone C (Figure 5-2).

5.2.3 Bioaccumulation Experiments

Bioaccumulation experiments were conducted by staff at NIWA Hamilton following a modified 28 day chronic test standard operating procedure (National Institiute of Water and Atmospheric Research (NIWA), 1995). The chronic test usually measures the growth and survival of juvenile amphipods; however, in this experiment adult amphipods were used and only bioaccumulation of metals in tissue was measured.

Adult (3-5 mm) estuarine amphipods, *Chaetocorophium* c.f. *lucasi*, collected from Raglan Harbour, were placed in whole sediments containing phosphorite nodules and bottom seawater from sites G87 and CRP-1 for 28 days to ensure steady state between the amphipods and metals in the test water was met. The experiments were conducted in aeriated 680 mL polypropylene jars containing a 2 cm layer of whole sediment and 450 mL of site deep seawater. Ten amphipods were used per replicate experiment. The experiment was conducted at a constant temperature of 20 ±1 °C and a salinity of 35 ‰. A control experiment was run concurrently using sediment collected from Raglan Harbour, where the test amphipods were collected from, and used to monitor the test validity. The test is deemed invalid if the overall

mortality is ≥ 25 % in the control experiment. The Chatham Rise test sediments used had been preserved by refrigeration at ~4 °C since collection. Chemical analyses were performed by Hill Laboratories, Hamilton. A bulk sample of 10 adult amphipods from each experiment were dried and prepared for analysis using a biological materials digestion method involving HNO_3 and HCl digestion at 85 °C for 1 hour (Appendix B-6).

Sediment and phosphorite nodules were also analysed for trace metals by Hill Laboratory Hamilton (Appendix B-2, Appendix B-4). Sediment samples were oven dried (60 °C) before analysis, and phosphorite nodules were sieved (>2 mm) from the residual collected sediment, ground, and oven dried by Dr. Chris Hickey, NIWA before trace metal analysis by Hill Laboratory Hamilton.

5.2.4 Leaching column cleaning procedure

The column cleaning procedures follow the USGS (2004) recommendations for cleaning of equipment used for water samples. The procedure for inorganic trace element analysis is as follows:

1. Wash in dilute soapy detergent

2. Rinse in either tap water or deionised water if the tap water supply is not clean.

3. Immerse components in 5 % v/v HCl for 30 minutes. Rinse thoroughly.

4. Immerse rinsed components in 10 % v/v HNO_3 for a minimum of 3 hours.

5. Rinse thoroughly in deionised water (18.2 MΩ water).

Components of the apparatus, as well as bottles used to store samples should be stored in a solution of HNO_3 acidified deionised water of a pH of 1.6 until used (Berman et al., 1983). Storage of samples in Teflon or high density polythene bottles is recommended (Batley & Gardner, 1977; Berman et al., 1983).

For this experiment the Viton and Perspex components of the apparatus were first cleaned with soapy (dishwashing liquid) tap water immediately after manufacture. 18.2 MΩ water and tissues (Kimtech delicate task wipes) were then used to clean each part individually. The

parts were then transferred to a clean borosilicate 3 L beaker and soaked in 18.2 MΩ water for up to 3 days. The parts were then rinsed 3x with 18.2 MΩ water. The apparatus was then soaked in 5 % v/v double sub-boiled analytical grade HCl for three days. The parts were then rinsed 3x with 18.2 MΩ water, and submerged in 10 % v/v double sub-boiled analytical grade HNO_3. The apparatus was soaked in the acid for a minimum of 3 days, and remained in the acid solution until needed for the experiment, but for no more than 30 days. Upon being removed from the HNO_3, the apparatus parts were rinsed 3x with 18.2 MΩ water prior to initiating the experiments.

Nalgene brand low density polyethylene bottles (LDPE, 60 ml) were used for sample storage. To ensure the bottles were chemically clean, each was filled with 18.2 MΩ water and 8 drops of concentrated Optima grade HNO_3. The bottles were placed underneath a hotplate set to 120 °C for 2-4 days. The bottles were rinsed 3x with 18.2 MΩ water and allowed to air dry in an ultra-clean laminar flow cupboard (Class 10).

5.2.5 Leaching Experiment Method

The column leaching experiments were designed to provide an improved alternative to the bottle procedure and give an indication of long term chemical equilibration processes. This apparatus facilitated longer duration measurements than the previous elutriate experiments by Hickey et al. (2014). The column leaching method proposed is an adaption based on the standard elutriate procedure by U.S. Environmental Protection Agency (1991).

First, a process blank of 18.2 MΩ water was run through the chemically clean apparatus (for cleaning procedure see section 5.2.4) for five days to identify any contaminants originating from the manufacturing process (

Table 5-5). The peristatic pump began operating at 30 rpm (Gilson Miniplus 3 peristaltic pump with a standard pump head, using 4x 1.3 mm I.D. tubing with an approximate 20 mL/min total flow rate) as soon as the water had been added to the column. Except for when samples were being taken, the pump operated continuously throughout the experiment.

Sediment and deep water from site CRP-1 that was collected in April 2015, and had subsequently been kept in refrigerated (4 °C) storage for a year, was used for the preliminary column leaching experiment. The sediment sat at ambient room temperature for a few hours

before the experiment commenced to allow for temperature equilibration. A 200 ml volume sub- sediment sample of bulk surface sediment containing phosphorite nodules was added to 800 ml of sea water from site CRP-1 for the leaching column. This was duplicated in a second 500 ml chemically clean bottle, with the same 1:4 ratio, but at a smaller scale of 100 ml sediment: 400 ml seawater. Another 400 ml sub-sample of seawater was added to a third chemically clean bottle, functioning as an elutriate blank.

The three bottles were inverted every five minutes for 30 minutes to agitate and mix the sediment and seawater. At the end of the 30 minute agitation period, the 200 ml: 800 ml sediment: seawater sample was added to the clean and empty leaching column. A further 200 ml of seawater was added to the reservoir. All three experiments were allowed to sit and settle for 1 hour. A 25 ml sub-sample was taken from each experiment. After the first subsample was taken, the peristaltic pump on the column was turned on at a speed of 30 rpm. Further subsamples were taken from each of the three experiments after 2 hours, 24 hours, 48 hours, and a week. Photographs were taken after 30 minutes, 1 hour, 24 hour, and 48 hours (Figure 5-8). pH was measured when samples were taken, using a glass body Omega Engineering Brand Alpha series probe calibrated using standard NIST buffer solutions.

As the column apparatus is a proto-type, the sample collection set-up had not been fully developed in time for this initial test. To collect samples, the peristaltic pump was first switched off. A plug was opened on the end of the return flow manifold, and the sample was collected in a clean polypropylene container (30 ml). The volume of leachate removed was replaced with seawater.

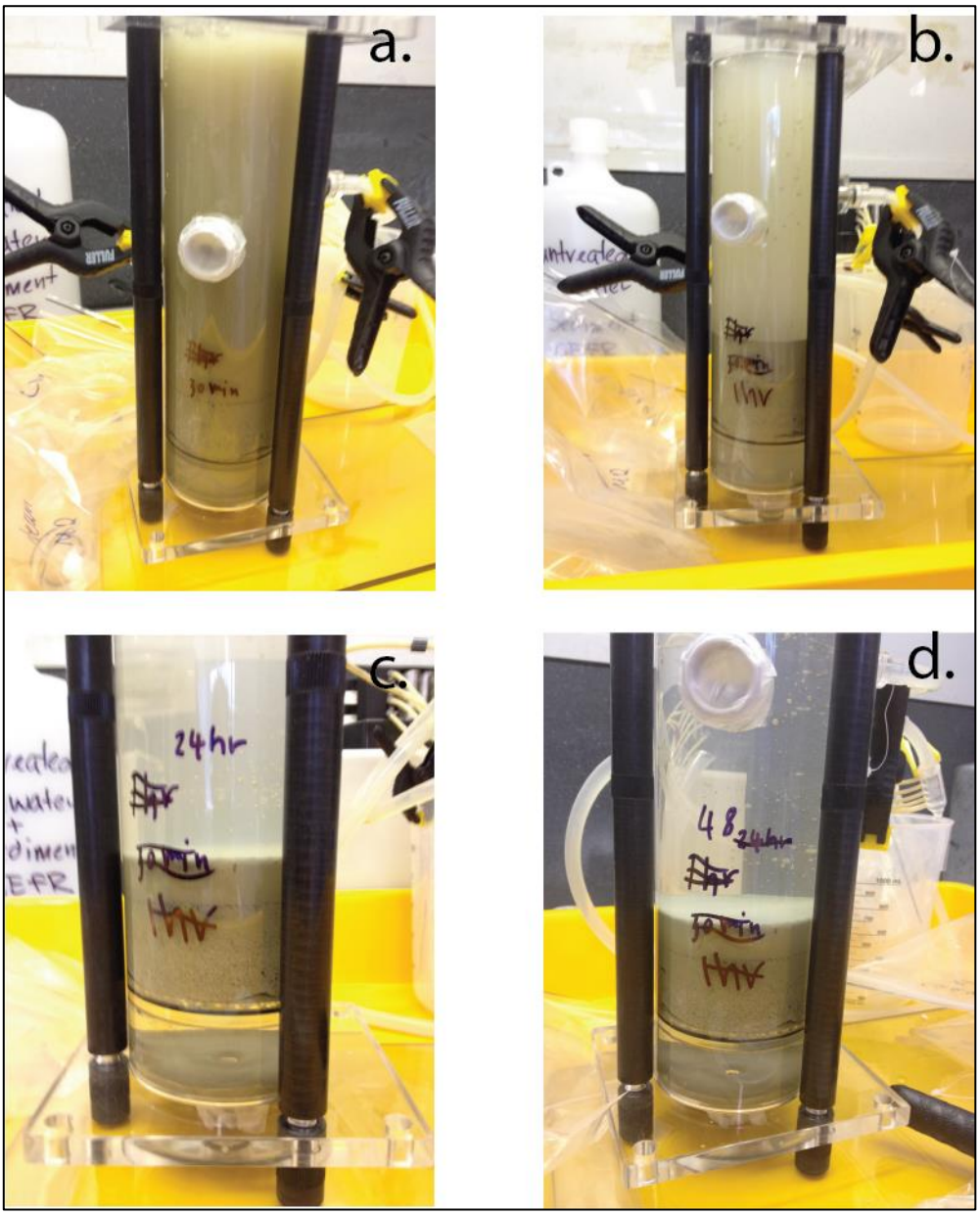

Figure 5-8: Photos of column leaching experiment. a: after 30 minutes b: after 1 hour. c: after 24 hours. d: after 48 hours.

Sub-samples collected for dissolved metal analysis were filtered using Biofil syringe filters with a pore size of 0.22 µm, after both the syringe and filter has been rinsed three times with 18.2 MΩ water. Samples were preserved in ultra-pure Optima Grade HNO_3 (68 -70%). A pH of <1.5 to 2 (0.05 M of H^+ ions) is the commonly accepted preservation method in preventing metals from adsorbing to the surface of the container of which the sample is stored (Batley & Gardner, 1977; Berman et al., 1983; Oliver, 2009). Along with metal samples, an

additional sample for Non-Purgeable Organic Carbon content was taken from each of the three experiments after 48 and 168 hours, and were not treated with acid. All samples were transferred to refrigerated storage until they were analysed by Hill Laboratories Ltd (Appendix B-8).

5.3 Results

5.3.1 Site Seawater

Seawater from near the seafloor was collected from two sites; G87 and CRP-1, and analysed for key trace metals and nutrients. Depths were calculated from pressure readings using the conversion equation of Fofonoff and Millard (1983) in the oce R package developed by Kelley and Richards (2016).

Surface seawater from site G87 was collected from an average depth of 9.11 mbsl. The average temperature of the surface seawater was 16 °C, and average salinity (S) was 35 ‰. Deep water from site G87 was collected from an average depth of 382 mbsl. The average temperature was 9 °C, and average salinity (S) was 34.6 ‰.

Surface seawater from site CRP-1 was collected from an average depth of 11mbsl. The average temperature of the surface water at the time of collection was 15°C, with an average salinity (S) of 34.6 ‰. Deep water from site CRP-1 was collected from an average depth of 368 mbsl. The average temperature at the time of deep water collection was 8 °C, with an average salinity (S) of 34.4‰. pH measurements are reported in Table 5-2 **.**

Seawater chemical analyses were conducted by Hill Laboratories, Hamilton (Appendix B-2). The concentrations of dissolved metals and nutrients of the bottom water from both sites were identical (Table 5-1).

5.3.2 Sediment geochemical analysis

An extensive suite of metal analyses was performed on the phosphorite nodules (> 2 mm) and the sediment matrix (< 2 mm fraction) to characterise enriched metals that may potentially be released in elutriates and tissue bioaccumulation. The samples were analysed by Hill Laboratories Ltd to ensure the methodology and results were consistent with results from the elutriate and amphipod tissue analyses. Concentrations are reported in Appendix B-4 for >2 mm and < 2 mm fractions. Concentrations for bulk sediment samples are reported in Appendix B-2.

Sediment and phosphorite trace element concentrations were normalised to average upper crust values to identify enriched elements (Figure 5-9). In the < 2 mm sieved sediment fraction from both sites, Ca, B, Sr, Cd and Hg are enriched relative to average upper crust, with U and As also enriched at CRP-1 (Figure 5-9). Phosphorite nodules > 2 mm from both sites are enriched in U, B, P, Ca, Sb, As, Sr, Hg, Cd and V, with CRP-1 also enriched in Mo and Tl, and G87 in K, La, Pb and Fe relative to average upper crust (Figure 5-9).

The bulk sediment, which includes both the < 2 mm and > 2 mm fractions, from both sites are enriched in B, Ca, Sr, Cd and Hg, with CRP-1 also enriched in U and As (Figure 5-9). Se, Bi and Ag are below the detection limit, therefore are not included in these results. The < 2 mm sediment fraction for G87 is less enriched in B, U and Cd, and more depleted in most other metals relative to CRP-1.

Major elements for both phosphorite and sediment samples are within the range of Chatham Rise sediments and phosphorites analysed in Chapter 4, except for K enrichment relative to the upper crust in site G87 phosphorite nodules. Uranium enrichment in phosphorites from site G87 is higher than the range of phosphorites analysed in Chapter 4, and Mo shows more depletion. All other trace elements are within the range of Chatham Rise phosphorites analysed in Chapter 4.

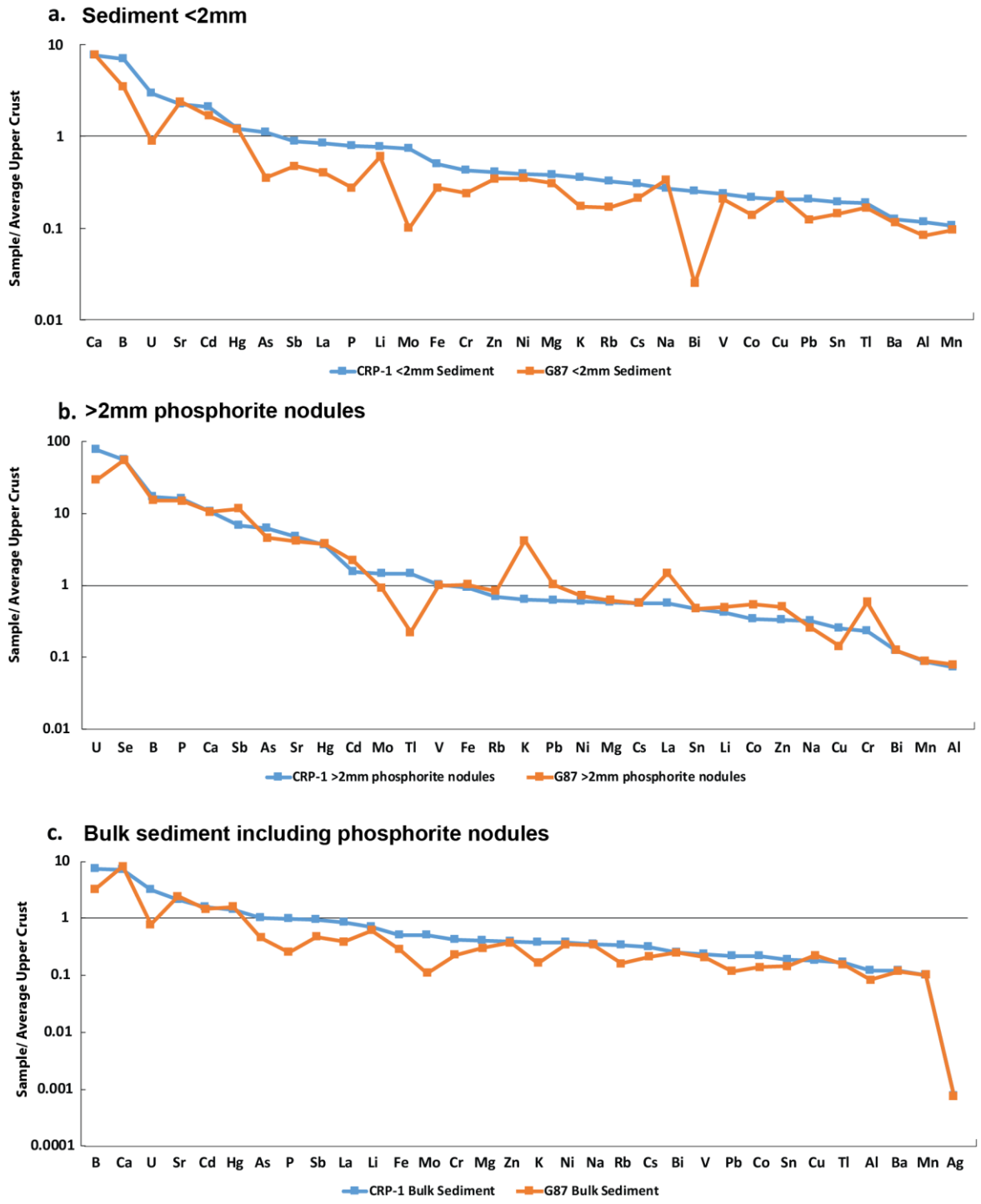

Figure 5-9: Sediment fractions from sites G87 and CRP-1 normalised to average upper crust. Upper crust values from Rudnick and Gao (2014). a. sieved sediment <2mm normalised to average upper crust for sites CRP-1 (sample P07) and G87 (sample P08). Samples prepared by Dr. C. Hickey, NIWA. b. sieved phosphorite nodules >2mm normalised to the average upper crust for sites CRP-1 (P020) and G87 (sample P019). Samples prepared by Dr. C. Hickey. c. bulk sediment, including phosphorite nodules, normalised to average upper crust for sites CRP-1(CRP1-_CR2_2-S ED) and G87 (sample G87_CR2_2-sed1).

5.3.3 Elutriate Experiments

Australian and New Zealand Environment Conservation Council (2000a) environmental trigger guidelines were used to identify concentrations of potentially ecotoxic elements that could be of concern. For metals and nutrients without water quality guidelines, concentration increases of 5x above background are used in place of trigger values to highlight potential concern (Hickey et al., 2014).

Pore water collected from site G87 has elevated concentrations of Fe (> 412.5x) and Mn (< 41x) relative to background ambient seawater levels (Table 5-1). For dissolved metals that have background concentrations below the detection limit, the detection limit is used as an indicator only. Background seawater levels for Zn (3.25x) were exceeded, as well as ANZECC(2000a) environmental trigger values for Zn (2x) and Mn (2x).

Sulphide measurements are below the detection limit for elutriate experiments conducted on sediment from both CRP-1 and G87 sites. Nitrite-N + Nitrate-N do not exceed ANZECC(2000a) trigger values for 99 % species protection or the 5x baseline site deep water values. Dissolved reactive phosphorus does not have a trigger value, but is below 5x the site deep water baseline for both site G87 and CRP-1. Non-purgeable organic carbon does not have an ANZECC(2000a) trigger value; however, elutriate concentrations at both sites G87 (5.7x) and CRP-1 (8.25x) exceed 5 x the baseline site deep-water values.

Parameter	Units	G87-CR3-Pore Water	G87 12-Apr-2015 Elutriate	Deep Water G87	CRP1 13-Apr-2015 Elutriate	CRP1 Deep Water	Distilled Water filter blank	Elutriate Blank	ANZECC Trigger Value 99%
pH	pH units		7.35	7.42	7.32	7.59	–	7.53	<0.2 change
Dissolved As	g/m^3	<0.004	<0.004	<0.004	<0.004	<0.004	<0.004	<0.004	NG
Dissolved Cd	g/m^3	<0.0002	<0.0002	<0.0002	<0.0002	<0.0002	<0.0002	<0.0002	0.0007
Dissolved Ca	g/m^3	390	390	380	350	370	<1	390	NG
Dissolved Cr	g/m^3	<0.01	<0.01	<0.001	<0.01	<0.001	0.001	<0.01	0.0077 (3+)
Dissolved Co	g/m^3	<0.0006	<0.0006	<0.0006	<0.0006	<0.0006	<0.0006	<0.0006	0.001[1]
Dissolved Cu	g/m^3	**0.0026**	<0.0010	<0.0010	<0.0010	<0.0010	<0.0010	<0.0010	0.0003
Dissolved Fe	g/m^3	**1.65**	<0.004	<0.004	<0.004	<0.004	<0.004	<0.004	NG
Dissolved Pb	g/m^3	<0.0010	<0.0010	<0.0010	<0.0010	<0.0010	<0.0010	<0.0010	0.0022
Dissolved Mn	g/m^3	**0.041**	0.0027	<0.001	**0.0171**	<0.001	<0.0010	<0.0010	0.020 (updated)[2]
Total Hg	g/m^3	<0.00008	<0.00008	<0.00008	<0.00008	<0.00008	–	–	0.0001
Dissolved Mo	g/m^3	0.0101	0.0111	0.0117	0.0103	0.0109	<0.0010	0.0111	NG
Dissolved Ni	g/m^3	<0.006	<0.006	<0.006	<0.006	<0.006	<0.006	<0.006	0.007
Dissolved Sr	g/m^3	7.7	8	7.6	7.1	7.4	0.0005	7.9	NG
Dissolved Tl	g/m^3	<0.0002	<0.0002	<0.0002	<0.0002	<0.0002	<0.0002	<0.0002	NG
Dissolved U	g/m^3	0.0004	0.0031	0.0031	0.0028	0.0030	<0.0004	0.0031	NG
Dissolved V	g/m^3	<0.0010	0.0030	0.0018	0.0054	0.0015	<0.0010	0.003	0.05
Dissolved Zn	g/m^3	**0.013**	0.009	<0.004	**0.056**	<0.004	**0.016**	<0.004	0.007
F	g/m^3	–	1.4	1	1.4	1	–	–	5[3]
Nitrite-N	g/m^3	–	<0.002	<0.002	<0.002	<0.002	–	–	NG
Nitrate-N	g/m^3	–	0.24	0.2	0.31	0.2	–	–	45
Nitrate-N+Nitrite-N	g/m^3	–	0.24	0.2	0.31	0.2	–	–	>45
Dissolved Reactive Phosphorus	g/m^3	–	0.138	0.04	0.132	0.038	–	–	NG
Non-Purgeable Organic	g/m^3	–	**4**	0.7	**6.6**	0.8	–	–	NG
Total Sulphide	g/m^3	–	<0.002	–	<0.02	–	–	–	10 (as H_2S)

Table 5-1: : Compiled results of the elutriate chemistry for Chatham Rise sites G87 and CRP-1, and sediment pore water chemistry.

Red shading indicates concentration in blank, grey fill indicates exceedance of ANZECC(2000a) trigger value, bold type with black outline indicates exceedance of 5 times the concentration of the baseline site deep water. 1. 95% protection value used for Co, as Hickey et al. (2014) considers the 99% value a statistical artefact. 2. Updated and unpublished ANZECC(2000a) value for Mn cited by (Hickey et al., 2014). 3. Total fluoride guideline for marine waters (Hickey et al., 2004, cited by (Hickey et al., 2014). NG= No guideline.

Despite elevated concentrations of Cu (2.6x) and Fe (>412 x) in site G87 pore water relative to baseline deep water concentrations, elutriate results (Table 5-1) show concentrations below the analytical detection limit in elutriates from both sample sites CRP-1 and G87. Mn is below ANZECC(2000a) trigger values in both elutriate experiments; however, it exceeds 5x the approximate deep water baseline value for site CRP-1.

Zn exceeded ANZECC(2000a) values at site CRP-1 (1.3x) and G87 (8x). Zn also exceeded background ambient seawater detection limit concentrations by < 2.2x at site G87 and > 14x at site CRP-1. Zn is also elevated in the filter blank relative to the elutriate blank, which may be contributing to higher Zn concentrations in both elutriate experiments and sediment pore water. Zn concentrations in elutriates should be interpreted with caution. Dissolved Mn exceeds ambient site seawater concentrations by >2.7x at site G87, and 17.1x at site CRP-1. Non-purgeable Organic Carbon concentrations exceeded site ambient seawater concentrations at both sites G87 (5.7x) and CRP-1 (8.2x).

ANZECC (2000a) guidelines state that a pH change of > 0.2, under the 99 % species protection trigger values, is an indicator for potential environmental risk. The elutriate experiments for site CRP-1 exceed the ANZECC (2000a) trigger values for 99 % species protection, but G87 did not.

pH measurements of sediment pore water show an increase of acidity down the sediment profile at both sites (Table 5-2). Pore water in the first 5 cm of the sediment profile, at both sites, has a similar pH to that measured in bottom water. Site CRP-1 has a consistent trend of decreasing pH from surface water to pore water at 5 cm sediment depth. By contrast, site G87 has an anomaly where the pore water at 3 cm depth has an alkaline pH.

	CRP-1 pH measurement	G87 pH measurement
Surface Water	7.82	7.69
Deep Water	7.59	7.42
Sediment pore water 0.5cm depth	7.46	7.5
Sediment pore water 3cm depth	7.34	7.9
Sediment pore water 5cm depth	7.31	7.1

Table 5-2. pH measurements of pore water in surficial sediments and site surface and deep water.

5.3.4 Bioaccumulation Experiments

Relative bioaccumulation in amphipod tissues is assessed by comparing it to metal concentrations in the sediment matrix and phosphorite nodules. The patterns of bioaccumulation relative to concentrations of different metals measured in sediments and phosphorite nodules are the same from each site, except for Mo where the amphipod tissue concentration at Site G87 is significantly higher relative to sediments compared to amphipod tissues exposed to sediments from site CRP-1 (Figure 5-10, Figure 5-11). The highest bioaccumulation in the amphipod tissue is seen for Cd, Cu and Zn for both site G87 and CRP-1. Sr shows some potential for bioaccumulation relative to the sediment matrix concentration. For both sites, Cr, Co, Fe, Pb, Mn, Hg, Ni, U and V show little to no accumulation in the amphipod tissues relative to the concentrations measured in sediments and phosphorite nodules. In addition, Tl shows very little to no accumulation in amphipods exposed to bulk sediment from site CRP-1.

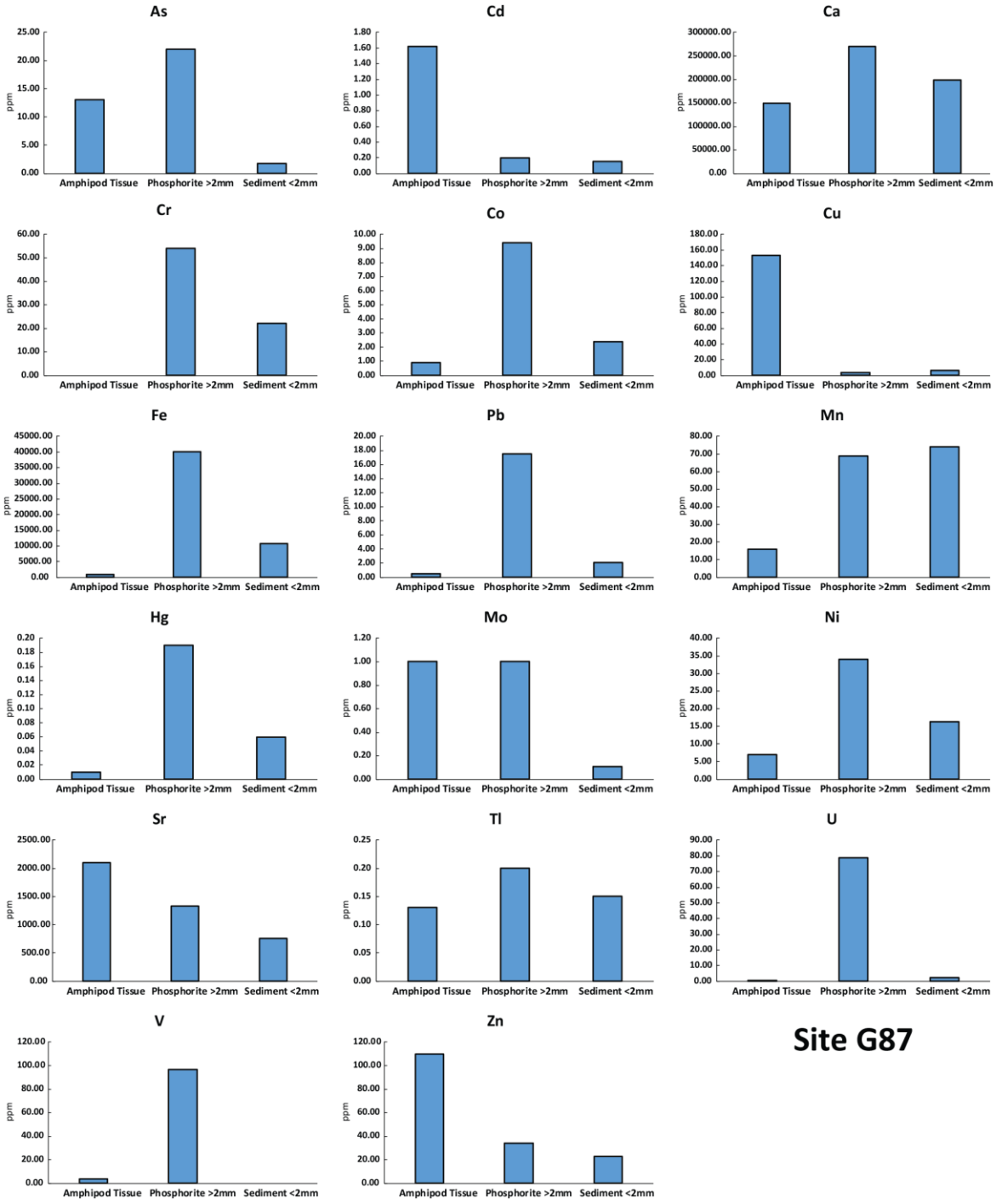

Figure 5-10: Amphipod (n=10 adults) metal body burden by element relative to sieved sediment (<2 mm) and phosphorite nodules (>2 mm) for site G87.
Units of ppm used as amphipod tissue (mg/kg) and sediment (g/m^3) analyses were reported in different, but equivalent units

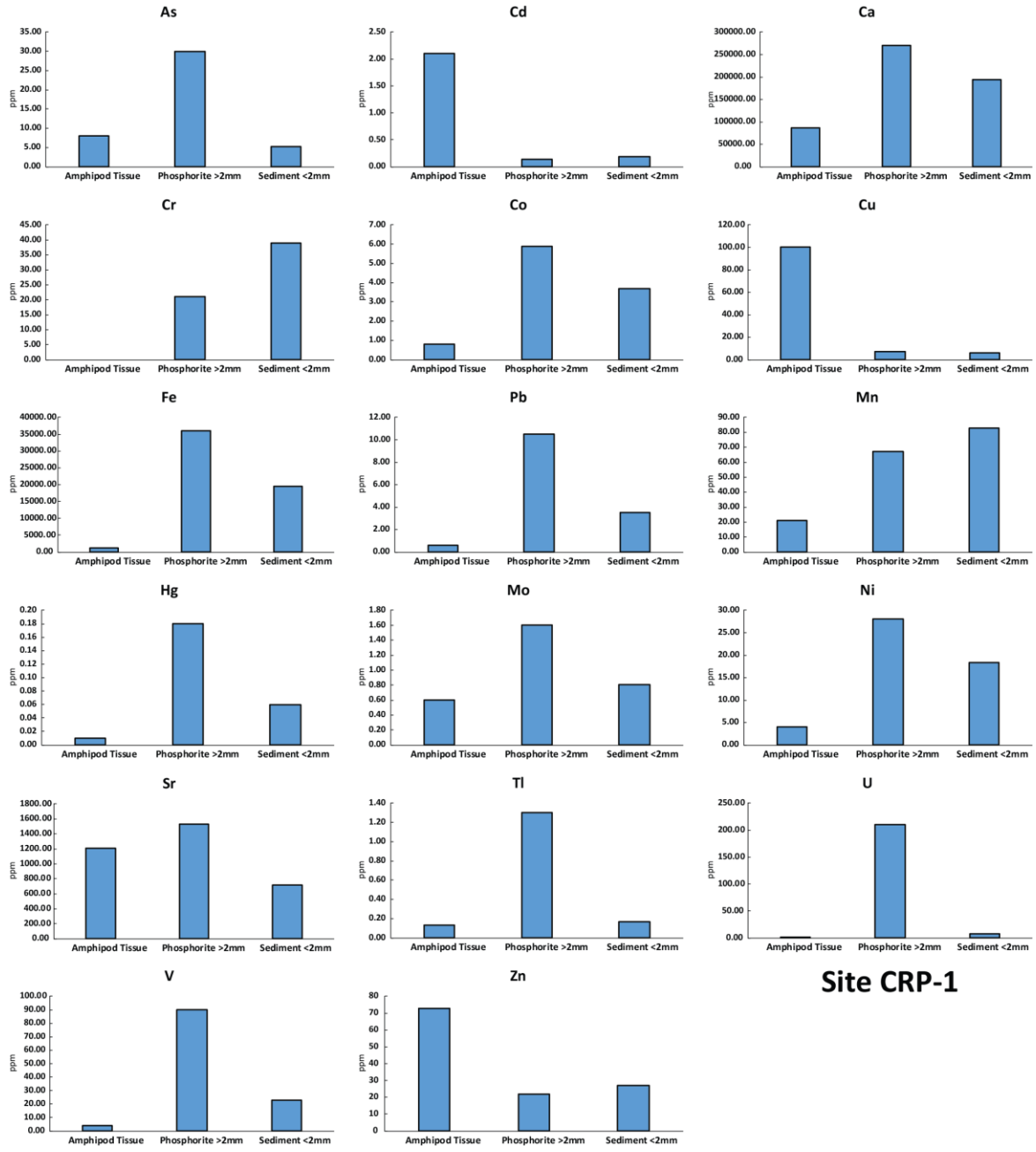

Figure 5-11: Amphipod (n=10 adults) metal body burden by element relative to sieved sediment (<2 mm) and phosphorite nodules (>2 mm) for site CRP-1.
Units of ppm used as amphipod tissue (mg/kg) and sediment (g/m^3) analyses were reported in different, but equivalent units.

Another quantitative method to assess the relative bioaccumulation potential of metals is a bioconcentration factor (BCF) (Arnot & Gobas, 2006);

Equation 7. $$BCF = C_f / C_l ,$$

where C_f is the dry weight concentration of the metal in the amphipod tissue and C_l is the total dissolved concentration of the metal in the sediment pore water. Results are compiled in Table 5-3. A BCF value of > 5000 indicates the metal bioaccumulates (CEPA, Canadian Environmental Protection Act, 1999 (Government of Canada 1999; Government of Canada 2000) cited by Arnot and Gobas (2006)), and a BCF of >10,000 can be regarded as a trigger point (ANZECC, 2000b).

Element	BCF: site G87 pore water exposure	BCF: site CRP-1 pore water exposure
As*	3250.00	2000.00
Cd*	8100.00	10500.00
Ca	384.62	220.51
Cr*	0.00[1]	0.00[1]
Co*	1500.00[1]	1333.33[1]
Cu	58846.15	38461.54
Fe	612.12	739.39
Pb*	500.00	600.00
Mn	385.37	512.20
Hg[2]	-	-
Mo	99.01	59.41
Ni*	1166.67	666.67
Sr	272.73	157.14
Tl*	650.00	650.00
U	625.00	975.00
V*	3600.00	4200.00
Zn	8461.54	5615.38

*Table 5-3:: BCF values calculated for amphipods exposed to sediment elutriates from sites G87 and CRP-1. Grey shading indicates bioaccumulation (BCF >5000).*Concentrations below the detection limit. Detection limits are used as a minimum BCF indicator only. 1. Cr and Co concentrations below detection limits in amphipod tissues. 2. Hg is below the detection limit in both pore water measurements and amphipod tissue, therefore is not included.*

The BCF factors indicate that Cd, Cu and Zn bioaccumulate in amphipod tissue (Table 5-3). The Cd BCF should be used with caution the dissolved Cd concentration in sediment pore water measurements is below the analytical detection limit. Very little bioaccumulation of Ca, Cr, Fe, Pb, Mn, Hg, Mo, Sr, Ni and Tl is indicated by the BCF values. Cu exceeds the trigger point BCF value of 10,000 by 3-5x. Although the BCF factors for Zn and Cu from site CRP-1 suggest these metals bioaccumulate, the concentrations are very similar to concentrations found in the control amphipod tissue (Table 5-4).

Element	Control (mg/kg)	Amphipods for G87 (P07) (mg/kg)	Amphipods for CRP-1 (PQ8) (mg/kg)
As	6.90	13.00	8.00
Cd	0.63	1.62	2.10
Ca	84000.00	150000.00	86000.00
Cr	1.60	<3	<3
Co	0.90	0.90	0.80
Cu	109.00	153.00	100.00
Fe	2100.00	1010.00	1220.00
Pb	1.33	0.50	0.60
Mn	66.00	15.80	21.00
Hg	<0.13	<0.3	<0.3
Mo	0.50	1.00	0.60
Ni	1.90	7.00	4.00
Sr	1220.00	2100.00	1210.00
Tl	<0.07	<0.13	<0.13
U	0.12	0.25	0.39
V	4.90	3.60	4.20
Zn	71.00	110.00	73.00

Table 5-4: Metal concentrations in amphipod tissues (mg/kg dry weight) in amphipods exposed to Chatham Rise sediments relative to the control.
The control experiment is comprised of amphipods that were kept in sediment from Raglan Harbour, from where the organisms were collected for the 28 day experiment.

5.3.5 Column blank

A blank of 18.2 MΩ water was run through the column for 5 days to measure any potential contaminants from the machining process. The blank was below detection limit for all metals analysed aside from Zn (

Table 5-5).

Dissolved Metals	g/m^3
As	< 0.0010
Cd	< 0.00005
Ca	< 0.05
Cr	< 0.0005
Co	< 0.0002
Cu	< 0.0005
Fe	< 0.02
Pb	< 0.00010
Mn	< 0.0005
Hg	< 0.00008
Mo	< 0.0002
Ni	< 0.0005
Sr	< 0.0005
Tl	< 0.00005
U	< 0.00002
V	< 0.0010
Zn	0.0138

Table 5-5: Concentration of dissolved metals measured from a MilliQ water blank to ensure metal contamination is minimal.

5.3.6 Column Leaching Experiment

Analysis of dissolved metals, and non-purgeable organic carbon of the leachate in addition to sediment trace metals were conducted by Hill Laboratories Limited, Hamilton (Appendix B-8). The pH in all three experiments changed over time. Relative to the seawater blank, both the control and column elutriates had an immediate pH drop from 8.01 to 7.82 and 7.95, respectively (Figure 5-13, Figure 5-14). Both the seawater blank and control elutriate show a drop in pH from 2 to 24 hours (from 8 and 7.85 to 7.84 and 7.63, respectively). The column

showed a similar pH drop, but delayed until 48 hours. After seven days, the pH in all three experiments.

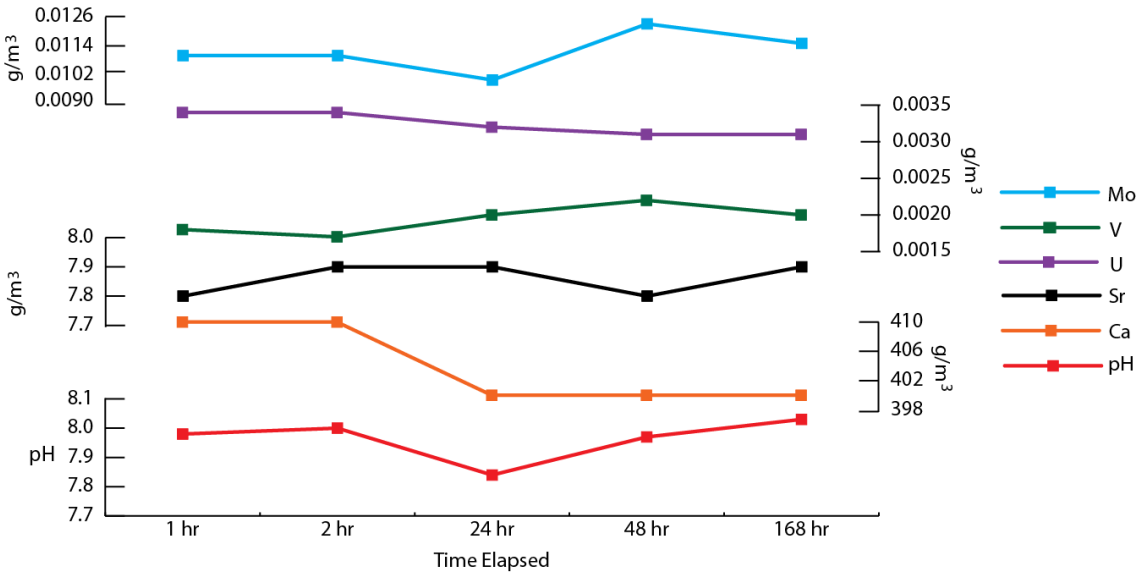

Figure 5-12: Dissolved metals concentrations in seawater blank over time.
Only dissolved metals that had concentrations above the detection limit are shown. Seawater used from site CRP-1 had been in refrigerated storage for 1 year prior to experiment.

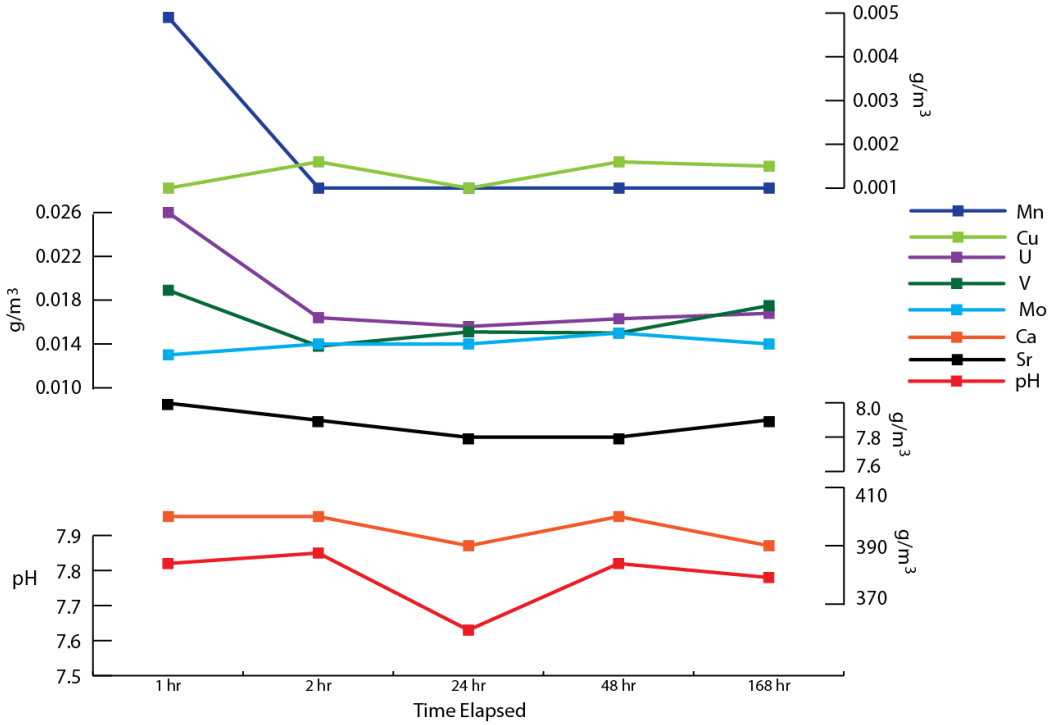

Figure 5-13: Metals concentration and pH over time for the control elutriate experiment.
Only dissolved metals that had concentrations above the detection limit are shown. Seawater and sediment used from site CRP-1 had been in refrigerated storage for 1 year prior to experiment.

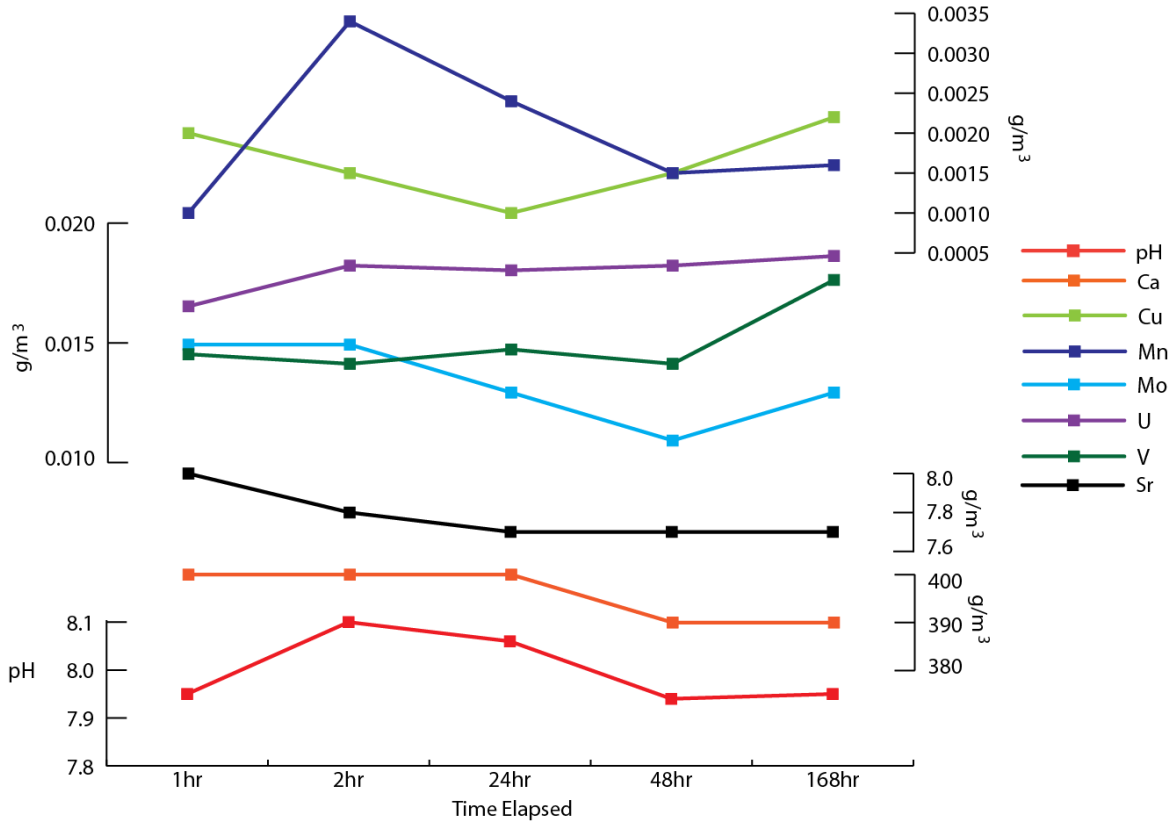

Figure 5-14: Metals concentration and pH over time for the column experiment.
Only dissolved metals that had concentrations above the detection limit are shown. Seawater and sediment used from site CRP-1 had been in refrigerated storage for 1 year prior to experiment.

had stabilized to that of their respective pH measured at the initial one hour timestamp. The pH drop in the control experiment mirrored that of the observed pH drop in the seawater control blank.

The dissolved Ca concentration of the eluent appeared to be directly proportional to the changes in pH for each of the three experiments (Figure 5-12, Figure 5-13, Figure 5-14). The column experiment showed a delayed drop in pH relative to the other two experiments, and this delay is also seen in the drop in dissolved Ca concentration after 48 hours (Figure 5-14).

Dissolved Cd remained below detection limit (<0.0002 g/m^3) until 48 hours after the experiment had been initiated for all three experiments and hence was not included in Figure 5-14. After 48 hours, dissolved Cd had increased to 0.0003 g/m^3 in the control elutriate, with a further increase to 0.0005 g/m^3 by seven days of leaching (Table 5-6). The increase of dissolved Cd coincided with a relative drop in pH. The column experiment experienced a similar increase in dissolved Cd, but not until day 7. This increase of dissolved Cd in the column experiment also coincided with a decrease in pH. Dissolved Cd in the seawater blank remained below the detection limit. Despite an increase in dissolved Cd concentration in both the column and control elutriate experiments, the concentrations did not exceed the ANZECC(2000a) trigger guideline values trigger guideline value for 99% species protection of 0.0007 g/m^3 (Table 5-6).

The concentration of dissolved Mn remained below the detection limit for the duration of the experiment for the blank (Figure 5-12). For the control elutriate experiment, Mn was initially elevated, but after 2 hours decreased to below the detection limit for the duration of the experiment (Figure 5-13).

Mn concentrations in the column experiment remained above the detection limit for the entirety of the experiment. In the column experiment the Mn increased in concentration as pH increased, and vice versa (Figure 5-14). Despite the elevation in dissolved Mn in both the column and elutriate control experiments, the levels did not exceed ANZECC (2000a) trigger values (Table 5-6).

Initial dissolved Mo concentrations in the control and column elutriates were higher than that of the blank (Figure 5-12, Figure 5-13, Figure 5-14). The dissolved Mo in the control elutriate experiment remained higher than that of the blank, and the increases and decreases appear to be coeval with changes in the pH level. The column experiment initially had relatively high concentrations of dissolved Mo compared to the control and seawater blank experiments; however, after 24 hours, the dissolved Mo concentration dropped to below that of the seawater blank. This decrease also coincides with a drop in the pH.

Sample	Units	Blank (B1)	Blank (B2)	Blank (B3)	Blank (B4)	Blank (B5)	ANZECC Trigger Value (99%)
Temperature	°C	20.1	20.2	20.3	20.4	21	-
Time Elapsed	hours	1	2	24	48	168	-
pH	-	7.98	8	7.84	7.97	8.03	>0.2 change
Dissolved As	g/m^3	<0.004	<0.004	<0.004	0.004	<0.004	NG
Dissolved Ca	g/m^3	410	410	400	400	400	NG
Dissolved Cd	g/m^3	<0.0002	<0.0002	<0.0002	<0.0002	<0.0002	0.0007
Dissolved Cr	g/m^3	<0.001	<0.001	<0.001	<0.001	<0.001	0.0077 (3+)
Dissolved Co	g/m^3	<0.0006	0.0009	<0.0006	<0.0006	<0.0006	0.001[1]
Dissolved Cu	g/m^3	<0.001	0.0011	<0.001	<0.001	<0.001	0.0003
Dissolved Fe	g/m^3	<0.004	<0.004	<0.004	<0.004	<0.004	NG
Dissolved Pb	g/m^3	<0.001	<0.001	<0.001	<0.001	<0.001	0.0022
Dissolved Mn	g/m^3	<0.001	<0.001	<0.001	<0.001	<0.001	0.02[2]
Dissolved Mo	g/m^3	0.011	0.011	0.01	0.0123	0.0115	NG
Dissolved Ni	g/m^3	<0.006	<0.006	<0.006	<0.006	<0.006	0.007
Dissolved Sr	g/m^3	7.8	7.9	7.9	7.8	7.9	NG
Dissolved Tl	g/m^3	<0.0002	<0.0002	<0.0002	<0.0002	<0.0002	NG
Dissolved U	g/m^3	0.0034	0.0034	0.0034	0.0031	0.0031	NG
Dissolved V	g/m^3	0.0018	0.0017	0.002	0.0022	0.002	0.05
Dissolved Zn	g/m^3	-	-	-	-	-	0.007
NOPC	g/m^3	-	-	-	<3	<3	NG

Table 5-6: Compiled results of the leaching column chemistry for Chatham Rise site CRP-1 sediment and deep water. Red shading indicates potential contamination, grey fill indicates exceedance of ANZECC (2000a) trigger value, bold type with black outline indicates exceedance of 5 times the concentration of the baseline site deep water values from Table 5-1. 1. 95% protection value used for Co, as Hickey et al. (2014) considers the 99% value a statistical artefact. Updated and unpublished ANZECC(2000a) value for Mn cited by Hickey et al. (2014). NG= No guideline.

Sample	Units	Control (CE1)	Control (CE2)	Control (CE3)	Control (CE4)	Control (CE5)	ANZECC Trigger Value (99%)
Temperature	°C	20.3	20.8	20.3	20.4	21.07	-
Time Elapsed	hours	1	2	24	48	168	-
pH	-	7.82	7.85	7.63	7.82	7.78	>0.2 change
Dissolved As	g/m³	<0.004	<0.004	<0.004	<0.004	0.004	NG
Dissolved Ca	g/m³	400	400	390	400	390	NG
Dissolved Cd	g/m³	<0.0002	<0.0002	<0.0002	0.0003	0.0005	0.0007
Dissolved Cr	g/m³	<0.001	<0.001	<0.001	0.0017	<0.001	0.0077 (3+)
Dissolved Co	g/m³	<0.0006	<0.0006	<0.0006	<0.0006	<0.0006	0.001
Dissolved Cu	g/m³	<0.001	0.0016	<0.001	0.0016	0.0015	0.0003
Dissolved Fe	g/m³	<0.004	<0.004	<0.004	<0.004	<0.004	NG
Dissolved Pb	g/m³	<0.001	<0.001	<0.001	<0.001	<0.001	0.0022
Dissolved Mn	g/m³	**0.0049**	<0.001	<0.001	<0.001	<0.001	0.02
Dissolved Mo	g/m³	0.013	0.014	0.014	0.015	0.014	NG
Dissolved Ni	g/m³	<0.006	<0.006	<0.006	<0.006	<0.006	0.007
Dissolved Sr	g/m³	8	7.9	7.8	7.8	7.9	NG
Dissolved Tl	g/m³	<0.0002	<0.0002	<0.0002	<0.0002	<0.0002	NG
Dissolved U	g/m³	**0.026**	**0.0164**	**0.0156**	**0.0163**	**0.0168**	NG
Dissolved V	g/m³	**0.0189**	**0.0138**	**0.0151**	**0.015**	**0.0146**	0.05
Dissolved Zn	g/m³	-	-	-	-	-	0.007
NPOC	g/m³	-	-	-	<3	<3	NG

Table 5-6 continued.

Sample	Units	Column (C1)	Column (C2)	Column (C3)	Column (C4)	Column(C5)	ANZECC Trigger Value (99%)
Temperature	°C	20.3	20.7	20.3	20.4	21.07	-
Time Elapsed	hours	1	2	24	48	168	-
pH	-	7.95	8.1	8.06	7.94	7.95	>0.2 change
Dissolved As	g/m³	<0.004	<0.004	0.004	0.004	<0.004	NG
Dissolved Ca	g/m³	400	400	400	390	390	NG
Dissolved Cd	g/m³	<0.0002	<0.0002	<0.0002	<0.0002	0.0003	0.0007
Dissolved Cr	g/m³	<0.001	<0.001	<0.001	<0.001	<0.001	0.0077 (3+)
Dissolved Co	g/m³	<0.0006	<0.0006	<0.0006	<0.0006	<0.0006	0.001
Dissolved Cu	g/m³	0.002	0.0015	<0.001	0.0015	0.0022	0.0003
Dissolved Fe	g/m³	<0.004	<0.004	<0.004	<0.004	**0.006**	NG
Dissolved Pb	g/m³	<0.001	<0.001	<0.001	<0.001	<0.001	0.0022
Dissolved Mn	g/m³	<0.001	**0.0034**	**0.0024**	**0.0015**	**0.0016**	0.02
Dissolved Mo	g/m³	0.015	0.015	0.013	0.011	0.013	NG
Dissolved Ni	g/m³	<0.006	<0.006	<0.006	<0.006	<0.006	0.007
Dissolved Sr	g/m³	8	7.8	7.7	7.7	7.7	NG
Dissolved Tl	g/m³	<0.0002	<0.0002	<0.0002	<0.0002	<0.0002	NG
Dissolved U	g/m³	**0.0166**	**0.0183**	**0.0181**	**0.0183**	**0.0187**	NG
Dissolved V	g/m³	**0.0146**	**0.0142**	**0.0148**	**0.0142**	**0.0177**	0.05
Dissolved Zn	g/m³	<0.004	0.006	<0.004	<0.004	0.035	0.007
NOPC	g/m³	-	-	-	<3	<3	NG

Table 5-6 continued.

The concentration of dissolved Cu in the seawater blank was below the detection limit, except after 2 hours, but stayed below the dissolved Cu concentrations in the control and column elutriate experiments (Figure 5-12). Cu concentrations in the elutriate control experiment appear to have changed with corresponding changes in pH throughout the experiment (Figure 5-13). Despite dissolved Cu being higher than the detection limit after 2 hours, the value of 0.0011 g/m^3 is so close to the baseline that contamination is unlikely.

In the column experiment (Figure 5-14), Cu decreased over the first 24 hours, and increased again after a week to equilibrium. Cu did not appear to follow changes in pH as was observed in the elutriate control experiment. In the elutriate control experiment, all analyses after 2 hours indicated the dissolved Cu concentration had exceeded the ANZECC(2000a) trigger

value by ~ 5x (Table 5-6). The dissolved Cu concentration in the column leaching experiment consistently exceeded ANZECC(2000a) trigger guidelines, by ~ 5 - 7x.

Dissolved Sr concentrations in both the column and elutriate control experiments changed little relative to that of the baseline. Dissolved Sr concentrations do not appear to have varied with pH or dissolved calcium concentration in any of the experiments.

Dissolved U was elevated above baseline levels (seawater blank) in both the elutriate control (Figure 5-13) and column experiments (Figure 5-14). In the column experiment, dissolved U was at its lowest concentration, and observed to reach equilibrium after 2 hours (Figure 5-14). There is no further change, even with the observed changes in pH. Dissolved U in the control elutriate experiment (Figure 5-13) also reached equilibrium after 2 hours; however, initial concentrations were higher, and decreased as equilibrium was reached. There are currently no ANZECC(2000a) trigger guidelines for U; however, dissolved uranium does exceed 5x the concentration of baseline dissolved uranium measured in the CRP-1 site seawater (Table 5-1).

Dissolved V concentrations for both the control elutriate and column experiment are above the seawater blank baseline. In the control elutriate, dissolved V had equilibrated with little variance after 2 hours (Figure 5-13). It is difficult to tell if the small variance in dissolved V concentration after 2 hours is due to pH changes. Similarly, dissolved V in the column experiment appears to have reached equilibrium almost immediately, however between 48 hours and a week of leaching, the V concentration increased (Figure 5-14). This increase in dissolved V concentration does not appear to coincide with a change in pH. Concentrations of V in both the control elutriate and column leaching experiment exceeded 5x the background value for CRP-1 deep water (Table 5-6)(Table 5-1), but did not exceed the ANZECC(2000a) guideline trigger value.

5.4 Discussion

5.4.1 Elutriate Experiments and Sediment Pore Water

The redox conditions of the natural sediment profile are important, as different metals have different solubilities in reducing/anoxic conditions relative to oxic conditions. In addition, the release of high concentrations of sulphides from sediment pore water can be highly toxic for marine biota (Brown et al., 2011). In this study, total sulphides were below the detection limit in shipboard elutriate experiments (Section 5.3.3, Table 5-1), and therefore pose no toxicity threat to local biota if the sediment were to be disturbed. No direct pore water measurements of sulphide concentrations were collected; however, dissolved metal concentrations can give insights into the redox conditions in the surficial sediments.

Sediment pore waters displayed higher dissolved Fe and Mn concentrations relative to the elutriate experiments (Table 5-1). The high concentrations of Fe and Mn indicate that the redox conditions in the surficial sediment of these two sites of Chatham Rise could be suboxic as there was an absence of a sulphur odour during sampling suggests the sediment is not anoxic/reducing, which is consistent with previous studies (Golder Associates (NZ) Limited, 2014b; Hickey et al., 2014). If conditions were oxic, it would be expected that dissolved Fe would be low, as Fe oxidised into an insoluble oxyhydroxide species in oxygenated conditions (Morse, 1991).

In anoxic/suboxic conditions, Fe^{2+} is the stable species. Upon exposure to more oxic conditions Fe^{2+} is rapidly oxidised to insoluble oxyhydroxides, initially over the course of hours to days (Morse, 1991). The decrease in dissolved Fe and Mn concentrations in elutriate experiments relative to direct surficial sediment pore water measurements indicates that upon mixing with oxygenated seawater, Fe accompanied by Mn, is rapidly oxidised and re-precipitated.

Significantly, sediment pore water extracted directly from the sediments at site G87 showed elevated Cu concentrations that exceeded both ANZECC (2000a) trigger guidelines (8.6x) and site ambient seawater concentrations (<2.6x) (Table 5-1). Dissolved Cu concentrations were below the detection limit of 0.001 g/m^3 in deep water from both sites. Thus, no definite background value can be assigned.

A decrease of dissolved Cu concentration in the elutriate experiments relative to sediment pore water was also observed, similar to Fe and Mn. This suggests that the decrease in dissolved Cu could be linked to Fe and Mn. Dissolved Cu has been found to efficiently be removed from solution by adsorption to iron oxyhydroxides (Moon & Peacock, 2012).

Non-purgable organic carbon (organic matter) is observed to be higher than 5x the baseline deep water levels by 5.7 and 8.2 times at site G87 and CRP-1, respectively (Table 5-1). Dissolved organic carbon can have an effect on heavy metal bioavailability, as metals can strongly adsorb to organic matter and become unavailable, leading to a reduction in toxicity (Australian and New Zealand Environment Conservation Council, 2000b). Fe and Mn oxyhydroxides complexed with organic matter derived ligands have been found to be more effective in removing dissolved Cu than non-complexed oxyhydroxides (Moon & Peacock, 2012). Therefore, the decrease in Cu observed between sediment pore water samples and elutriate experiments could be due to the scavenging of dissolved Cu by released organic matter, or oxyhydroxides possibly complexed with ligands derived from organic matter. Dilution with seawater could also decrease Cu concentrations observed in the elutriate experiments.

Elevated Cu concentrations in pore water indicates a potential issue if mining were to commence, agitation of the surface sediments due to mining could release dissolved Cu into the immediate environment. A 200x initial dilution of disturbed sediment is shown in plume modelling studies for the Chatham Rise (Golder Associates (NZ) Limited, 2014b), but the validity of these models has been questioned (Environmental Protection Agency, 2015). In the standard elutriate experiments, sediment is diluted in a 1:4 ratio with seawater. Results from this study show that 4x dilution is enough to reduce elevated Cu concentrations in the sediment pore water by at least 2.6x to below the detection limit (Table 5-1). However, the analytical detection limit is 3x the ANZECC (2000a) guideline trigger value for Cu. Therefore, the combined dilution and scavenging of dissolved Cu released during sediment disturbance does effectively dilute dissolved Cu concentrations; however, the exact diluted concentration in elutriates is still unknown.

Surface seawater pH measurements taken during sampling in this study are more acidic than expected. The average pH of oceanic surface water is 8.1 (Millero et al., 2009). Cool Sub Antarctic surface water off the coast of Otago, New Zealand, has been measured using spectrophotometric methods, with an average pH of 7.84 ±0.002 (Ohline et al., 2007), which is consistent with the surface water pH measurement of 7.82 for site CRP-1 in this study. The surface water measurement of 7.69 from site G87; however, is significantly lower. Furthermore, the sampling sites in this study are situated in the Sub-Tropical Front (Figure 1-1), and not under the influence of cooler Sub Antarctic waters. It is possible that problems with the pH probe performance in saline solutions have caused the lower than expected pH measurements, rather than a natural occurrence.

A comparison of previous elutriates, and column experiments indicate that the shipboard elutriate experiments from this study have anomalously low pH (Figure 5-15). The column experiments in this study used a sub-sample of the same bottom water from site CRP-1, but were measured with a different type of pH probe.

The inconsistent measurements suggest the pH probe used for shipboard elutriates may not have performed properly in seawater. This could arise from the buffers used to calibrate the pH probe: standard buffer solutions were used; however, calibration with artificial seawater buffers give more accurate results when using standard potentiometric methods of pH measurement by matching the salinity (Marion et al., 2011; Millero et al., 1993).

The pH of the sediment pore water decreases down the sediment profile at both site G87 and CRP-1 (Table 5-2). Slightly more acidic pH measurements of bottom water are expected as there is a higher concentration of dissolved CO_2 due to respiration and organic matter decomposition (C. Hickey, Pers. Comm. 2016)

Results from column and elutriate experiments from this study are compared to previous experiments by Hickey et al. (2014) (Figure 5-15). These experiments exceeded ANZECC (2000a) guidelines for Cu concentrations in both elutriates (15-22x) and in the seawater used from the Alderman Islands (16x). By contrast, elutriates and baseline deep water dissolved Cu concentrations for both sites analysed here were below detection limit. However, dissolved Cu concentrations for column leaching experiments exceeded ANZECC(2000a) guideline trigger values (by 5-7x) (Table 5-6). It should be noted ;however, that the detection

limit for Cu, 0.001 g/m^3, is 3x higher than the ANZECC(2000a) guideline trigger value of 0.0003 g/m^3, indicating that methods with lower detection limits are required.

U values in the previously reported 30 minute elutriates showed an elevation of < 4.3x (Hickey et al., 2014), and exceeded 5x site CRP-1 baseline deep water concentrations in both column leaching and elutriate control experiments reported here. Conversely, dissolved U concentrations in the shipboard elutriate experiments did not exceed site deep water values by more than 1x. This could indicate that the freeze-thaw process and/or long term refrigeration storage could affect the mobility of U, hence increasing dissolved U concentrations.

In contrast to these metals, dissolved Sr is similar across all the experiments. This indicates that conducting experiments on old material cannot confidently give a true indication of the concentration of dissolved metals released during sediment disturbance. The long-term storage of sediments, either by freezing or refrigerating will not preserve the sediments well enough to conduct elutriate experiments that are representative of the true response. In future, samples should be processed within a shorter time period, preferably at the time of sample collection.

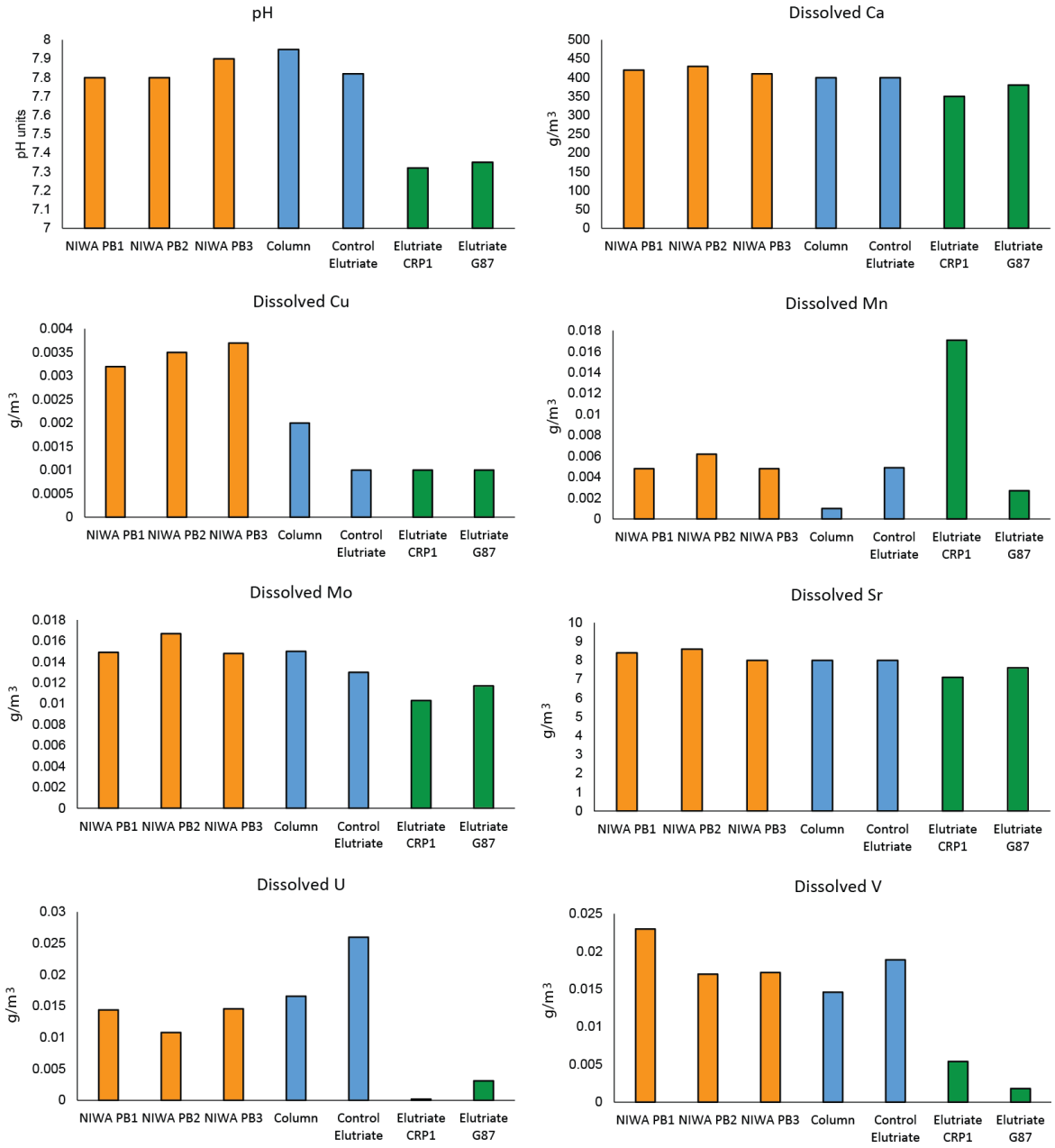

Figure 5-15: A comparison of results for all elutriate and column experiments conducted on Chatham Rise sediment 0.5 to 1 hour after agitation.

Yellow fill: data from Hickey et al. (2014), blue fill: data from column experiments (Section 5.3.6), green fill: data from ship board elutriate experiments (section 5.3.3). Only dissolved metals displaying concentrations above the detection limit are included.

5.4.2 Bioaccumulation Experiments

The sensitivity of amphipods to metal contaminants depends on a number of factors, for example, whether or not the amphipod species is infaunal tube-dwelling and filter feeding on particulates in the water column, or is epibenthic (King et al., 2006). Infaunal amphipods are more insensitive to high dissolved Cu and Zn metal concentrations (King et al., 2006). The two major pathways in which infaunal amphipods can be exposed to dissolved metals are through sediment pore water (King et al., 2006) or ingestion of sediment particles (Marsden & Rainbow, 2004) and thus, the elevated levels of Cu observed in the sediment pore water samples (Table 5-1) may be of concern if surficial sediment disturbance due to mining were to occur.

Many traditional metal accumulation studies expose test organisms to one element at a time in controlled laboratory experiments. Different metal combinations or mixtures can cause differences in bioavailability and toxicity in some organisms, for example, an excess of Fe can result in higher Cd accumulation in talitrid amphipods (Casini & Depledge, 1997). The accumulation experiments in this study used whole sediments, therefore the accumulation observed would be closely matched to what would be expected in the natural environment.

Using whole sediments also decreases the uncertainty about whether the observed accumulation, or lack thereof, is representative of the natural environment after sediment disturbance. A further consideration in the context of seabed mining of Chatham Rise is that processed sediments returned to the seafloor are the <2mm fraction, whereas experiments in this study used whole sediments including the >2mm fraction. Considering elements that are highly enriched in the phosphorite nodules e.g. U were not shown to be released in significant concentrations it can be assumed that the main contribution of dissolved metals is from the sediment matrix, and the sediment pore water. Future bioaccumulation studies should also be conducted using <2mm and >2mm fractions to assess not only the intial seafloor sediment disturbance, but also the return of the fine <2mm fraction to the seafloor.

The bioaccumulation experiment undertaken here is only used as an indicator of potential relative bioaccumulation. Consequently, metals that are enriched in sediment and phosphorite nodules but do not bioaccumulate are of most significance. At site G87, the matrix sediment is enriched in Hg (Figure 5-9-a), and the phosphorite nodules are enriched

in Hg, Pb, Fe and U (Figure 5-9-b). These elements are not observed to have accumulated in amphipods exposed to elutriate leachate from the same site (Figure 5-10). Similarly, U and Hg are enriched in matrix sediments (Figure 5-9-a) and U, Hg and V is enriched in phosphorite nodules from site CRP-1 (Figure 5-9-b), and are also not observed to significantly bioaccumulate (Figure 5-11).

This indicates that the dissolution of solid phases in sediments during agitation, especially phosphorites, is unlikely. Since dissolved concentrations of U were below baseline levels in the elutriate experiments conducted in this study, it is likely that low concentrations of dissolved U are also contributing to low observed levels of U bioaccumulation in amphipod tissues.

Cr, Co, Mn and Ni are not enriched in phosphorite nodules (Figure 5-9-b) or the sediment matrix (Figure 5-9-a) from both G87 and CRP-1, nor is Tl at site CRP-1. These metals display little to no bioaccumulation in amphipod tissues (Figures 5-10, 5-11), indicating that these metals are either not bioavailable under the conditions of the experiment, or are not released in high enough concentrations to bioaccumulate.

A change in redox conditions can change the bioavailability of some metals species, for example, Fe and Mn are more bioavailable in the reduced form. The high concentrations of Fe and Mn measured in sediment pore water rapidly oxidise and precipitate when mixed with oxygen rich bottom water as observed in elutriates, therefore, despite Fe and Mn being enriched in sediment pore water, little to no bioaccumulation is observed (Figure 5-10, Figure 5-11).

Cu concentrations in sediment pore water are high, but below detection limits in the elutriate experiments in this study (Table 5-1). However, Cu is observed to be highly bioaccumulative in amphipods exposed to sediment elutriates from both site G87, and CRP-1. The BCF factor for Cu in amphipod tissues is 3-5x the trigger value of 10,000.

Cu concentrations in the sediment matrix are higher at site G87 (6.3 ppm), and slightly lower at site CRP-1 (5.8 ppm). Conversely, phosphorite nodules from site CRP-1 (7 ppm) have a higher Cu concentration than G87 (4 ppm). Site G87 also shows higher relative bioaccumulation in both absolute concentration in amphipod tissue, and BCF factors. This

could indicate that concentrations of bioavailable Cu are site dependant. However, the differences in Cu concentrations in the sediment matrix and phosphorite nodules is small, and since the uncertainties in the analyses were not supplied with the results, it is not possible to determine if the differences between the Cu concentrations at each site are statistically significant, or if they are within error.

Cu concentrations in the control experiment are comparable to concentrations observed in amphipods exposed to whole sediment from site CRP-1 (Table 5-4). Cu is an essential trace element and commonly accumulates in the tissues of aquatic organisms without toxic effects. However, too high concentrations of Cu can also be toxic, with invertebrates such as amphipods being the most sensitive to excess Cu (Australian and New Zealand Environment Conservation Council, 2000b), especially infaunal species (King et al., 2006). Therefore, some accumulation is expected in the amphipod tissues, and it is possible that the amphipods exposed to whole marine sediments have retained their naturally high concentrations of Cu from the collection site. Cu concentrations in amphipod tissues exposed to sediment from site CRP-1 show similar concentrations to amphipods kept in the control sediment (Table 5-4).

Whilst Zn concentrations were elevated in both sediment pore water and elutriate experiments, the results were interpreted with caution due to contamination observed in the filter blank. Both the bioaccumulation experiments and BCF factors indicate Zn is highly bioaccumuative in amphipods exposed to disturbed whole sediment from both sampling sites. However, Zn is an essential metal in aquatic organisms (Australian and New Zealand Environment Conservation Council, 2000b), therefore a certain degree of bioaccumulation is expected. Similar to Cu concentrations in amphipod tissues, amphipods exposed to site CRP-1 whole sediments had similar Zn concentrations to the control amphipod tissues (Table 5-4). Amphipods exposed to site G87 whole sediments had elevated Zn concentrations relative to the control. It is possible that Zn has accumulated above natural concentrations in the amphipods exposed to whole sediments from site G87; however, this cannot be confirmed without a critical bioassay, and a chemical analysis of the control sediment was not undertaken.

Dissolved Cd concentrations were below detection limit in the shipboard elutriate experiments, but in the long-term column experiment had concentrations above the detection limit, but below ANZECC (2000a) guideline trigger values after 48 hours (Table 5-6). The bioaccumulation experiments also show that the non-essential metal Cd is bioaccumulative in amphipods exposed to whole marine sediments. This is validated by the observation that concentrations in the tissue of amphipods exposed to whole sediments from sites G87 and CRP-1 have over double the concentrations observed in the control experiment (Table 5-4).

The amphipod *Chaetocorophium* c.f. *lucasi* is a filter feeder and the most likely uptake pathways are from particulates or from Cd dissolved in the water. This could suggest that Cd release/dissolution takes much longer than other metals, but Cd was able to significantly bioaccumulate within the 28 days exposure of the experiments. Another possibility is that the amphipods could have ingested excess Cd from particulates. More long term and detailed studies into Cd dissolution would provide more certainty into if this is the case or if the low concentrations of dissolved Cd are sufficient over the 28 days to concentrate in the amphipod tissues without toxic effects.

Differences in the degree of bioaccumulation are also observed in amphipods exposed to the two different whole sediments. Mo shows relatively higher bioaccumulation of almost 2x in amphipods exposed to sediments from site G87 relative to site CRP-1(Table 5-4), coupled with a higher BCF factor (Table 5-3), despite site G87 sediments having lower concentrations of Mo. This indicates that differences in local sediment chemistry, including sediment pore water, and metal bioavailability can result in different effects on biota. To fully monitor the effects of sediment disturbance on marine biota, the entire substrate needs to be chemically characterized, as does the control sediment. Sediment geochemistry results (Chapter 4.) show that trace elements in surficial and chalk sediment from the Chatham Rise have site specific differences, notably in relative enrichments of Mo. Major element analyses of different size fractions also show differences in chemistry. The larger size fractions of 63µm to 8mm show higher enrichments in FeO, CaO, K_2O, P_2O_5, Al_2O_3, MnO and MgO (Figure 4-7), suggesting the sediments comprise different minerals at different size fractions. It has been previously found (Von Rad & Rosch, 1984) that the smallest size fractions are dominated by quartz erratics, and the larger size fractions (63µm -8mm) are dominated by foraminifera, chalk aggregates, glauconite, pumice, and phosphorite. Different ratios of these components will

also lead to different site specific chemistry surficial sediment chemistry, and hence to potentially different effects on biota.

However, Mo is an essential metal for aquatic organisms (Australian and New Zealand Environment Conservation Council, 2000b), therefore some accumulation is expected. The extent of toxicity of marine organisms to Mo remains unknown, as the ANZECC (2000a) trigger guideline values for the marine environment were based solely on dinoflagellates (Australian and New Zealand Environment Conservation Council, 2000b). More research into the toxicity of Mo in marine organisms is required as it is clear from the relative bioaccumulation observed in this study that Mo has some bioaccumulation potential.

Chaetocorophium c.f. *lucasi* is a burrowing Amphipod (Dewitt et al., 1999), which can lead to difficulties in being able to determine precise effects of trace metals in sediments as the amphipods tested in a laboratory setting are exposed not only to the ambient surface water, but also the sediment pore water and sediment (Marsden & Rainbow, 2004). In this instance, the BCF factor is not an ideal method of quantifying the concentration of metals in tissue as a limitation is that the measurement does not consider metal uptake from food sources. The BCF factor only considers the concentration of metals in the organism relative to the water in which the organism is exposed.

In calculating the BCF factors for this study, direct sediment pore water concentrations were used instead of elutriate extracts, because of the very low concentrations in the elutriate extracts (Appendix B-4). This may result in lower BCF values for Fe, Mn and Cu as these elements have high concentrations in sediment pore water (Table 5-1). Direct measurements of sediment pore water are only available for site G87, therefore using the same values to calculate BCF factors for amphipods exposed to site CRP-1 sediments may not give a robust indication of potential bioaccumulation. However, Since sediment chemistry is heterogeneous between sites (Figure 5-9), it is likely that the sediment pore water at site CRP-1 will also have a different chemistry.

Another limitation of the BCF method applied to this study is that many of the analyses for dissolved metals in the pore water extracts were below detection limit, and the detection limit was substituted as a value. This would result in the calculated BCF values being either underestimated or overestimated.

5.4.3 Column Leaching Experiments

pH and dissolved Ca concentrations are observed to change in unison in all three experiments. The experiments in this study were exposed to the atmosphere, therefore changes to pH due to atmospheric $_pCO_2$ is possible (Aranda, 2008), as well as microbial processes, as the experiment was exposed to light and non-sterile atmosphere which could have encouraged the growth of some photosynthesising organisms (Andersson, 2014).

The relationship of CO_2 and pH in seawater is shown below. Equations are from Andersson (2014):

Equation 8. $CO_2 + H_2O \leftrightharpoons H_2CO_3$

Equation 9. $H_2CO_3 \leftrightharpoons H^+ + HCO_3^{2-}$

Equation 10. $H^+ + CO_3^{2-} \leftrightharpoons HCO_3^{2-}$

Giving the overall equation:

Equation 11. $CO_2 + H_2O + CO_3^{2-} \leftrightharpoons 2HCO_3^-$

As CO_2 dissolves in seawater, H^+ ions are produced, causing the pH to drop. The excess H^+ can react with carbonate species already dissolved in the water, or cause the dissolution of $CaCO_3$, hence CO_3^{2-} also decreases when pH decreases. This can cause an excess of Ca^{2+} and speciation changes in metals complexed with CO_3^{2-} in solution (Millero et al., 2009). Conversely, if the pH becomes too high, H_2CO_3 can disassociate, creating an excess of H^+ ions, leading to a pH drop. This is an equilibrium process, and provides an effective buffer for pH in seawater

If the above buffer system is responsible for the changes in pH throughout the experiment ; however, it would be expected that dissolved Ca would increase with a decrease in pH, not change in unison. It could be that the scale of the changes is large, as very few measurements were taken over a long period, thus the leads and lags of the pH and dissolved Ca concentration cannot be observed in enough detail.

Alternatively, pH can also change the speciation and concentration of dissolved metals in a solution. For example, dissolved Cu concentration was observed to vary in unison with pH, especially in the static elutriate control experiment (Figure 5-13). The initial pH of the elutriate control experiment was 7.8, and under these conditions the main species of Cu in a

carbonate dominated system (such as seawater) are $CuCO_3$ (69%), Cu^{2+} (14.9%), and $Cu(CO_3)_2^{2-}$ (10.5%) (Millero et al., 2009). During the experiment, the pH dropped to ~7.6. Under these conditions the main Cu species are expected to be $CuCO_3$ (66%), Cu^{2+} (22%), and $Cu(CO_3)_2^{2-}$ (6.2%) (Millero et al., 2009), resulting in a ~7% increase in free Cu^{2+} speciation.

In more acidic conditions, the solubility of metals is also expected to increase, therefore it is expected that the absolute concentrations of free Cu will increase. This was not observed in these preliminary experiments, most likely due to the large time gaps between sampling which does not allow the observation of the rate of dissolved metal concentration in enough detail. The uncertainties in the analyses are not known, therefore the actual variation could be much smaller, and the system is most likely more complex. Metal complexion with organic and OH^- ligands are also affected by pH (Millero et al., 2009), and could exert some influence on the dissolved metals concentrations over time in this experiment.

An excess of free Cu^{2+} can be toxic for aquatic organisms (Australian and New Zealand Environment Conservation Council, 2000b), therefore the effects of an increase in $_pCO_2$, and hence ocean acidification, on the dissolution and speciation of metals in marine sediments and minerals needs to be explored.

Determining the speciation of the dissolved metals was beyond the scope of this thesis; however, it is clear from these experiments that a CO_2 based pH control system needs to be implemented as the next stage of development for this apparatus. With a pH control system implemented, the factors influencing the concentrations of dissolved metals can be isolated, and the apparatus can also be used to observe the effects of ocean acidification on the release of metals from sediments in a laboratory environment.

Temperature effects are very important when trying to model a natural response in laboratory conditions. Most leaching experiments are conducted at room temperature (Aranda, 2008), as were the experiments in this study. The temperature of the natural system is usually much lower however. For example, in this study the ambient temperature at 365 -380 m below sea level is ~ 8.2 to 8.9 °C (Section 5.3.1). Lower temperatures can affect the solubility of different metal species (Aranda, 2008), therefore to fully understand long term chemical

release over time, experiments at different temperatures, in addition to pH, should be conducted on the material.

The long term behaviour of some metals in the dynamic circulating column tests differed from those of the static control elutriate experiment. For example Mn decreased rapidly to equilibrium in the control elutriate, whereas in the column Mn continued to increase until 2 hours, and then slowly decreased in concentration over the week. Aranda (2008) conducted static agitation tests, and static and dynamic leaching experiments on sediments, similar to this study. Aranda (2008) also found that in the dynamic experiments where the leachate is constantly circulating, the behaviour of the dissolved metals differed from that of the static tests over time. That study concluded that the dynamic experiments were better for observing long term behaviour of dissolved metals.

Overall, the relative changes in dissolved metal concentration over the week of leaching in all experiments was very low. Despite an increase in dissolved Cd after a week to 0.0005 g/m^3, this concentration is still below the ANZECC(2000a) guideline trigger value of 0.0007 g/m^3. Dissolved Cu exceeded ANZECC(2000a) guideline trigger values in both the column and control elutriate experiments; however, as discussed in Sections 5.4.1 and 5.4.2, the dissolved Cu is from the sediment pore water, and the long term storage of sediment changes the concentrations of dissolved metals. This indicates that significant dissolution of solid phases such as phosphorite nodules, or release of high concentrations of dissolved metals is unlikely to occur within a week of sediment disturbance under the conditions of the column experiments in this study.

Chapter 6. Conclusions

This study sought to characterise the bulk geochemistry of New Zealand offshore phosphorite nodules, evaluate the potential release of dissolved ecotoxic metals during seafloor sediment disturbance and evaluate the effectiveness of amphipods as a potential biomonitor.

Section 6.1 summarises the key findings from the bulk major and trace element characterisation of New Zealand offshore phosphorite nodules and geochemical considerations regarding phosphorite use as a fertilizer. In addition to the main aim of bulk geochemical characterisation, key findings relating to the formation history of Chatham Rise phosphorite nodules are also presented. Section 6.2 summarises the key findings from elutriate, bioaccumulation, and column leaching experiments used to determine the ecotoxicity of seafloor sediment disturbance. An overall conclusion is given in section 6.3 relating the key findings from the characterisation of the phosphorite nodule geochemistry and ecotoxicity investigations. This chapter is concluded by suggestions for future research.

6.1 Geochemistry

Phosphorite chemistry

- The bulk geochemistry of the Chatham Rise and Offshore South Island phosphorite nodules is characterised by enrichment in CaO, P_2O_5, Sr, U, Y, Mo and depletion in TiO_2, Al_2O_3, MnO, MgO, FeO, K_2O, Sc, Cr, Cu, Ga, Rb, Cs, Ba, Hf, Ta, Pb, and Th relative to the average upper crust.
- The bulk geochemistry of phosphate-rich nodules from Bollons Seamount is characterised by enrichment in first row transition metals; Co, Ni, Cu, Zn, in addition to Sr, Y, Mo, U, MnO, CaO, and P_2O_5, and by depletion in TiO_2, Al_2O_3, MgO, K_2O, FeO, SiO_2, Sc, Cr, Ga, Rb, Cs, Hf, and Th relative to the average upper crust.
- The chemical composition of the nodules is strongly dependant on their constituent minerals e.g. Bollons Seamount nodules contain Mn crusts, therefore display higher enrichment of MnO relative to Chatham Rise nodules. For Chatham Rise phosphorite nodules, the proportion of mineral phases in individual nodules is dependent on nodule size, and there is a strong correlation of the abundance of many elements with nodule size.

Nodule diagenesis and element enrichment

- The iron pump model of Froelich et al. (1988) is proposed for the formation of Chatham Rise phosphorite nodules to explain the concentric zoning of different minerals. The oxic, suboxic, and anoxic sections of the sediment profile have fluctuated during phosphorite nodule formation. Pyrite, observed in the outer zones of some nodules, formed in the anoxic section of the sediment profile. As the anoxic section of the sediment profile migrated downwards relative to the nodules, some pyrite could dissolve and reprecipitate as goethite. Apatite precipitated in the suboxic zone, together with glaucony minerals.
- The REE content of bulk Chatham Rise nodules is highly influenced by the glaucony rim minerals. Therefore, based on REE the diagenetic conditions interpreted for Chatham Rise phosphorite nodules in this study only give insights into the rim mineral formation, which was in suboxic conditions.
- Bollons Seamount phosphorite samples and Chatham Rise bulk phosphorite and chalk sediment samples display seawater REE patterns, due to quantitative uptake of REE primarily through adsorption with minor substitution. The observed negative Eu and Ce and positive Gd anomalies are inherited from oxygenated bottom seawater.
- U enrichment in the Chatham Rise phosphorite nodules depends on the local conditions of diagenesis. In some localities, phosphorite nodules likely persisted in the anoxic section of the sediment profile for longer, resulting in site-specific enrichment of U that is independent of nodule size and P_2O_5 wt %, leading to the high relative variability of U concentration both spatially and within nodule size fractions.
- The trace elements Ga, Nb, Ta and Hf associate with the glaucony rim minerals in Chatham Rise phosphorite nodules.
- Site specific enrichments in Ba, V, Co, Ni, Cu, Zn, Y, Cd, Pb observed in Chatham Rise phosphorite nodules are inherited from material either incorporated into the precursor carbonate, or that contributed to dissolved concentrations in sediment pore water. Specifically, Ba, Cu and Zn enrichment likely derives from a high flux of organic matter.

Suitability as fertilizers

- Low Cd and Th concentrations in bulk Chatham Rise phosphorite nodules make them suitable as a direct application fertilizer. U and Ni concentrations are higher than other comparable deposits, however.
- Bollons Seamount phosphorites have low Cd and U concentrations. They are also enriched in Co and Cu, which are depleted in New Zealand soils.
- Offshore South Island nodules have low concentrations of Mo, Cd, Pb and Th, but higher Cs relative to other phosphate deposits. This study is the first report of phosphorite nodules from both this particular area and Bollons Seamount, therefore no economic estimates exist for these deposits and the scale of these phosphorites is still unknown. The Offshore South Island deposit analysed in this study may be a part of the Snares Depression phosphorite deposit reported by Summerhayes (1967).

6.2 Ecotoxicity

Ecotoxic elements in the nodule environment

- Elutriate and leaching experiments should only be conducted on fresh materials, otherwise there is a risk that the degradation of the samples in storage can alter the mobility of some key, potentially ecotoxic metal species, e.g. U, V, Mo, Mn. U mobility, and hence its dissolved concentration in experiments, appears to increase significantly upon freezing and/or refrigerating and thawing sediment samples.
- Direct sediment pore water measurements show concentrations of Cu and Zn that exceed ANZECC(2000a) trigger guideline values for 99% species protection. Excess dissolved Cu being released into the immediate environment if surficial sediments are disturbed could be of concern, and monitoring is recommended.
- High dissolved Fe and Mn concentrations in sediment pore water indicates surficial sediments are likely to be suboxic.
- It is unlikely that potentially ecotoxic elements are released from phosphorite nodules during sediment agitation involved in standard elutriate procedures, or leaching column experiments of longer duration.
- pH fluctuations during column leaching experiments demonstrate methods of pH control need to be developed to study dissolved metal behaviour over time.

Implications from amphipod bioaccumulation experiments

- Most significantly, elements observed to be enriched in the matrix sediment and phosphorite nodules were not observed to bioaccumulate in amphipod tissues, indicating the solid phases in the sediment are not dissolving and releasing metals.
- In the bioaccumulation experiments using amphipods exposed to whole sediments from both study sites, Cu, Zn and Cd were also observed to bioaccumulate in amphipod tissues. Cu and Zn are essential metals; therefore bioaccumulation is expected. Thus, conclusions as to whether the bioaccumulation of these metals is due to excess exposure during experiments or an artefact of their natural environment cannot be made. Characterisation of the control sediment chemistry may help to resolve this uncertainty.
- Analysis of amphipod tissues exposed to whole sediments indicate that Cr, Co, Fe, Pb, Mn, Hg, Ni, U and V did not bioaccumulate at both study sites. In addition, Mo and Tl did not bioaccumulate in amphipods exposed to whole sediment from site CPR-1.
- For amphipods exposed to whole sediment from both sites, Sr has the potential to bioaccumulate, as did Mo in amphipods exposed to sediment from G87. Overall, this indicates some site-specific influences on exposure and bioavailability of dissolved metals.

6.3 Overall Conclusions and implications for future chemical changes and environmental impacts at phosphorite nodule localities

It is evident from the geochemical characterisation of the major and trace elements of Bollons Seamount phosphorites, Offshore South Island, and Chatham Rise phosphorite nodules and sediments, that the bulk phosphate and sediment chemistry is heterogeneous on both site and regional spatial scales as a result of complex formation processes. This was also seen in the geochemical analyses of fresh surficial sediments collected from sites G87 and CRP-1.

These site-specific chemical differences were observed to affect the biota responses when exposed to disturbed sediments. For example, Mo was depleted in site G87 sediments relative to site CRP-1 sediments, but was observed to have more bioaccumulation potential in amphipods exposed relative to sediment concentrations and BCF indicator values. This

indicates that to fully investigate the potential effects of seafloor disturbance on local biota, and hence formulate appropriate protection strategies, the chemistry of the substrate, including sediment pore water, needs to be fully characterised at multiple sites.

An amphipod biomonitor shows promise for further development, especially if species native to sites can be found and cultivated in the laboratory environment.

The potential effects of small changes in pH on metal solubility in the sediment-water system has been highlighted in this study. This has implications for changing seafloor environment through ocean acidification. Phosphorite nodules are exposed on the seafloor on both Chatham Rise and Bollons Seamount, but it is currently unknown what effects exposure to more acidic seawater will have.

6.4 Future work

Despite initial leaching column testing giving reasonable results, there is still scope for improvement. Exact flow rate calibrations are also required for the leaching column. Sediments containing different quantities of mud% and sand% will result in different flow rates. This is an important calibration. It is apparent that temperature and pH are two variables that need to be assessed for any future experiments. Temperature fluctuations can be kept to a minimum by conducting experiments in a temperature controlled laboratory; however keeping pH constant is more complicated. A pH control system utilizing CO_2 is already in development to solve this problem. The system is inspired by existing methods of mining tailing leaching experiments (Hammarstrom et al., 2009) and existing CO_2 controlled aquariums at NIWA, Wellington. Alternating between the introduction of CO_2 gas and atmosphere using a controller can keep pH constant over time, as utilised by Payán et al. (2012). This could also prove useful to study metal release from seafloor sediments influenced by ocean acidification, as a more acidic pH has the potential to increase the solubility of and change the speciation of many metals, which could make them more bioavailable (Millero et al., 2009).

Of particular importance, methods used to analyse samples for the ecotoxicity experiment samples have detection limits for several metals that are too high to be useful in this study,

which meant that the baseline chemistry of deep seawater could not be characterised effectively.

Preliminary bioaccumulation experiments from this study show promise for using amphipods as biomonitors for dissolved metal release from disturbed sediments in the marine environment. Current limitations of the bioaccumulation experiments in this study include: 1. the response of biota from the Chatham Rise is still unknown as a surrogate species had to be used in this study; 2. a standard control sediment for New Zealand offshore sediments is needed; 3. the high bioaccumulation of Cu and Zn observed in amphipod tissues cannot be concluded to be either due to exposure from test sediments, or previously accumulated from the organism's natural environment.

A Smart Ideas proposal for a project by NIWA to develop crustacean biomonitors, and use the leaching column constructed in this thesis to test more marine sediments has been granted funding by the Ministry of Business, Innovation, and Employment. The scope of this new project will allow some of these analytical limitations to be addressed, and aims to provide a more robust biomonitoring system for New Zealand's offshore marine environments.

The geochemical analysis in this study has highlighted the methodological difficulties with measuring trace elements in phosphorite and marine sediment samples using dissolution methods. Method development is required to solve wetting and precipitation issues. More work is needed on characterizing phosphate SRMs for the full range of trace metals. SRM NIST120c performed better than BCR-32 for dissolution methods, producing accurate values for a larger suite of trace metals; however it has not yet been well characterised for all elements of potential interest.

Whilst bulk geochemical characterization is useful for characterizing the overall major and trace element composition of bulk material, the different mineral phases, e.g. glaucony rim minerals, contain and contribute different trace elements. Pairing μXRF mapping with laser ablation inductively coupled mass spectrometry (LA-ICPMS) using methods developed by Walsh (2009) for phosphorite nodules could prove to be a powerful method of identifying which trace metals are associated with which major phases. Transects measuring the full suite of REE and U from rim to core could offer more insights into paleo-redox conditions during

the formation, and hence a more detailed formation history for New Zealand phosphorite nodules.

References

Abed, A. M., Sadaqah, R., & Kuisi, M. A. (2008). Uranium and Potentially Toxic Metals During the Mining, Beneficiation, and Processing of Phosphorite and their Effects on Ground Water in Jordan. *Mine Water and the Environment, 27*(3), 171. doi:10.1007/s10230-008-0039-3

Al-Hwaiti, M. S., Ranville, J. F., & Ross, P. E. (2010). Bioavailability and mobility of trace metals in phosphogypsum from Aqaba and Eshidiya, Jordan. *Chemie der Erde - Geochemistry, 70*(3), 283-291. doi:http://dx.doi.org/10.1016/j.chemer.2010.03.001

Alibo, D. S., & Nozaki, Y. (1999). Rare earth elements in seawater: particle association, shale-normalization, and Ce oxidation. *Geochimica et Cosmochimica Acta, 63*(3–4), 363-372. doi:http://dx.doi.org/10.1016/S0016-7037(98)00279-8

Amante, C., & Eakins, B. (2009). *Etopo1 1 arc-minute global relief model: Procedures, data sources and analysis.* Retrieved from http://www.ngdc.noaa.gov/mgg/global/relief/ETOPO1/docs/ETOPO1.pdf

Andersson, A. J. (2014). 8.19 - The Oceanic CaCO3 Cycle A2 - Holland, Heinrich D. In K. K. Turekian (Ed.), *Treatise on Geochemistry (Second Edition)* (pp. 519-542). Oxford: Elsevier.

Aranda, C. B. A. (2008). *Leaching tests comparison for solidified and stabilized contaminated sediments : Assessment of selected inorganic contaminants* (Master's Thesis), University of Oslo, Norway.

Arnot, J. A., & Gobas, F. (2006). A review of bioconcentration factor (BCF) and bioaccumulation factor (BAF) assessments for organic chemicals in aquatic organisms. *Environmental Reviews, 14*(4), 257-297. doi:10.1139/A06-005

Australian and New Zealand Environment Conservation Council [ANZECC]. (2000a). *Australian and New Zealand Guidelines for Fresh and Marine Water Quality* (National Water Quality Management Strategy Paper, No. 4., Vol. 1). Retrieved from http://www.environment.gov.au/system/files/resources/53cda9ea-7ec2-49d4-af29-d1dde09e96ef/files/nwqms-guidelines-4-vol1.pdf

Australian and New Zealand Environment Conservation Council [ANZECC]. (2000b). *Australian and New Zealand Guidelines for Fresh and Marine Water Quality. Aquatic Ecosystems — Rationale and Background Information* (National Water Quality Management Strategy Paper, No. 4., Vol. 2.). Retrieved from http://agriculture.gov.au/SiteCollectionDocuments/water/nwqms-guidelines-4-vol2.pdf

Aydin, I., Aydin, F., Saydut, A., Bakirdere, E. G., & Hamamci, C. (2010). Hazardous metal geochemistry of sedimentary phosphate rock used for fertilizer (Mazıdag, SE Anatolia, Turkey). *Microchemical Journal, 96*(2), 247-251. doi:http://dx.doi.org/10.1016/j.microc.2010.03.006

Barnes, P. M., & Shane, P. A. R. (1992). Late Neogene unconformity- bounded tuffaceous sequences: Northwestern Chatham Rise, New Zealand. *New Zealand Journal of Geology and Geophysics, 35*(4), 421-435. doi:10.1080/00288306.1992.9514537

Batley, G. E., & Gardner, D. (1977). Sampling and storage of natural waters for trace metal analysis. *Water Research, 11*(9), 745-756. doi:http://dx.doi.org/10.1016/0043-1354(77)90042-2

Bau, M., & Dulski, P. (1996). Geology and Geochemistry of the transvaal supergroup. Distribution of yttrium and rare-earth elements in the Penge and Kuruman iron-formations, Transvaal Supergroup, South Africa. *Precambrian Research, 79*(1), 37-55. doi:http://dx.doi.org/10.1016/0301-9268(95)00087-9

Benitez-Nelson, C. R. (2000). The biogeochemical cycling of phosphorus in marine systems. *Earth-Science Reviews, 51*(1–4), 109-135. doi:http://dx.doi.org/10.1016/S0012-8252(00)00018-0

Bennett, E. M., & Schipanski, M. E. (2013). The Phosphorus Cycle. In K. C. Weathers, D. L. Strayer, & G. E. Likens (Eds.), *Fundamentals of Ecosystem Science* (pp. 159-178): Academic Press.

Berman, S. S., Sturgeon, R. E., Desaulniers, J. A. H., & Mykytiuk, A. P. (1983). Preparation of the sea water reference material for trace metals, NASS-1. *Marine Pollution Bulletin, 14*(2), 69-73. doi:http://dx.doi.org/10.1016/0025-326X(83)90195-9

Brown, K. A., McGreer, E. R., Taekema, B., & Cullen, J. T. (2011). Determination of Total Free Sulphides in Sediment Porewater and Artefacts Related to the Mobility of Mineral Sulphides. *Aquatic Geochemistry, 17*(6), 821-839. doi:10.1007/s10498-011-9137-0

Burns, D. A. (1984). Nannofossil Dating and Paleoenvironmental Interpretation of some Chatham Rise Sediments Collected on the SONNE-17 Cruise. *Geologisches Jahrbuch, 65*, 91-97.

Burns, M. M. (1952). Phosphates in New Zealand Agriculture. *New Zealand Geographer, 8*(2), 125-137. doi:10.1111/j.1745-7939.1952.tb01803.x

Carson, G. A., & Crowley, S. F. (1993). The glauconite-phosphate association in hardgrounds: examples from the Cenomanian of Devon, southwest England. *Cretaceous Research, 14*(1), 69-89. doi:http://dx.doi.org/10.1006/cres.1993.1006

Carter, L., Carter, R. M., & McCave, I. N. (2004). Evolution of the sedimentary system beneath the deep Pacific inflow off eastern New Zealand. *Marine Geology, 205*(1–4), 9-27. doi:http://dx.doi.org/10.1016/S0025-3227(04)00016-7

Carter, R. M. (1985). The Mid-Oligocene Marshall Paraconformity, New Zealand: Coincidence with Global Eustatic Sea-Level Fall or Rise? *The Journal of Geology, 93*(3), 359-371.

Casini, S., & Depledge, M. H. (1997). Influence of Copper, Zinc, and Iron on Cadmium Accumulation in the Talitrid Amphipod, Platorchestia platensis. *Bulletin of Environmental Contamination and Toxicology, 59*(3), 500-506. doi:10.1007/s001289900506

Chatham Rock Phosphate Limited. (2014). Overview June 2014. Retrieved from http://static1.squarespace.com/static/51d24098e4b0d519d0c065f5/t/538e3629e4b0ba4a68dd30e4/1401828905177/Overview+Factsheet+June+2014+v2.pdf

Chatham Rock Phosphate Limited. (2016a). NZX Announcement: Chatham issues July 2016 Update. Retrieved from http://www.rockphosphate.co.nz/news/2016/7/11/nzx-announcement-chatham-issues-july-2016-update

Chatham Rock Phosphate Limited. (2016b). NZX Announcement: Namibian green light for marine phosphate mining "hugely significant". Retrieved from http://www.rockphosphate.co.nz/news/2016/10/21/nzx-announcement-namibian-green-light-for-marine-phosphate-mining-hugely-significant

Cooper, J., Lombardi, R., Boardman, D., & Carliell-Marquet, C. (2011). The future distribution and production of global phosphate rock reserves. *Resources, Conservation and Recycling, 57*(0), 78-86. doi:http://dx.doi.org/10.1016/j.resconrec.2011.09.009

Cooper, R. A. & Agterberg, F. P. 2004. *The New Zealand geological timescale* Lower Hutt, N.Z., Institute of Geological & Nuclear Sciences.

Cordell, D., Drangert, J.-O., & White, S. (2009). The story of phosphorus: Global food security and food for thought. *Global Environmental Change, 19*(2), 292-305. doi:http://dx.doi.org/10.1016/j.gloenvcha.2008.10.009

Cullen, D. J. (1965). Autochthonous rocks from the Chatham Rise, east of New Zealand. *New Zealand Journal of Geology and Geophysics, 8*(3), 465-474. doi:10.1080/00288306.1965.10426417

Cullen, D. J. (1980). Distribution, composition, and age of submarine phosphorites on Chatham Rise, east of New Zealand. *The Society of Economic Paleontologists and Mineralogists (SEPM) Special Publication*, 139-148.

Cullen, D. J. (1987). *The submarine phosphate resource on central Chatham Rise*. (Division of marine & fresh water science reports No. 2.). Retrieved from http://docs.niwa.co.nz/library/public/DMFSreport2.pdf

Cullen, D. J., & Singleton, R. J. (1977). The distrobution of submarine phosphorite deposits on central Chatham Rise, east of New Zealand:1 Surface distrobution from underwater photographs (Vol. 10, pp. 24).

Davy, B. (2006). Bollons Seamount and early New Zealand–Antarctic seafloor spreading. *Geochemistry, Geophysics, Geosystems, 7*(6), Q06021. doi:10.1029/2005GC001191

Delaney, M. L. (1998). Phosphorus accumulation in marine sediments and the oceanic phosphorus cycle. *Global Biogeochemical Cycles*, *12*(4), 563-572.

Dewitt, T. H., Hickey, C. W., Morrisey, D. J., Nipper, M. G., Roper, D. S., Williamson, R. B., & Williams, E. K. (1999). Do amphipods have the same concentration-response to contaminated sediment in situ as in vitro? *Environmental Toxicology and Chemistry, 18*(5), 1026-1037. doi:10.1002/etc.5620180530

Dulski, P. (1994). Interferences of oxide, hydroxide and chloride analyte species in the determination of rare earth elements in geological samples by inductively coupled plasma-mass spectrometry. *Fresenius' Journal of Analytical Chemistry, 350*(4), 194-203. doi:10.1007/bf00322470

Elderfield, H., & Greaves, M. J. (1982). The rare earth elements in seawater. *Nature, 296*(5854), 214-219.

Elderfield, H., & Sholkovitz, E. R. (1987). Rare earth elements in the pore waters of reducing nearshore sediments. *Earth and Planetary Science Letters, 82*(3), 280-288. doi:http://dx.doi.org/10.1016/0012-821X(87)90202-0

Environmental Protection Agency [EPA]. (2015). *Decision on Marine Consent Application: Chatham Rock Phosphate Limited to Mine Nodules on the Chatham Rise*. Retrieved from www.epa.govt.nz

Falconer, R. K. H., von Rad, U., & Wood, R. (1984). Regional Structure and High-Resolution Seismic Stratigraphy of the Central Chatham Rise (New Zealand). *Geologisches Jahrbuch, 65*, 29-56.

Fert Research, & AgResearch. (1999). Use of trace elements in New Zealand pastoral farming. In J. D. Morton, N. D. Grace, & M. B. O'Connor (Eds.).

Fertiliser Matters. (2005). Cadmium in New Zealand – An Update. *New Zealand Fertiliser Manufacturers' Research Association Newsletter*, (34). Retrieved from http://www.fertiliser.org.nz/Site/resource_center/newsletter_fertiliser_matters/archives.aspx

Filippelli, G. M. (2011). Phosphate rock formation and marine phosphorus geochemistry: The deep time perspective. *Chemosphere, 84*(6), 759-766. doi:http://dx.doi.org/10.1016/j.chemosphere.2011.02.019

Fofonoff, N., Millard, R., Joint Panel on Oceanographic Tables Standards, Unesco, & SCOR Working Group 51. (1983). *Algorithms for computation of fundamental properties of seawater / by N.P. Fofonoff and R.C. Millard ; endorsed by Unesco/SCOR/ICES/IAPSO Joint Panel on Oceanographic Tables and Standard and SCOR Working Group 51*. Paris]: Unesco.

Föllmi, K. B. (1996). The phosphorus cycle, phosphogenesis and marine phosphate-rich deposits. *Earth-Science Reviews, 40*(1–2), 55-124. doi:http://dx.doi.org/10.1016/0012-8252(95)00049-6

Fordyce, R. E. (1984). Preliminary Report on Cetacean Bones from Chatham Rise (New Zealand). *Geologisches Jahrbuch, 65*.

Froelich, P. N., Arthur, M. A., Burnett, W. C., Deakin, M., Hensley, V., Jahnke, R., & Vathakanon, C. (1988). Early diagenesis of organic matter in Peru continental margin sediments: Phosphorite precipitation. *Marine Geology, 80*(3–4), 309-343. doi:http://dx.doi.org/10.1016/0025-3227(88)90095-3

Froelich, P. N., Bender, M. L., Luedtke, N. A., Heath, G. R., & DeVries, T. (1982). The marine phosphorus cycle. *American Journal of Science, 282*(4), 474-511. doi:10.2475/ajs.282.4.474

Froelich, P. N., Klinkhammer, G. P., Bender, M. L., Luedtke, N. A., Heath, G. R., Cullen, D., & Maynard, V. (1979). Early oxidation of organic matter in pelagic sediments of the eastern equatorial Atlantic: suboxic diagenesis. *Geochimica et Cosmochimica Acta, 43*(7), 1075-1090. doi:http://dx.doi.org/10.1016/0016-7037(79)90095-4

Fulthorpe, C. S., Carter, R. M., Miller, K. G., & Wilson, J. (1996). Marshall Paraconformity: a mid-Oligocene record of inception of the Antarctic circumpolar current and coeval glacio-eustatic lowstand? *Marine and Petroleum Geology, 13*(1), 61-77. doi:http://dx.doi.org/10.1016/0264-8172(95)00033-X

Gadd, M., Layton-Matthews, D., & Peter, J. (2016). Non-hydrothermal origin of apatite in SEDEX mineralization and host rocks of the Howard's pass district, Yukon, Canada. *American Mineralogist, 101*(5-6), 1061

Glenn, C. R., & Arthur, M. A. (1988). Petrology and major element geochemistry of Peru margin phosphorites and associated diagenetic minerals: Authigenesis in modern organic-rich sediments. *Marine Geology, 80*(3–4), 231-267. doi:http://dx.doi.org/10.1016/0025-3227(88)90092-8

Gnandi, K., Boroon, M. H. R., & Dimitri, D. D. (2009). Distribution, Speciation, and Extractability of Cadmium in the Sedimentary Phosphorite of Hahotoé-Kpogamé (Southern Togo). *Aquatic Geochemistry, 15*(4), 485-495. doi:10.1007/s10498-009-9062-7

Golder Associates (NZ) Limited. (2014a). *Chatham Rock Phosphate Limited. Proposed Mining Operation, Chatham Rise: Marine Consent Application and Environmental Impact Assessment* (Vol. 1).

Golder Associates (NZ) Limited. (2014b). *Review of Sediment Chemistry and Effects of Mining.* (Report Number: 1178207517/013_Rev 4).

Graham, W. F., & Duce, R. A. (1979). Atmospheric pathways of the phosphorus cycle. *Geochimica et Cosmochimica Acta, 43*(8), 1195-1208.

Gromet, L. P., Haskin, L. A., Korotev, R. L., & Dymek, R. F. (1984). The "North American shale composite": Its compilation, major and trace element characteristics. *Geochimica et Cosmochimica Acta, 48*(12), 2469-2482. doi:http://dx.doi.org/10.1016/0016-7037(84)90298-9

Grundl, T., & Delwiche, J. (1993). Kinetics of ferric oxyhydroxide precipitation. *Journal of Contaminant Hydrology, 14*(1), 71-87. doi:http://dx.doi.org/10.1016/0169-7722(93)90042-Q

Hammarstrom, J. M., Cravotta, C. A., Galeone, D., Jackson, J. J., & Dulong, F. (2009). *Development and Interpretation of the ADTI-WP2 Leaching Column Method (Kinetic test procedure for the prediction of coal mine drainage quality).* (EPA method 1627 : U.S. Office of Surface Mining Reclamation and Enforcement CT-5-30040).

Hayward, B. W., Grenfell, H. R., Carter, R., & Hayward, J. J. (2004). Benthic foraminiferal proxy evidence for the Neogene palaeoceanographic history of the Southwest Pacific, east of New Zealand. *Marine Geology, 205*(1–4), 147-184. doi:http://dx.doi.org/10.1016/S0025-3227(04)00022-2

Herzer, R. H., Challis, G. A., Christie, R. H. K., Scott, G. H., & Watters, W. A. (1989). The Urry Knolls, late Neogene alkaline basalt extrusives, southwestern Chatham Rise. *Journal of the Royal Society of New Zealand, 19*(2), 181-193. doi:10.1080/03036758.1989.10426447

Herzer, R. H., & Wood, R. A., S. (1988). The Geology and Structure of Mernoo Bank and Surrounding Area, Western Chatham Rise. *New Zealand Geological Survey, 29*.

Hickey, C. W., Albert, A., Thompson, K. A., & Martin, M. L. (2014). *Chatham Rise Sediment Elutriates: Toxicity and Chemistry*. Retrieved from Hamilton, New Zealand:

Horn, M., & Uenzelmann-Neben, G. (2015). The Deep Western Boundary Current at the Bounty Trough, east of New Zealand: Indications for its activity already before the opening of the Tasmanian Gateway. *Marine Geology, 362*, 60-75. doi:http://dx.doi.org/10.1016/j.margeo.2015.01.011

Hughes, J. M. (2015). The many facets of apatite. *American Mineralogist, 100*(5-6), 1033-1039. doi:10.2138/am-2015-5193

James, N. P., Jones, B., Nelson, C. S., Campbell, H. J., & Titjen, J. (2011). Cenozoic temperate and sub-tropical carbonate sedimentation on an oceanic volcano - Chatham Islands, New Zealand. *Sedimentology, 58*(4), 1007-1029. doi:10.1111/j.1365-3091.2010.01193.x

Jarosewich, E., Nelen, J. A., & Norberg, J. A. (1980). Reference Samples for Electron Microprobe Analysis*. *Geostandards Newsletter, 4*(1), 43-47. doi:10.1111/j.1751-908X.1980.tb00273.x

Jarvis, I., Burnett, W., Nathan, Y., Almbaydin, F., Attia, A., Castro, L., . . . Zanin, Y. (1994). Phosphorite geochemistry: state-of-the-art and environmental concerns. *Eclogae Geologicae Helvetiae, 87*(3), 643-700.

Jochum, K. P., Nohl, U., Herwig, K., Lammel, E., Stoll, B., & Hofmann, A. W. (2005). GeoReM: A New Geochemical Database for Reference Materials and Isotopic Standards. *Geostandards and Geoanalytical Research, 29*(3), 333-338. doi:10.1111/j.1751-908X.2005.tb00904.x

Joosu, L., Lepland, A., Kirsimäe, K., Romashkin, A. E., Roberts, N. M. W., Martin, A. P., & Črne, A. E. (2015). The REE-composition and petrography of apatite in 2 Ga Zaonega Formation, Russia: The environmental setting for phosphogenesis. *Chemical Geology, 395*, 88-107. doi:http://dx.doi.org/10.1016/j.chemgeo.2014.11.013

Kelley, D., & Richards, C. (2016). oce: Analysis of Oceanographic Data. R package version 0.9-18. Retrieved from https://CRAN.R-project.org/package=oce

King, C. K., Gale, S. A., Hyne, R. V., Stauber, J. L., Simpson, S. L., & Hickey, C. W. (2006). Sensitivities of Australian and New Zealand amphipods to copper and zinc in waters and metal-spiked sediments. *Chemosphere, 63*(9), 1466-1476. doi:http://dx.doi.org/10.1016/j.chemosphere.2005.09.020

Kolodny, Y., & Kaplan, I. R. (1970). Uranium isotopes in sea-floor phosphorites. *Geochimica et Cosmochimica Acta, 34*(1), 3-24. doi:http://dx.doi.org/10.1016/0016-7037(70)90148-1

Kreuzer, H. (1984). K-Ar Dating of Glauconite Rims of Phosphorite Nodules (Chatham Rise, New Zealand). *Geologisches Jahrbuch, 65*, 121-127.

Kudrass, H., & von Rad, U. (1984a). Geology and some mining aspects of the Chatham Rise phosphorite: a synthesis of Sonne-17 results. *Geologisches Jahrbuch, 65*, 233-252.

Kudrass, H. R., & Von Rad, U. (1984b). Underwater Television and Photography Observations, Side-Scan Sonar and Acoustic Reflectivity Measurements of Phosphorite-Rich Areas on the Chatham Rise (New Zealand). *Geologisches Jahrbuch, 65*, 69-89.

Kudrass, H. R., & Cullen, D. J. (1982). Submarine Phosphorite Nodules from the Central Chatham Rise of New Zealand: Composition, Distrobution, and Reserves (VALDIVA-Cruise 1978). Hannover, Germany: Bundesanstalt für Geowissenschaften und Rohstoffe und den Geologischen Landesämtern in der Bundesrepublik Deutschland.

Lamboy, M. (1993). Phosphatization of calcium carbonate in phosphorites: microstructure and importance. *Sedimentology, 40*(1), 53-62. doi:10.1111/j.1365-3091.1993.tb01090.x

Lawless, A. S. (2012). *Nature, Distribution, Origin and Economics of Glauconite in Carbonate-Phosphate-Glauconite Surficial Deposits on Central Chatham Rise, Southwest Pacific.* (Master of Science thesis), The University of Waikato, Hamilton, New Zealand.

Lécuyer, C., Reynard, B., & Grandjean, P. (2004). Rare earth element evolution of Phanerozoic seawater recorded in biogenic apatites. *Chemical Geology, 204*(1–2), 63-102. doi:http://dx.doi.org/10.1016/j.chemgeo.2003.11.003

Leote, C., Epping, E., & Van Cappellen, P. (2013). Phosphate sorption from seawater solutions: Particle concentration effect. *Marine Chemistry, 148*, 52-62. doi:http://dx.doi.org/10.1016/j.marchem.2012.12.002

Li, Y. H., & Schoonmaker, J. E. (2014). Chemical Composition and Mineralogy of Marine Sediments. In H. D. Turekian & K. K. Holland (Eds.), *Treatise on Geochemistry (Second Edition)* (pp. 1-32). Oxford: Elsevier.

Mackay, A. D., Gregg, P. E. H., & Sysers, J. K. (1980). A preliminary evaluation of Chatham Rise phosphorite as a direct- use phosphatic fertiliser (New Zealand). *New Zealand Journal of Agricultural Research, 23*(4), 441-449. doi:10.1080/00288233.1980.10417867

Marion, G. M., Millero, F. J., Camões, M. F., Spitzer, P., Feistel, R., & Chen, C. T. A. (2011). pH of seawater. *Marine Chemistry, 126*(1–4), 89-96. doi:http://dx.doi.org/10.1016/j.marchem.2011.04.002

Marsden, I. D., & Rainbow, P. S. (2004). Does the accumulation of trace metals in crustaceans affect their ecology—the amphipod example? *Journal of Experimental Marine Biology and Ecology, 300*(1–2), 373-408. doi:http://dx.doi.org/10.1016/j.jembe.2003.12.009

Masuda, A., & Ikeuchi, Y. (1979). Lanthanide tetrad effect observed in marine environment. *Geochemical Journal, 13*, 19 - 22.

Masuda, A., Kawakami, O., Dohmoto, Y., & Takenaka, T. (1987). Lanthanide tetrad effects in nature: two mutually opposite types, W and M. *Geochemical Journal, 21*(3), 119-124.

Maynard, J. B. (2014). Manganiferous Sediments, Rocks, and Ores. In H. D. Turekian & K. K. Holland (Eds.), *Treatise on Geochemistry (Second Edition)* (pp. 327-349). Oxford: Elsevier.

Mazumdar, A., Banerjee, D. M., Schidlowski, M., & Balaram, V. (1999). Rare-earth elements and Stable Isotope Geochemistry of early Cambrian chert-phosphorite assemblages from the Lower Tal Formation of the Krol Belt (Lesser Himalaya, India).

Chemical Geology, 156(1–4), 275-297. doi:http://dx.doi.org/10.1016/S0009-2541(98)00187-9

McArthur, J. M., Sahami, A. R., Thirlwall, M., Hamilton, P. J., & Osborn, A. O. (1990). Dating phosphogenesis with strontium isotopes. *Geochimica et Cosmochimica Acta, 54*(5), 1343-1351. doi:http://dx.doi.org/10.1016/0016-7037(90)90159-I

McArthur, J. M., & Walsh, J. N. (1984). Rare-earth geochemistry of phosphorites. *Chemical Geology, 47*(3–4), 191-220. doi:http://dx.doi.org/10.1016/0009-2541(84)90126-8

McCoy-West, A. J. (2009). *The Petrogenesis of Mid-Cretaceous Continental Intraplate Volcanism in Marlborough, New Zealand, during the Break-up of Gondwana.* (Master of Science thesis), Victoria University of Wellington.

McDowell, R. W., Taylor, M. D., & Stevenson, B. A. (2013). Natural background and anthropogenic contributions of cadmium to New Zealand soils. *Agriculture, Ecosystems & Environment, 165*, 80-87. doi:http://dx.doi.org/10.1016/j.agee.2012.12.011

McLennan, S. M. (1989). Rare-earth elements in sedimentary-rocks: Influence of provenance and sedimentary processes. *Reviews in Mineralogy and Geochemistry, 21*, 169-200.

McLennan, S. M. (1994). Rare earth element geochemistry and the "tetrad" effect. *Geochimica et Cosmochimica Acta, 58*(9), 2025-2033. doi:http://dx.doi.org/10.1016/0016-7037(94)90282-8

Millero, F. J., Woosley, R., DiTrolio, B., & Waters, J. (2009). Effect of Ocean Acidification on the Speciation of Metals in Seawater. *Oceanography, 22*(4), 72–85. doi:http://dx.doi.org/10.5670/oceanog.2009.98

Millero, F. J., Zhang, J.-Z., Fiol, S., Sotolongo, S., Roy, R. N., Lee, K., & Mane, S. (1993). The use of buffers to measure the pH of seawater. *Marine Chemistry, 44*(2), 143-152. doi:http://dx.doi.org/10.1016/0304-4203(93)90199-X

Moon, E. M., & Peacock, C. L. (2012). Adsorption of Cu(II) to ferrihydrite and ferrihydrite–bacteria composites: Importance of the carboxyl group for Cu mobility in natural environments. *Geochimica et Cosmochimica Acta, 92*, 203-219. doi:http://dx.doi.org/10.1016/j.gca.2012.06.012

Morse, J. W. (1991). Oxidation kinetics of sedimentary pyrite in seawater. *Geochimica et Cosmochimica Acta, 55*(12), 3665-3667. doi:http://dx.doi.org/10.1016/0016-7037(91)90064-C

Namibian Marine Phosphate (Pty) Ltd. (2011). Environmental Impact Assessment Background Information. Retrieved from http://www.namphos.com/project/sandpiper/environment/item/57-environmental-marine-impact-assessment-report.html

National Institiute of Water and Atmospheric Research [NIWA]. (1995). *Amphipod chronic (28 d) sediment toxicity test procedure.* (Standard Operating Procedure No. 18). Hamilton, New Zealand: National Institute of Water and Atmospheric Research

Nelson, C. S., & Cooke, P. J. (2001). History of oceanic front development in the New Zealand sector of the Southern Ocean during the Cenozoic—a synthesis. *New Zealand Journal of Geology and Geophysics, 44*(4), 535-553. doi:10.1080/00288306.2001.9514954

Nodder, S. D., Pilditch, C. A., Probert, P. K., & Hall, J. A. (2003). Variability in benthic biomass and activity beneath the Subtropical Front, Chatham Rise, SW Pacific Ocean. *Deep Sea Research Part I: Oceanographic Research Papers, 50*(8), 959-985. doi:http://dx.doi.org/10.1016/S0967-0637(03)00094-3

Nodder, S. D., Bowden, D. A., Pallentin, A., & Mackay, K. (2012). Seafloor habitats and benthos of a continental ridge: Chatham Rise, New Zealand. In P.T. Harris & E.K. Baker (Eds.*), Seafloor Geomorphology and Benthic Habitat: GeoHab Atlas of seafloor geomorphic features and benthic habitats* (pp. 763-776). St. Louis: Elsevier Science.

Ogunleye, P. O., Mayaki, M. C., & Amapu, I. Y. (2002). Radioactivity and heavy metal composition of Nigerian phosphate rocks: possible environmental implications. *Journal of Environmental Radioactivity, 62*(1), 39-48. doi:http://dx.doi.org/10.1016/S0265-931X(01)00149-7

Ohline, S. M., Reid, M. R., Husheer, S. L. G., Currie, K. I., & Hunter, K. A. (2007). Spectrophotometric determination of pH in seawater off Taiaroa Head, Otago, New Zealand: Full-spectrum modelling and prediction of pCO2 levels. *Marine Chemistry, 107*(2), 143-155. doi:http://dx.doi.org/10.1016/j.marchem.2007.06.018

Oliver, W. (2009). Sampling and Sample Treatments *Practical Guidelines for the Analysis of Seawater*: CRC Press.

Pante, E., & Simon-Bouhet, B. (2013). marmap: A Package for Importing, Plotting and Analyzing Bathymetric and Topographic Data in R. *PLoS ONE, 8*(9), e73051. doi:doi:10.1371/journal.pone.0073051

Pantelica, A. I., Salagean, M. N., Georgescu, I. I., & Pincovschi, E. T. (1997). INAA of some phosphates used in fertilizer industries. *Journal of Radioanalytical and Nuclear Chemistry, 216*(2), 261-264. doi:10.1007/BF02033788

Panter, K. S., Blusztajn, J., Hart, S. R., Kyle, P. R., Esser, R., & McIntosh, W. C. (2006). The Origin of HIMU in the SW Pacific: Evidence from Intraplate Volcanism in Southern New Zealand and Subantarctic Islands. *Journal of Petrology, 47*(9), 1673-1704. doi:10.1093/petrology/egl024

Pasho, D. W. (1976). *Distribution and morphology of Chatham Rise phosphorites*. Wellington, New Zealand: New Zealand Oceanographic Institute.

Pattan, J. N., Pearce, N. J. G., & Mislankar, P. G. (2005). Constraints in using Cerium-anomaly of bulk sediments as an indicator of paleo bottom water redox environment: A case study from the Central Indian Ocean Basin. *Chemical Geology, 221*(3–4), 260-278. doi:http://dx.doi.org/10.1016/j.chemgeo.2005.06.009

Payán, M. C., Verbinnen, B., Galan, B., Coz, A., Vandecasteele, C., & Viguri, J. R. (2012). Potential influence of CO2 release from a carbon capture storage site on release of trace metals from marine sediment. *Environmental Pollution, 162*, 29-39. doi:http://dx.doi.org/10.1016/j.envpol.2011.10.015

Rao, V. P., Hegner, E., Naqvi, S. W. A., Kessarkar, P. M., Ahmad, S. M., & Raju, D. S. (2008). Miocene phosphorites from the Murray Ridge, northwestern Arabian Sea. *Palaeogeography, Palaeoclimatology, Palaeoecology, 260*(3–4), 347-358. doi:http://dx.doi.org/10.1016/j.palaeo.2007.12.003

Reynard, B., Lécuyer, C., & Grandjean, P. (1999). Crystal-chemical controls on rare-earth element concentrations in fossil biogenic apatites and implications for paleoenvironmental reconstructions. *Chemical Geology, 155*(3–4), 233-241. doi:http://dx.doi.org/10.1016/S0009-2541(98)00169-7

RSC Consulting Ltd. (2014). *Chatham Rise Project: Independent JORC (2012) Technical Report and Mineral Resource Estimate on the Chatham Rise Project in New Zealand*. Retrieved from http://www.epa.govt.nz/eez/EEZ000006/EEZ000006_Appendix05_Sterk_JORC%20Resource%20Estimate.pdf

Rudnick, R. L., & Gao, S. (2014). 4.1 - Composition of the Continental Crust A2 - Holland, Heinrich D. In K. K. Turekian (Ed.), *Treatise on Geochemistry (Second Edition)* (pp. 1-51). Oxford: Elsevier.

Sabiha, J., Mehmood, T., Chaudhry, M. M., Tufail, M., & Irfan, N. (2009). Heavy metal pollution from phosphate rock used for the production of fertilizer in Pakistan. *Microchemical Journal, 91*(1), 94-99. doi:http://dx.doi.org/10.1016/j.microc.2008.08.009

Schenau, S. J., Slomp, C. P., & De Lange, G. J. (2000). Phosphogenesis and active phosphorite formation in sediments from the Arabian Sea oxygen minimum zone. *Marine Geology, 169*(1–2), 1-20. doi:http://dx.doi.org/10.1016/S0025-3227(00)00083-9

Schipper, L. A., Sparling, G. P., Fisk, L. M., Dodd, M. B., Power, I. L., & Littler, R. A. (2011). Rates of accumulation of cadmium and uranium in a New Zealand hill farm soil as a result of long-term use of phosphate fertilizer. *Agriculture, Ecosystems & Environment, 144*(1), 95-101. doi:http://dx.doi.org/10.1016/j.agee.2011.08.002

Schoute, E. (2013). *Phosphate Mining on the Chatham Rise*. Paper presented at the European Marine Sand and Gravel Group (EMSAGG) Seminar 'Opportunities for European Mineral Resources'.

Shaffer, G. (1986). Phosphate pumps and shuttles in the Black Sea. *Nature, 321*(6069), 515-517.

Shields, G., & Stille, P. (2001). Diagenetic constraints on the use of cerium anomalies as palaeoseawater redox proxies: an isotopic and REE study of Cambrian phosphorites. *Chemical Geology, 175*(1–2), 29-48. doi:http://dx.doi.org/10.1016/S0009-2541(00)00362-4

Starinsky, A., Katz, A., & Kolodny, Y. (1982). The incorporation of uranium into diagenetic phosphorite. *Geochimica et Cosmochimica Acta, 46*(8), 1365-1374. doi:http://dx.doi.org/10.1016/0016-7037(82)90272-1

Statistics New Zealand. (2014). *Harmonised trade imports - Natural calcium phosphates, natural aluminium calcium phosphates and phosphatic chalk; unground*. [Data file] Retrieved from http://www.stats.govt.nz/infoshare/ViewTable.aspx?pxID=0bdfadbb-7cb7-4801-ad46-5795086af424.

Stilwell, J. D., Consoli, C. P., Sutherland, R., Salisbury, S., Rich, T. H., Vickers-Rich, P. A., & Wilson, G. J. (2006). Dinosaur sanctuary on the Chatham Islands, Southwest Pacific: First record of theropods from the K–T boundary Takatika Grit. *Palaeogeography, Palaeoclimatology, Palaeoecology, 230*(3–4), 243-250. doi:http://dx.doi.org/10.1016/j.palaeo.2005.07.017

Summerhayes, C. P. (1967). Marine environments of economic mineral deposition around New Zealand: A review. *New Zealand Journal of Marine and Freshwater Research, 1*(3), 267-282. doi:10.1080/00288330.1967.9515204

Taylor, M. D. (2007). Accumulation of uranium in soils from impurities in phosphate fertilisers. *Landbauforschung Völkenrode, 2*(57), 133-139.

The Treasury. (2014). *New Zealand Economic and Financial Overview 2014*. Retrieved from http://www.treasury.govt.nz/economy/overview/2014

Timm, C., Hoernle, K., Werner, R., Hauff, F., den Bogaard, P. v., White, J., . . . Garbe-Schönberg, D. (2010). Temporal and geochemical evolution of the Cenozoic intraplate volcanism of Zealandia. *Earth-Science Reviews, 98*(1–2), 38-64. doi:http://dx.doi.org/10.1016/j.earscirev.2009.10.002

The Treasury. (2010). *The Economy of New Zealand: Overview*. Retrieved from www.treasury.govt.nz/economy/overview/2010/04.htm.

The Treasury. (2013). Special Topic: Recession and recovery: how do we compare? Retrieved from www.treasury.govt.nz/economy/mei/nov13/08.htm

U.S. Environmental Protection Agency. (1991). Evaluation of Dredged Material Proposed for Ocean Disposal Testing Manual (No. EPA-503/8-91/001.).

USGS. (2004). Cleaning of Equipment for Water Sampling. In F. D. Wilde (Ed.), *National Field Manual for the Collection of Water-Quality Data*. United States Geological Survey. Retrieved from https://water.usgs.gov/owq/FieldManual/chapter3/final508Chap3book.pdf

Vaccari, D. A., & Strigul, N. (2011). Extrapolating phosphorus production to estimate resource reserves. *Chemosphere, 84*(6), 792-797. doi:http://dx.doi.org/10.1016/j.chemosphere.2011.01.052

Van Raalte. G., Van Doorn. T., & Steenbrink. S. (2013). *System Design for Sustainable Phosphate Mining Operations.* Paper presented at the Australian Institute of Mining and Metallurgy (AUSIMM), Nelson, New Zealand.

Van Vuuren, D. P., Bouwman, A. F., & Beusen, A. H. W. (2010). Phosphorus demand for the 1970–2100 period: A scenario analysis of resource depletion. *Global Environmental Change, 20*(3), 428-439. doi:http://dx.doi.org/10.1016/j.gloenvcha.2010.04.004

Von Rad, U., & Rosch, H. (1984). Geochemistry, texture, and petrography of phosphorite nodules and associated foraminiferal glauconite sands (Chatham Rise, New Zealand). *Geologisches Jahrbuch, 65*, 129-178.

Walsh, S. R. (2009). *Trace Elements in Sedimentary Phosphorites.* (PhD thesis), Southern Cross University, Lismore, New South Wales, Australia.

Weedon, G. P., & Hall, I. R. (2004). Neogene palaeoceanography of Chatham Rise (Southwest Pacific) based on sediment geochemistry. *Marine Geology, 205*(1–4), 207-225. doi:http://dx.doi.org/10.1016/S0025-3227(04)00024-6

Wei, T., & Simko, V. (2016). corrplot: Visualization of a Correlation Matrix [R package version 0.77]. Retrieved from https://CRAN.R-project.org/package=corrplot

Wheat, G. C., Feely, R. A., & Mottl, M. J. (1996). Phosphate removal by oceanic hydrothermal processes: An update of the phosphorus budget in the oceans. *Geochimica et Cosmochimica Acta, 60*(19), 3593-3608. doi:http://dx.doi.org/10.1016/0016-7037(96)00189-5

Wignall, P. B., & Myers, K. J. (1988). Interpreting benthic oxygen levels in mudrocks: a new approach. *Geology, 16*(5), 452–455.

Wood, R. A., Andrews, P. B., & Herzer, R. H. (1989). *Cretaceous and Cenozoic Geology of the Chatham Rise Region, South Island, New Zealand*. Lower Hutt, New Zealand: New Zealand Geological Survey.

Yamagata, Y., Watanabe, H., Saitoh, M., & Namba, T. (1991). Volcanic production of polyphosphates and its relevance to prebiotic evolution. *Nature, 352*(6335), 516-519.

Zachos, J., Pagani, M., Sloan, L., Thomas, E., & Billups, K. (2001). Trends, Rhythms, and Aberrations in Global Climate 65 Ma to Present. *Science, 292*(5517), 686-693.

Zobel, B. (1984). Foraminiferal Age of Phosphorite Nodules from the Chatham Rise (SO-17 Cruise). *Geologisches Jahrbuch, 65*, 99-105.

Appendix A. Geochemical data: phosphorites and sediments

All supplementary information listed below can be found on the digital appendices CD located at the back of this thesis.

A-1. Sample information: A sample list of all phosphorite and sediment samples analysed for geochemical characterisation.

A-2. Major element data: All phosphorite and sediment XRF major element analyses used for geochemical characterisation.

A-3. Accuracy of XRF SRM: Accuracy of standard reference materials used for XRF major element calibration.

A-4. Trace element data: All phosphorite and sediment ICPMS trace element analyses used for geochemical characterisation.

A-5: Reproducibility of ICPMS data: Compiled duplicates used to monitor external precision.

A-6. Lost on Ignition data: Lost on ignition (LOI) for selected Chatham Rise and Bollons Seamount samples.

A-7. Processing blank for ceramic mortar and pestle: A quartz sand blank processed in the ceramic mortar and pestle used for sample preparation in this study to monitor contamination.

Appendix B. Hill Laboratories Analysis Reports

All supplementary information listed below can be found on the digital appendices CD located at the back of this thesis.

B-1. Sample list: B-1. Sample list and analysis report codes. Elutriate, seawater, sediment pore water, and bulk sediment samples collected during *R.V. Tangaroa* voyage TAN1503.

B-2. Hill Laboratory Analysis Report for elutriate experiments, seawater samples, sediment pore water, and bulk sediment samples collected during *R.V. Tangaroa* voyage TAN1503.

B-3: Sample list: Sample list of sediment and elutriate experiments analysed samples from amphipod bioaccumulation experiments. Elutriate results from this report are not included in this thesis. Samples prepared by Dr. C. Hickey, NIWA.

B-4 Hill Laboratory Analysis Report for sediment fractions analysed from amphipod bioaccumulation experiments.

B-5: Sample list: Sample list of amphipod tissue analyses from bioaccumulation experiments.

B-6: Hill Laboratory Analysis Report for amphipod tissues analysed from amphipod bioaccumulation experiments.

B-7: Sample List: Sample list of subsamples from column leaching experiments, including a key to analysis codes in the Hill Laboratory Analysis Report.

B-8: Hill Laboratory Analysis Report for samples analysed from the column leaching experiments.

B-9: Raw CTD data collected for seawater samples collected during *R.V. Tangaroa* voyage TAN1503.

Appendix C. Leaching Column Apparatus: Construction and Parts

This appendix can be found on the digital appendices CD located at the back of this thesis.